A GENERALIZED THEORY OF RADIATIONLESS TRANSITIONS

Thesis by

Charles Anderson Langhoff

In Partial Fulfillment of the Requirements

For the Degree of

Doctor of Philosophy

California Institute of Technology

Pasadena, California

1974

(Submitted November 15, 1973)

ACKNOWLEDGEMENTS

This thesis is dedicated to my parents to whom I wish to give my sincere thanks. Their encouragement throughout my life in and out of school has contributed greatly to the perseverance that went into this thesis. Of course, there is always the financial support they have given my family and me. For all these things and many more, I am forever grateful.

Secondly, thanks go to Professor G. W. Robinson. Even in times when I thought much of the work I was doing was not worthwhile, his continuing belief in the work and me always raised my spirits.

Thirdly, to my wife and son, who will make the agony of this thesis worthwhile in the future.

Finally, I wish to thank the National Institutes of Health which has supported me throughout my graduate career.

ABSTRACT

The problem of radiationless transitions in polyatomic molecules has been much discussed in recent years. Most attention has been focused on the large energy gap or statistical limit case where the lineshape is Lorentzian and the emission decay exponential. The weighted density of states is assumed to be constant with energy. The broad band approximation, which states that the exciting light uniformly and coherently excites the entire molecular resonance, is standardly employed. The cases of intermediate energy gap have not been extensively investigated. Also, the effect of a finite bandwidth excitation light has only been formally treated. The generalizations proposed here allow the weighted density function to assume general energy dependence. Using the techniques of scattering theory, we are able to present exact formulas for the spectrum and the emission decay which must be evaluated numerically. This enables a more thorough treatment of the intermediate energy gap case where the density is expected to be "line-like". The spectral line shapes become very complex and in no way resemble a Lorentzian. The emission decay curves are correspondingly complex showing quantum beat effects. The ability to detect these quantum beats is also discussed. Also, the excitation band is allowed to have finite width (and, of necessity, a finite time duration). The width and positioning of the excitation band has a dramatic effect on the emission decay. The above generaliza-

tions also lead to a new interpretation of the lifetimes of some intermediate case molecules such as NO_2, SO_2, and CS_2. Finally, we apply the formal results to the calculation of the second singlet spectrum of naphthalene in various mixed crystal hosts. We are able to get virtually exact fits to the spectrum using our simple formulas Also, we compute some emission decay curves and compare these curves with some measured gas phase emission curves.

TABLE OF CONTENTS

PART 1

HISTORICAL AND MATHEMATICAL BACKGROUND

The radiationless transition problem has been around almost since the origins of the quantum theory. The early work dealt mainly with phenomena such as the Auger effect and predissociation. Later, chemical physicists began to worry about the origins and properties of fluorescence and phosphorescence. This work led to the currently used terms "internal conversion" and "intersystem crossing". The most recent times have seen both simple and sophisticated mathematical tools applied to the problem with a bewildering array of results forthcoming. Robinson [1] has recently written a summary of the history of the development of the field. Earlier reviews by Henry and Kasha [2], Hochstrasser, et. al. [3], and Schlag, et. al. [4] present a great deal of the experimental and theoretical results obtained since 1965. Freed [5] has reviewed principally the theoretical work in the same period.

Before proceeding to discuss the theoretical models proposed to explain the phenomenon of the radiationless transition, we will present some of the experimental criteria characterizing it. We will henceforth deal only with the radiationless transitions due to internal conversion or intersystem crossing. We will ignore the problems of predissociation, dissociation, and any kind of photochemistry (see Ref. [3] for some discussion of the photochemistry problem). There are three areas in which the radiationless transition is manifested experimentally. These are the electronic absorption spectrum, the emission decay curve or lifetime, and the quantum yield.

The thing that one generally looks for in the absorption spectrum to indicate radiationless transitions is diffuseness or broadening. According to standard solutions of the Schroedinger equation, one would expect to see regular structure such as well defined, sharp lines whose positions are ascribable to electronic, vibrational, or rotational energy levels. For many molecules this is the case for the first and maybe the second and third electronic transitions. Almost in every case, however, the upper excited states are diffuse and frequently featureless. This is commonly known as Kasha's rule. This diffuseness is attributed to the presence of a continuum of states which interact with the zero-order vibrational and rotational levels of the electronic transition. The net result is that the zero order levels broaden. If the broadening is comparable to the spacing between consecutive zero-order energy levels, no structure would be resolvable. Hochstrasser [6] has recently provided a qualitative discussion of this diffuseness together with several examples. Bryne and Ross [7] have also presented an extensive discussion of the causes of diffuseness in electronic spectra along with many examples.

In addition to simple broadening caused by interaction with a continuum, there is another effect which is quite striking. When two electronic states are separated by a fairly small energy gap (roughly a few thousand wavenumbers), the interaction of the upper electronic state with the higher vibrational levels of the lower state gives rise to extra structure in the region of the higher electronic state. This

phenomenon has been observed in dilute mixed crystals of quinoxaline in a durene host [6] and naphthaline in durene, p-xylene, n-pentane and toluene hosts [8]. We will later present a detailed discussion of the naphthalene spectrum (see Part 5).

The decay curves are roughly related to the absorption spectrum via the uncertainty principle. Thus, a linewidth ΔE implies a lifetime $\Delta t \simeq \hbar/\Delta E$ [6]. Normally, the radiation field contributes a certain width to the spectrum and thus gives rise to a radiative lifetime. If a second continuum (say from a lower electronic state) interacts with the zero order level, then it also contributes a component to the width and lifetime. The presence of the second continuum thus shortens the lifetime. This is the usual case for larger molecules. Much experimental effort has been expended in determining lifetimes of single vibronic levels in benzene and perdeuterobenzene [11], β-naphthylamine [12], naphthalene vapor [13], acetone [14] and aniline [15]. These references are surely not all the work done in this area. If the diffuseness is of the second kind where sharp structure is introduced into what is otherwise a broad spectrum, then the uncertainty principle relationship is somewhat difficult to define. Indeed, one would not expect the decay curve to be even exponential. Some nonexponential decays of this type have been reported [9], but these claims have been questioned. At present the situation is not resolved.

A second decay time effect has been observed in small molecules and is discussed by Douglas [14]. In small molecules the densities

are not broad and almost constant, but rather line-like. This is due to the small number of vibrational degrees of freedom. As opposed to the above discussed case of lifetime shortening, the lifetime is apparently lengthened over that of the radiative lifetime. Here the radiative lifetime is estimated from the integrated absorption coefficient. The spectra in these cases are line-like, but they do not seem to obey the usual spectroscopic rules and as of now have not been assigned.

Quantum yields of emission have been measured for many molecules. By measuring the quantum yield and the fluorescent lifetime, one can get an estimate of the nonradiative decay rate separate from the radiative component. This technique has been applied only to molecules where the interacting states are a continuum of the first kind. In particular the most treated molecule has been benzene [16]. This has been used to map out the nonradiative rate as a function of energy. The same has been done for acetone [17] and formaldehyde [18]. The method has not been applied to any broadening of the second kind.

Having surveyed the experimental results, we will not briefly survey the theoretical models proposed to explain them. In all models we start with a zero-order set of states whose exact description we will ignore for the present. We will restrict our model somewhat more by allowing only one zero-order state (designated the primary state) to carry oscillator strength from the ground state. The continuum levels are called secondary levels. The zero-order states are eigenstates

of the zero-order Hamiltonian H_0. The true Hamiltonian is $H = H_0+V$. V is thus the interaction which causes the transition. More will be said about the nature of H_0 later. This will be called henceforth the canonical model. This model was originally proposed by O. K. Rice (see Ref. [1]) and was reintroduced into the radiationless problem by Robinson and Frosch [19]. The latter's treatment of the transition pictured it as a kind of "radiative transition" in which the photon absorbed had "zero energy". Thus, they employed Fermi's Golden Rule to the calculation of the rate.

Bixon and Jortner [20] assumed that the continuum was a ladder of equally spaced levels and calculated the molecular eigenstates after diagonalizing the Hamiltonian matrix. The mathematics is specialized to their model of the continuum, but the results were shown to be valid for a more general model of the continuum [21]. In both cases the broad band approximation is used. This assumes that the excitation source has an infinite bandwidth which excites the entire broadened band. This means that they have reduced their model back to the Robinson and Frosch model where it was assumed the entire primary state is excited [22]. One important result of this work was the prediction of the absorption band shape to be Lorentzian. Since this work, more sophisticated and powerful mathematical techniques have been applied to the problem with very little further physical insight forthcoming [23].

Two aspects of the problem that have been mostly ignored are

the effect of excitation bandwidth on decays and quantum yields, and the changes introduced by the intermediate level density cases. Rhodes [24] has discussed the first problem in detail formally, but then makes some simplifying approximations which reduce the generality of his results (see also Ref. [22] for a qualitative discussion). The changes due to intermediate level density have been discussed in a highly formal manner by Nitzan, Jortner, and Rentzepis [25]. Other than these papers, little attention has been paid to these two aspects of the problem.

One can go beyond the canonical model to situations where there is more than one state carrying oscillator strength from the ground state. The original treatment of this situation is due to Fano [26]. He was able to predict the line shape of a resonance where the primary and secondary states carried comparable oscillator strength. Freed and Jortner [23] also discussed a similar problem. Recently, Nitzan and Jortner [27] and Nitzan [28] have treated the problem in some detail. They computed the line shape for various cases under some simplifying assumptions. Tric [29] has also discussed a related problem. Again, most of these treatments are highly formal and invoke many simplifying approximations. It also seems that this type of model is not generally needed for describing the radiationless transition problem among the first few excited states. The argument that the continuum carries no oscillator strength because of spin selection rules (triplet continuum, singlet ground state) or because

of vanishingly small Franck-Condon factors seems to be generally valid. Such a model may be significant for higher electronic states such as Rydberg states [30].

The key quantity central to the entire field of radiationless transitions is the weighted density of states. This quantity is in general energy dependent and is formed from the product of the interaction energy matrix element between secondary and primary states and the density of secondary states both evaluated at a particular energy. For the situation in which the secondary state spectrum is continuous (a fact we shall soon show to be generally true), this quantity can be treated as a continuous function of the energy. As we shall show later (see also Ref. [3]), all observable properties of a molecular system can be calculated once knowledge of the weighted density is obtained.

There are several contributing components to the weighted density function. The two principal components are the radiation field and lower energy electronic states of the system. The radiation field states are a true continuum. The inclusion of these states in the problem are necessary to describe photon emission and absorption. Usually, and we also do so here, the assumption is made that the weighted density due to the radiation field is constant within the bandwidth of a line. The molecular weighted density can be divided into two components where applicable. The first is a constant component. The second is the line-like density due to a nearby electronic energy level [25]. This second component is not

present in the large energy gap situation.

The molecular weighted density is the inverse of the radiationless decay rate which is, of course, energy dependent in the general case. The ultimate aim is to extract this quantity from the total weighted density function. For the statistical limit case of benzene, this quantity has been calculated in a fashion [31], [32], and also measured experimentally (Spears and Rice, [11]). It has also been experimentally measured for SO_2 [33] and chloro- and bromoacetylene [34].

The calculational methods can be divided up into two groups. The first [35] considers the transition rate from a thermally averaged excited state. A more general formalism has been achieved by Lin [32] and Heller, et. al. [31]. These calculations allow for both frequency change and displacement of the oscillators. They are able to apportion the energy of the excited states among the various vibrational modes of the lower electronic state. Unfortunately, these calculations are totally within the harmonic approximation. The results of Burland and Robinson [36] seem to indicate that anharmonicities are very important in the values of the Franck-Condon factors and densities of states. Thus, there is still some lingering doubt as to the accuracy of these calculations in an absolute sense, but they do seem to reproduce relative values of radiationless rates quite well. These methods would seem also to be more accurate than the factorization technique of Robinson and Frosch [19], [36].

It should be noted that the above calculations [31]-[32] ignore the electronic interaction part of the whole interaction integral. There is at present a controversy over the exact nature of the coupling term. An equivalent question is, what is a proper choice of zero-order states? Most workers have used Born-Oppenheimer states for zero-order states. Burland and Robinson [37] and Sharf and Silbey [38] have suggested that Herzberg-Teller states are a more appropriate choice. Recently, Siebrand [39] has proposed some criteria for testing which of these choice of basis sets is correct or partially correct. The issue is still open to considerable debate. We will see that the assumption of one or the other basis set is not necessary for deriving the description of the total weighted density function from experiment. To extract the nonradiative rate from the total rate, some calculations must be done and these will involve some choice of basis. All calculations so far attempted have employed a Born-Oppenheimer basis set.

Most mathematical developments use the assumption that at time $t = 0$ the state is prepared in some state $|a\rangle$. We do not ask or need to know what the system looks like at times less than zero. One can worry about how crucial this assumption is to the results of our model. What the worrying amounts to is a consideration of the preparation of the state. For example, if one is using low energy electron impact excitation, the time characteristics of the preparation of the state are very different from using say a mode

locked laser because of the differences of sources. The problem conveniently divides itself up into two (or possibly three) convenient regions, each of which corresponds to a different type of experiment or theoretical treatment. We will now proceed to examine these experiments briefly. In all subsequent discussion we assume photon excitation solely.

If one uses an excitation pulse which is a delta function in time, the approximation of the above discussion is valid. The molecule suddenly at time t = 0(+) is in the excited state. Previous to the pulse it was not in the excited state. No emitted light can be detected before time t = 0. By the uncertainty principle, our excitation source must have an infinite bandwidth. This is the so-called broad band approximation used frequently in the literature [20]. Of course, the delta function time pulse is a mathematical construct. In the laboratory this limit can be reached if the time duration of the pulse is much less (say 0.01-0.001) than the decay time. This means that the excitation bandwidth is wider (roughly 100-1000) than the absorption band. If the absorption band is a simple Lorentzian, not much more can be done experimentally. This is the statistical limit. If, however, the abosrption band is structured, i.e. the molecule lies in the intermediate or small molecule classification, then by not having a finite bandwidth to isolate various regions of the spectrum, some potential information is lost.

The opposite extreme is the situation where the excitation

is continuous and the bandwidth very narrow (a delta function mathematically) [14]. This is more appropriately discussed in terms of scattering theory [41]. Here we cannot really talk about the molecule being prepared in a definite state at a definite time. The quantities we must deal with are probabilities of absorption or of scattering most frequently measured in terms of cross sections. Also, one measures the quantum yield of each channel of the decay via these either computed or experimentally measured cross sections. The advantage of this type of experiment is that excellent spectral resolution is available. Again, with statistical limit molecules, nothing really interesting occurs. However, in an intermediate or small type molecule, one can very completely explore the details of the spectrum. The disadvantage of these experiments is that one has little, if any, time resolution.

The third type of experiment encompasses all the territory in between the two above limiting cases. We permit our excitation source to have a variable bandwidth and corresponding variable time duration. We have the advantage of some spectral as well as some time resolution. Technically, the language of this experiment should be scattering theory, but frequently we can resort to reasoning about the decay of prepared states. Thus, we combine some of the advantages of both above types of treatments and also reject many of the objectionable qualities. We will have some spectral and time resolution. and will be able to measure both time decays and absorption spectra.

This is a more general treatment and encompasses both previous experiments as limiting cases. We will be concerned with this type of description from here on.

In summary, the series of papers that follows will generalize the radiationless transition problem in two different ways. The first is permitting the weighted density of states to assume a general energy dependence. This allows us to encompass all the different classifications (statistical limit, intermediate, and small molecule) under "one roof" so to speak. We do not have to resort to approximations to the density such as a constant continuum or a "ladder" of states. In treating the naphthalene problem (Section IV), we will make no assumptions about the density, but let the spectrum tell us what it should be. The second generalization will be in letting the excitation bandwidth assume a general width. By doing this we avoid the limiting case of the broad band approximation. This should allow a closer comparison with experiments where very narrow excitation is used. Also, the physics of the narrow band situation is different from the broad band approximation because a pure zero order state is not excited. This will be a crucial factor in understanding intermediate or small molecule absorption spectra and emission curves.

REFERENCES

[1] Robinson, G. W., "Molecular Electronic Radiationless Transitions," in Excited States, E. C. Lim, ed. (Academic Press).

[2] Henry, B. R., and Kasha, M., 1968, Ann. Rev. of Phys. Chem., 19, 161.

[3] Hochstrasser, R. M., Jortner, J., and Rice, S. A., 1971, Adv. in Photochem., 7, 149.

[4] Schlag, E. W., Schneider, S., and Fischer, S. F., 1971, Ann. Rev. Phys. Chem., 22, 465.

[5] Freed, K. F., Topics in Current Chem., (in press).

[6] Hochstrasser, R. M., 1968, Acc. Chem. Res., 1, 266.

[7] Byrne, J. P. and Ross, I. G., 1971, Aus. J. Chem., 24, 1107.

[8] (a) McClure, D. S., 1954, J. Chem. Phys., 22, 1668; ibid., 1956, J. Chem. Phys., 24, 1.

(b) Wessel, J. E., 1971, Thesis, U. of Chicago.

[9] (a) Busch, G. E., Rentzepis, P. M., and Jortner, J., 1972, J. Chem. Phys., 56, 361.

(b) Wannier, P., Rentzepis, P. M., and Jortner, J., 1971, Chem. Phys. Lett., 10, 193.

[10] Hochstrasser, R. M., and Wessel, J. E., Chem. Phys. Lett., 1973, 19, 156.

[11] Selinger, B. K., and Ware, W. R., 1970, J. Chem. Phys., 53, 3160; Spears, K. G., and Rice, S. A., 1971, J. Chem. Phys., 55, 5561.

[12] Schlag, E. W., and von Weyssenhoff, H., 1969, J. Chem. Phys., 51, 2508

[13] Laor, U., and Ludwig, P. K., 1971, J. Chem. Phys., 54, 1054.

[14] Douglas, A. E., 1966, J. Chem. Phys., 45, 1007.

[15] von Weyssenhoff, H., and Kraus, F., 1971, J. Chem. Phys., 54, 2387.

[16] Ware, W. R., Selinger, B. K., Parmenter, C. S., and Schuyler, M. W., 1970, Chem. Phys. Lett., 6, 342; see Spears and Rice, Ref. [11].

[17] Halpern, A. M., and Ware, W., 1971, J. Chem. Phys., 54, 1271.

[18] Yeung, E. S., and Moore, C. B., 1973, J. Chem. Phys., 58, 3988.

[19] (a) Robinson, G. W., and Frosch, R. P., 1962, J. Chem. Phys., 37, 1962.

(b) Ibid., 1963, J. Chem. Phys., 38, 1187.

[20] (a) Bixon, M., and Jortner, J., 1968, J. Chem. Phys., 48, 715.

(b) Ibid., 1969, J. Chem. Phys., 50, 4061.

(c) Ibid., 1969, J. Chem. Phys., 50, 3284.

[21] Chock, D. P., Jortner, J., and Rice, S. A., 1968, J. Chem. Phys., 49, 610.

[22] Rhodes, W., Henry, B. R., and Kasha, M., 1969, Proc. Nat'l Acad. Sci., 63, 31.

[23] Freed, K. F., and Jortner, J., 1969, J. Chem. Phys., 50, 2916; Tric, C., 1971, J. Chem. Phys., 55, 4303; Schmidt, P. P., 1970, J. Phys. B, 3, 443; Voltz, R., 1970, Mol. Phys., 19, 881.

[24] Rhodes, W., 1969, J. Chem. Phys., 50, 2885; Ibid., 1971, Chem. Phys. Lett., 11, 179.

[25] Nitzan, A., Jortner, J., and Rentzepis, P. M., 1972, Proc. Roy. Soc. Lond. A, 337, 367.

[26] Fano, U., 1961, Phys. Rev., 124, 1866.

[27] Nitzan, A., and Jortner, J., 1972, Mol. Phys., 24, 109.

[28] Nitzan, A., preprint.

[29] Tric, C., 1973, Chem. Phys. Lett., 21, 83.

[30] Scheps, R., Florida, D., and Rice, S. A., 1972, J. Chem. Phys., 56, 295; 1972, Chem. Phys. Lett., 15, 4.

[31] Heller, D. F., Freed, K. F., and Gelbart, W. M., 1972, J. Chem. Phys., 56, 2309.

[32] Lin, S. H., 1973, J. Chem. Phys., 58, 5760.

[33] Hui, M., and Rice, S. A., 1972, Chem. Phys. Lett., 17, 474.

[34] Evans, K., and Rice, S. A., 1972, Chem. Phys. Lett., 14, 8.

[35] Freed, K. F., and Jortner, J., 1970, J. Chem. Phys., 52, 6272; Fischer, S., 1970, J. Chem. Phys., 53, 3195.

[36] Burland, D. M., and Robinson, G. W., 1969, J. Chem. Phys., 51, 4548.

[37] Burland, D. M., and Robinson, G. W., 1970, Proc. Nat'l Acad. Sci. USA , 66, 257.

[38] Sharf, B., and Silbey, R., 1970, Chem. Phys. Lett., 4, 561.

[39] Orlandi, G., and Siebrand, W., 1973, J. Chem. Phys., 58, 4513.

[40] We assume that source power is low, so saturation effects, etc., can be ignored.

[41] Nitzan, A., and Jortner, J., 1973, J. Chem. Phys., 57, 2870.

MATHEMATICAL THEORY OF THE GREEN'S FUNCTION

As was shown in the previous section, our problem is to calculate the solution to the Schoedinger equation written in the form

$$H\psi = (H_0+V)\psi = E\psi \tag{1}$$

The situation of interest in the case where the eigenvalue spectrum we obtain from Eq. (1) is continuous. We can rewrite Eq. (1) as an inhomogeneous equation

$$(H_0-E)\psi = V\psi \tag{2}$$

where the solutions to the homogeneous part of Eq. (2),

$$(H_0-E)\psi_0 = 0 \tag{3}$$

are presumed known. By standard differential equation theory, Eq. (3) has a Green's function which satisfies

$$(H_0-E)\cdot G^+(\underset{\sim}{r},\underset{\sim}{r}';E) = -\delta(\underset{\sim}{r}-\underset{\sim}{r}') \tag{4}$$

The solution to the inhomogeneous equation (2) is then given by

$$\psi(\underset{\sim}{r},\xi) = \psi_0(\underset{\sim}{r},\xi) + \int G^+(\underset{\sim}{r},\underset{\sim}{r}';\varepsilon)\cdot V(\underset{\sim}{r}')\cdot\psi(\underset{\sim}{r}')d^3r' \tag{5}$$

This will give the true wavefunction of the system (if it can be solved).

The wavefunction in Eq. (5) contains all the information we need know about the system. However, in order to get meaningful results to compare with experiment, we do not need the wavefunction itself. All we essentially need is the eigenvalue spectrum together with formal manipulations. Thus, we circumvent the usually impossible job of solving Eq. (5). In particular the two quantities of interest which we wish to have are the absorption spectrum and the time evolution of the system. These are the observable quantities. This can be done without any detailed knowledge of the exact eigenstates of the system. The approach to be taken here is actually a type of perturbation theory where we use a series expansion to calculate the Green's function. From this Green's function, which is essentially a presentation of the eigenvalues of the system, we can get directly the quantities of interest. The approach used here is also called by some authors the resolvent method [1].

A brief summary of the Green's function theory to be used in Section II will be presented now. This summary will try to collect in one section most of the pertinent mathematical arguments and result. In later sections the results of the particular situation in question and the physical interpretation will be presented in greater detail.

The diagram expansion was an important development in the theory of Green's function [2]. Although to the uninitiated this

appears to be a formal mathematical device, it is in reality a powerful device because of its simplicity. Its use is not as significant here as in the many body problem [2]. A second important result is the Dyson's equation,

$$G = G_0+G_0VG \tag{6}$$

where G and G_0 are the Green's functions of the true and zero order Hamiltonians respectively, and V is the remaining part of the Hamiltonian as in Eqs. (1) and (2). It is this equation which gives the solution ultimately for the Green's function. Applications of these ideas can be found in many sources [3].

We deal with a matrix representation of the Green's function which is first computed in energy space. This will give the answer to the first part of the problem, the calculation of an absorption spectrum. If we express our true Green's function operator in the representation of the exact eigenstates (i.e., the eigenstates of $H = H_0+V$)

$$G(\varepsilon') = \int \frac{|\lambda)\rho(\lambda)<\lambda|}{\varepsilon'-\lambda}\, d\lambda \tag{7}$$

where ε' is a complex energy, λ a real energy eigenvalue of the molecular eigenstate $|\lambda>$ and $\rho(\lambda)$ is the number of eigenstates between λ and $\lambda+d\lambda$. Now set $\varepsilon'=\varepsilon+i\eta$, where ε and η are real and $\eta>0$. After letting $\eta\to 0$, we get the result,

$$G(\varepsilon) = \mathcal{P} \int \frac{|\lambda\rangle\rho(\lambda)\langle\lambda|}{\varepsilon-\lambda} - i\pi\delta(\varepsilon-\lambda)|\lambda\rangle\rho(\lambda)\langle\lambda|$$

The term $\frac{-1}{\pi}$ ImG(ε) is easily seen to be the density operator [4] for the system. This relationship of density of states with the Green's function is sometimes called the Lehman spectral representation of the Green's function [5]. In the representation of our zero order states, the density of the primary state is $D_p(\varepsilon)$,

$$D_p(\varepsilon) = -\frac{Im}{\pi}\langle p|G(\varepsilon|p\rangle \qquad (9)$$

This will be proportional to the absorption spectrum in our simple case. For situations where there is more than one primary level, the absorption spectrum is a more complicated expression involving several matrix elements of the Green's function.

One aspect of Green's function theory that has received considerable attention in the literature is the analytical properties of G and its related function R, the level shift operator. G and R are really functions of a complex energy variable and thus must obey the rules of complex function theory. As will be seen, when the zero order energy spectrum is discrete, the Green's function has a set of discrete poles. However, when the zero order eigenvalue problem is continuous, the situation is much more subtle. It is here that we must deal with the Green's function as a complex variable function whose properties in energy space will determine its behavior in time space.

As was noted earlier, the Green's function "operator" can be written in terms of the exact eigenstates of the system, or it is said that the Green's function is written in the molecular eigenstate representation. This matrix representation of the Green's function must be diagonal, and all the poles lie on the real axis. This must be so since the exact molecular eigenstates are stationary states of the system and have real energy eigenvalues. All of this is conveniently expressed by Eq. (7) where λ is a real energy. If we are concerned with a state which is not a stationary state but is a linear combination of stationary states, the diagonal matrix element in this new representation, i.e., that of our complete set of nonstationary states (the zero-order set) will be seen not to have poles on the real axis any longer. The poles are now complex reflecting the finite lifetime (nonstationarity) of these states.

Before proceeding, a slight diversion will be made to relate some of the above considerations to the actual experiment with which we are concerned here. This experiment involves the excitation of a molecule by a light source with the observation of the subsequent decay of resonance fluorescence. By the word decay it is clear that we must be dealing with a nonstationary state. Also note that any real molecule must have a continuous spectrum because of the radiation field. Thus, it is clearly impossible in any real experiment to deal with excited stationary states. The only representation of the Green's function which we will deal with is that of the zero-

order states. It will even turn out that the experimentalist has a certain amount of control over what state the experiment actually involves.

The important point to be noted here is that in our zero-order representation, the position of the poles of the Green's function, and thereby its analytical properties, will change from the molecular eigenstate representation. This is due to the fact that the state with which we deal in zero-order is a superposition of molecular eigenstates. Thus, we expect that the analytical properties of the diagonal matrix element involving this state would be different from any diagonal matrix element in the molecular eigenstate representation.

It can be shown in general [6] that a diagonal element of the Green's function matrix in some representation for the simple case we are dealing with can be written as

$$\langle a|G|a\rangle = G_a = \langle a|\frac{1}{\varepsilon'-H_0-R(\varepsilon)}|a\rangle = \frac{1}{\varepsilon'-\varepsilon_a-R_a(\varepsilon)} \tag{10}$$

where $\langle a|$ satisfies

$$H_0|a\rangle = \varepsilon_a|a\rangle \tag{11}$$

and

$$H_0 + V = H \tag{12}$$

H is the exact Hamiltonian for the system.

$R(\varepsilon)$ is the so-called level shift operator which is given by the equation

$$R(\varepsilon) = V + \int \rho_a(\lambda)d\lambda \frac{V(1-|a><a|)\lambda><\lambda|(1-|a><a|)V}{\varepsilon'-\varepsilon_\lambda} \tag{13}$$

with $|\lambda>$ being the eigenstates of the Hamiltonian

$$H_a|\lambda> = [H_0+(1-|a><a|)V(1-|a><a|)]\ |\lambda> = \varepsilon_\lambda|\lambda> \tag{14}$$

Since $1-|a><a| = \int|\ \gamma>\rho(\gamma)<\gamma|d\gamma$ where the $|\gamma>$'s are all the other states in our complete set, the Hamiltonian in our case reduces to

$$H_a = H_0 \tag{15}$$

since we define $<\gamma|V|\gamma> = 0$ (see Section I A). Also, since we take $<a|V|a> = 0$, for the equation for $R(\varepsilon)$ becomes

$$R(\varepsilon) = \int\rho(\gamma)d\gamma \frac{V|\gamma><\gamma|V}{\varepsilon'-\varepsilon} \tag{16}$$

Note that again ε_γ is real and ε' is complex. We can again explicitly show ε to be complex by writing

$$\varepsilon' \rightarrow \varepsilon \pm i\eta \tag{17}$$

where ε and η are real and $\eta>0$ as before. We must pick the plus sign in Eq. (17) to insure getting a causal or retarded Green's function [7].

Thus,

$$\lim_{\eta\to 0(+)} \langle a|R|a\rangle = \lim_{\eta\to 0(+)} R_a(\varepsilon+\eta) = \lim_{\eta\to 0(+)} \int \rho(\gamma)d\gamma \frac{|\langle a|V|\gamma\rangle|^2}{\varepsilon-\varepsilon\gamma+i\eta}$$

$$= \int \rho(\gamma)d\gamma \frac{|\langle a|V|\gamma\rangle|^2}{\varepsilon-\varepsilon_\gamma} - i\pi\rho(\varepsilon)|\langle a|V|\varepsilon\rangle|^2 \tag{18}$$

where use was made of a standard identity [8]

$$\lim_{\eta\to 0(+)} \int \frac{f(x)}{x\pm i\eta-x_0}\,dx = \mathcal{P}\int \frac{f(x)}{x-x_0}\,dx \mp i\pi f(x_0) \tag{19}$$

and $\mathcal{P}$ represents the Cauchy principle value integral.

We see that $R_a(\varepsilon')$ has both a real and an imaginary part,

$$\lim_{\eta\to 0(+)} R_a(\varepsilon+i\eta) = D(\varepsilon) - I(\varepsilon) \tag{20}$$

$I(\varepsilon)$ is always positive which we have indicated in Eq. (21) by the negative sign. Also, it is clear from Eq. (19) that

$$\lim_{\eta\to 0(+)} R_a(\varepsilon-i\eta) = D(\varepsilon) + I(\varepsilon) \tag{21}$$

which shows that $R_a(\varepsilon\pm i\eta)$ has a branch cut (discontinuity) along the the real axis. Dispersion relations can be then derived connecting $D(\varepsilon)$ and $I(\varepsilon)$, but we will not be concerned with these. Note that in

the discrete state limit, $R(\varepsilon)$ has only poles and no branch cut. This will prove to be a significant difference between the two cases.

Returning to the Green's function itself, we see that it can be written

$$\langle a|G|a\rangle = G_a(\varepsilon) = \frac{1}{\varepsilon-\varepsilon_a-R_a(\varepsilon)} = \frac{1}{\varepsilon-\varepsilon_a-D(\varepsilon)+iI(\varepsilon)} \tag{22}$$

The question is, where are the poles (if any) and the branch cut(s) (if any)? If for some reason, $D(\varepsilon)$ and $I(\varepsilon)$ are constants, or equivalently when $D(\varepsilon_a) \ll |\varepsilon_a|$ and $|I(\varepsilon_a)| \ll |\varepsilon_a|$, the pole of the Green's function is clearly located at

$$\varepsilon = \varepsilon_0 = \varepsilon_a + D(\varepsilon_a) - iI(\varepsilon_a) \tag{23}$$

which is a complex pole seemingly in the negative half plane. However, since $R_a(\varepsilon)$ has a branch cut along the real axis, we must be very careful. Expressing G_a specifically as a function of complex energy,

$$\lim_{\eta\to 0(+)} G_a(\varepsilon+i\eta) = G_a^+(\varepsilon) = \frac{1}{\varepsilon-\varepsilon_a-D(\varepsilon)+i(I(\varepsilon)} \tag{24a}$$

$$\lim_{\eta\to 0(+)} G_a(\varepsilon-i\eta) = G_a^-(\varepsilon) = \frac{1}{\varepsilon-\varepsilon_a-D(\varepsilon)-i(I(\varepsilon)} \tag{24b}$$

and

$$\lim_{\eta\to 0(+)} [G_a(\varepsilon-i\eta) - G_a(\varepsilon+i\eta)] = i\frac{2I(\varepsilon)}{(\varepsilon-\varepsilon_a-D(\varepsilon))^2+(I(\varepsilon))^2} \qquad (24c)$$

showing that $G_a(\varepsilon)$ also has a branch cut along the real axis. To get to the pole in Eq. (23) we must analytically continue R_a(and thus also G_a) into the second Riemann sheet which is reached when crossing the branch cut. This is done by defining

$$R_a^{II}(\varepsilon-i\eta) = R_a^{I}(\varepsilon+i\eta) = D(\varepsilon)-iI(\varepsilon) \qquad (25)$$

with $R_a^{II,I}$ being the value of R_a in the second and first Riemann sheets respectively. Then it is seen that the pole lies in the second Riemann sheet.

From this simple case one can give a very simple physical interpretation to the real and imaginary parts of $R_a(\varepsilon)$. The real part is seen to be the energy shift. This shift is related to (See Eq. (26)) the perturbative shifting of discrete zero order energy levels which are allowed to interact. The complex part is only non-zero for the continuous spectrum case. It represents the half-width of the band which now characterizes our once discrete state. Note that the term half-width (and the related lifetime) only has true meaning in this simple case where it is a constant. When it is strongly energy dependent, then the above interpretation is not valid.

One now has to worry about what happens when the conditions leading to our simple pole no longer exist. To get some understanding of this, let us return to the case where our zero-order energy spectrum is discrete. Then the poles are located by solving the equation (See Section II)

$$\varepsilon-\varepsilon_1-\sum_{i=2}^{n}\frac{|V1i|^2}{\varepsilon-E_i}=0 \tag{26a}$$

or

$$\prod_{i=1}^{n}(\varepsilon-E_i)-\sum_{i-2}^{n}|V_{1i}|^2\left[\frac{\prod_{i=}^{n}(\varepsilon-E_j)}{\varepsilon-E_j}\right]=0 \tag{26b}$$

The E_i's are the zero-order energy eigenvalues, ε is real, and $V_{1i} = \langle 1|V|i\rangle$. This is easily seen to be an nth order polynomial equation in ε which thus has n roots (eigenvalues). Thus, the Green's function has n poles. If we let $n\to\infty$ and $(E_j-E_{j-1})\to 0$, we get to our continuum case. Here we have an infinite set of poles all of which must be in the second Riemann sheet because of the properties of $R_a(\varepsilon)$ in this limit.

The second observable we desire is the emission decay curve. To get this quantity we must be concerned with the time evolution of our eigenstates. The calculation of the time evolution of the system will give us directly the emission decay curve. The important result here is the following [9]:

$$U(t,t') = \frac{1}{2\pi i}\int_C \frac{1}{\lambda - H} e^{-ih^{-1}H(t-t')}d\lambda = \int_C G_{op}(E)e^{-ih^{-1}\lambda(t-t')}dE$$

where $U(t,t')$ is the time evolution operator, $G_{op}(E)$ is the Green's function operator, the contour of integration is a Cauchy contour (counterclockwise, closed path encircling all the poles of G) and λ is a complex energy. When $t-t'>0$, we can push the contour in the lower half plane to infinity and the integration along this path goes to zero because the integrand approaches zero. The only path that contributes is that above the real axis in the first Riemann sheet. We can then lower this contour to the real axis because there are no poles in the first sheet, and we obtain [10]

$$U(t,t') = \frac{1}{2\pi i}\int_{-\infty}^{\infty} G_{op}(E)\, e^{-ih^{-1}\lambda(t-t')}dE \qquad (28)$$

which is the Fourier transform of the entire Green's function . E is now a real energy variable.

In applying this time evolution operator to the initial wavefunction, we must ask exactly what the quantity is we wish to follow. Since our experiment involves the detection of photons, the quantity to calculate is the time dependent transition probability,

$$T(t) = \Sigma|\langle 0|\underset{\sim}{e}\cdot\underset{\sim}{r}|\Psi(t)\rangle|^2$$

$$= \Sigma|\langle 0|\underset{\sim}{e}\cdot\underset{\sim}{r}|U(t,0)\cdot\Psi(0)\rangle|^2 \qquad (29)$$

where $\langle 0|$ is the ground state, $\underset{\sim}{e}\cdot\underset{\sim}{r}_{\lambda}$ the dipole moment with polarization λ, and $\Psi(0)$ is the state that we prepare at time zero. Note that we are here tacitly assuming that the excitation pulse is a delta function in time (See Part 4). We can expand $T(t)$ in our zero order representation, and assume that $|\Psi(0)\rangle = |a\rangle$. In Section III we will show that this last assumption can be relaxed if certain modifications are made to the Green's function. Continuing, we get

$$
\begin{aligned}
T(t) &= \sum_{\lambda}\{|\langle 0|\underset{\sim}{e}\cdot\underset{\sim}{r}|a\rangle\langle a|U(t,0)|a\rangle|^2\} \\
&= |\langle 0|\underset{\sim}{e}\cdot\underset{\sim}{r}_{\lambda}|a\rangle|^2|\langle a|U(t,0)|a\rangle|^2 \qquad (30) \\
&= |\langle 0|\mu|a\rangle|^2 \left|\frac{1}{2\pi i}\int_{-\infty}^{\infty}\langle a|G|a\rangle e^{-ih^{-1}Et}dE\right|^2
\end{aligned}
$$

where in the last step we used Eq. (29) and also we assumed only one component of the dipole transition moment is non-zero. If we have more than one optically allowed state, this transition moment would be somewhat more complicated.

In some very simple cases we can get an approximation to the emission decay probability, Eq. (30). Using the discussion of the analytical properties of $G_a(\epsilon \pm i\eta)$, in particular Eq. (23) and the assumptions behind it, we see that $T(t)$ is simply evaluated by the Cauchy integral formula. $\langle a|G|a\rangle$ has a simple pole on the second Riemann sheet which is within closed contour of Eq. (27). Thus,

using Eqs. (28) and (23) and the theorem of residues from complex variable theory,

$$\frac{1}{2\pi i}\int_{-\infty}^{\infty} \langle a|G|a\rangle\, e^{-iEt} dE - e^{-i(\varepsilon a + D(\varepsilon a) - iI(\varepsilon a))t} \tag{31}$$

$$= e^{-i(\varepsilon a + D(\varepsilon a))t} \cdot e^{-I(ta)t}$$

Upon taking the magnitude squared,

$$T(t) = |\langle 0|\mu|a\rangle|^2 \frac{1}{4\pi^2} e^{-2\cdot I(\varepsilon a)t} \tag{32}$$

which is the standard exponential decay. Note that this is only an approximation to the true decay because of the assumptions involved in Eq. (23). However, as discussed in Goldberger and Watson [11] and by Galitskii and Migdal [5], the approximations are generally good ones and deviations only occur at long times. This confirms the opinion one has from experimental results for many molecules and experiments.

REFERENCES

[1] Ziman, J. M., 1969, Elements of Advanced Quantum Theory (Cambridge U. Press).

[2] Mattuck, R. D., 1968, A Guide to Feynman Diagrams in the Many-Body Problem (McGraw-Hill).

[3] (a) Pines, D., 1961, The Many-Body Problem (Benjamin).

(b) Parry, W. E., et.al., 1969, Many-Body Problems (Benjamin).

[4] See Ref. [1], p.

[5] Galitskii, V., and Migdal, A., 1958, Soviet Physics JETP, 7, 96.

[6] Goldberger, M. L., and Watson, K. M., 1964, Collision Theory (Wiley & Sons), p. 440.

[7] See Ref. [1], p. 81.

[8] Heitler, W., 1954, The Quantum Theory of Radiation (Oxford U. Press), pp. 69 ff.

[9] Zumino, B., 1961, In Lectures on Field Theory and the Many-Body Problem, E. R. Caianello, ed., (Academic Press), p. 37.

[10] See Ref. [6], p. 434.

[11] See Ref. [6], pp. 446-450.

[12] See Ref. [6], Chapter 8.

PART 2

RADIATIONLESS TRANSITIONS: THEIR EFFECT ON ABSORPTION LINE SHAPES AND EMISSION DECAY CURVES

I. INTRODUCTION

The subject of radiationless transitions in large polyatomic molecules has been extensively discussed in the literature for the last ten years beginning with the papers by Robinson and Frosch [1]. A review of theoretical work up to 1968 can be found in the article by Henry and Kasha [2]. Within the past four years there has been a large number of theoretical papers published in this area. The article by Jortner, et al. [3], provides an extensive review of much of this work plus some good experimental background in the field. Two other review articles more recent than those above and with slightly different emphasis have come to the author's attention [4].

One basic starting model used in radiationless transition theory has not changed since the Robinson and Frosch treatment. The zero order states consist of a single, discrete quantum state (primary level), carrying all the oscillator strength, which interacts with a quasi-continuum of quantum states (secondary levels). Using this basic model many workers have computed the radiationless transition rate by a variety of techniques and approximations [5]. A second derivable property is the spectral line shape due to the interaction of discrete and continuum states. This latter property, mentioned only briefly in earlier work [6], is the subject of this paper.

Fano [7] first discussed in detail the line shape of a state interacting with a continuum of states in connection with the autoionization of helium. His line shapes were based on a model where both the discrete state and the continuum have comparable oscillator strength. Thus [8] his model does not coincide exactly with ours.

Bixon and Jortner, using Fano's formalism, compute the line shape to be a symmetric Lorentzian. Their model assumes a uniform density of states and an energy independent interaction. Their line shape is thus an idealized one. Sharf [9] discusses line shapes in somewhat more detail than Bixon and Jortner but still employs the same basic model and assumptions. The paper by Byrne and Ross [10] provides an extensive discussion of many mechanisms of line broadening. They provide many examples of spectra which are broadened both by electronic relaxation mechanisms and by other mechanisms. Like Byrne and Ross, Hochstrasser, et al., [10, 11] discuss the broadening of spectra from the experimentalist's viewpoint. Hochstrasser's discussion [11d] is particularly relevant to the topic of this paper, although his discussion is more qualitative than ours.

In this paper we present a general formalism that allows the calculation of the spectral line shape of a single resonance and its fluorescence decay curve. We place no restriction on the coupled states (i.e., they may vary anywhere from a true continuum to a set of discrete coupled levels) or on the energy dependence of the interaction matrix element. In order to get a visual idea of what real line shapes might look like, we pick some representative examples and plot the line shape and decay curve. These model examples hopefully provide some idea of what may be observed in real spectra. Discussion of the properties of these line shapes is presented. We restrict ourselves in this paper to the particular case of one single discrete state carrying all the oscillator strength interacting with a secondary set of states. Broad band excitation is assumed. The situation of more than one discrete

level, or where the secondary states also carry oscillator strength, or where the excitation bandwidth is finite and narrow with respect to the broadened line will be dealt with in a subsequent paper. For a discussion of the latter aspect of the radiationless transition problem, see the article by Kasha, et al. [12], and the one by Rhodes [13].

II. THEORY

The method of the Green's Function has been applied to the problem of radiationless transitions by several authors. These results are identical to earlier ones concerned with the decay of metastable particles [14]. We briefly present our derivation for completeness. Our formalism has its origins in the theory of mixed crystal spectra [15, 16]. In this theory, impurities are viewed as perturbations on the delocalized electronic wavefunction of the pure crystal. The problem with which we wish to deal is formally equivalent to the mixed crystal problem in which there is only a single impurity atom present in the otherwise pure crystal. In this treatment, assumptions as to the functional energy dependence of either the density of secondary states or of the interaction matrix elements between primary and secondary states may be deferred until the end of the calculation.

We define a zero order Hamiltonian matrix $\underset{\sim}{H}_0$ consisting of the true molecular Hamiltonian matrix $\underset{\sim}{H}$ minus the interaction matrix $\underset{\sim}{V}$, which connects the primary level with the secondary levels. The secondary levels at first are assumed to be a set of discrete states. This is done for mathematical convenience, and the limit to a density of states function is taken after some initial manipulations. We define

the Green's function as follows:

$$\underset{\sim}{G} = \frac{1}{\underset{\sim}{\varepsilon} - \underset{\sim}{H}_0 - \underset{\sim}{V}} = \frac{1}{\underset{\sim}{G}_0^{-1} - \underset{\sim}{V}} \tag{1}$$

where $\underset{\sim}{\varepsilon}$ is the matrix of complex energy eigenvalues measured with respect to an appropriate zero of energy, $\underset{\sim}{V}$ is the matrix of interaction integrals between states, and $\underset{\sim}{G}_0 = [\underset{\sim}{\varepsilon} - \underset{\sim}{H}_0\ ]^{-1}$. $\underset{\sim}{G}$ could also be expressed in a diagram expansion [16]

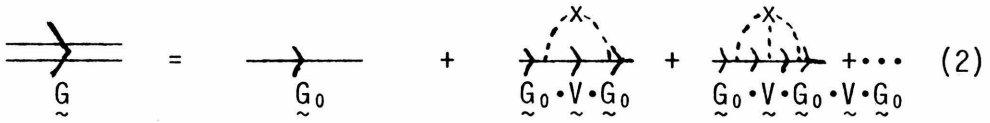

(2)

where dotted lines represent an interaction $\underset{\sim}{V}$, and arrows represent $\underset{\sim}{G}_0$ in a manner indicated by the first term on the RHS. The diagram expansion is not so useful in this very simple case. In some cases (see Ref. [14]), the construction of the diagram expansion and rearrangement of the diagrams allows one to obtain the approximate Green's function using the technique of partial summation.

From (1) then, the true Green's function is found by calculating the inverse of the matrix,

$$G_0^{-1} - V = \begin{pmatrix} \varepsilon - E_1 & \cdots & -V_{1i} & \cdots \\ \vdots & & & \\ -V_{i1} & & \varepsilon - E_i & \\ \vdots & & & \end{pmatrix} \tag{3}$$

where the states have been arranged so that E_1 is the zero order energy of the primary state. The first row and column contain the interaction

matrix elements, and E_i is the zero order energy of the ith continuum state. We assume that the continuum states are prediagonalized. The ordering of the diagonal elements is done solely for convenience. The inverse is calculated in a standard fashion as indicated in Appendix I. The density of states resulting from the perturbation was calculated from the relationship [16],

$$\text{Density of states} = \frac{-1}{\pi} \text{ Im tr } \underset{\sim}{G}. \tag{4}$$

The calculation of the trace is repeated in Appendix I. The result is

$$\text{tr } \underset{\sim}{G} = [\varepsilon - E_1 - \sum_{k \neq 1} \frac{|V_{1k}|^2}{\varepsilon - E_k}]^{-1} \cdot \{1 + \sum_{i \neq 1} \frac{1}{\varepsilon - E_i} (\varepsilon - E_1 - \sum_{k \neq i,1} \frac{|V_{1k}|^2}{\varepsilon - E_k})\} \tag{5}$$

Since the line shape is dependent only on the primary state, which is the sole carrier of oscillator strength, we need only be concerned with that diagonal element in the Green's function matrix dealing with this state. This matrix element is

$$G_{11} = \frac{1}{\varepsilon - E_1 - \sum_{k \neq 1} \frac{|V_{1k}|^2}{\varepsilon - E_k}} .$$

We now make the transition to the density of states function by transforming the sums over discrete secondary states to integrals over an energy dependent density of states function $D_0(\varepsilon)$. The transformation is in this case not really an approximation. Since all real eigenstates have a certain amount of breath, they cannot truly be described by delta

functions in energy space. Thus, any sum over energy levels is in fact more correctly described as an integration over a density function. The density function at a point in energy space is the sum of the amplitudes of all energy levels at that point. The density may be quite smooth, or rapidly varying, even line-like, depending on the situation. (cf. Nitzan and Jortner, Ref. [17] sec III).

Thus, the denominator of tr G becomes

$$\varepsilon-E_1-\int \frac{D_0(E')|V(E')|^2}{\varepsilon - E'}dE'=\varepsilon-E_1-\mathcal{P}\int\frac{D_0(E')|V(E')|^2}{\varepsilon - E'}dE'-i\pi D_0(\varepsilon)|V(\varepsilon)|^2$$

$$=\varepsilon-E_1-\mathcal{P}(\varepsilon)-i\pi D_0(\varepsilon)|V(\varepsilon)|^2 \qquad (7)$$

where the integration is over the energy spectrum of the continuum states. After lowering the contour of integration to the real axis, use was made of the standard identity [18],

$$\lim_{\Delta\to 0}\int \frac{f(x)}{\lambda-x+i\Delta}dx=\mathcal{P}\int\frac{f(x)}{\lambda-x}dx - i\pi f(\lambda).$$

The principle value integral corresponds to a level shift operator for the E_1 level. The adjusted energy is denoted $\bar{E}_1$. For constant $D_0(\varepsilon)$ and $|V(\varepsilon)|^2$, the level shift is seen to be zero.

The final density function for the primary state is

$$-\frac{1}{\pi}\mathrm{Im}\,[G]_{11}=\frac{|V(\varepsilon)|^2D_0(\varepsilon)}{(\varepsilon-\bar{E}_1)^2+[\pi|V(\varepsilon)|^2D_0(\varepsilon)]^2}\,. \qquad (8)$$

This function describes how the originally discrete primary state is broadened, due to the interaction with the secondary states.

A. Addition of Radiation Field

The above case considers the coupling of the discrete state to one continuum, supposed to be the upper vibrational levels of a lower electronic state [1]. In actuality, this is a very artificial model, as the discrete state is coupled to a lot of things. If it is assumed that the molecule is isolated in the gas phase or in a low temperature matrix, the principle other coupling is to the radiation field. We approximate this, or some other set of interacting states, by a second continuum orthogonal and uncoupled, at least directly, to the first continuum.

The matrix $\underset{\sim}{G}^{-1}$ is calculated as before and is given by

$$\underset{\sim}{G}^{-1} = \begin{pmatrix} \varepsilon-E_1 \cdots V_{1i} \cdots -W_{1k} \cdots \\ \vdots \quad \ddots \\ -V_{i1} \quad \varepsilon-E_i \quad \ddots \\ \vdots \quad \ddots \\ -W_{k1} \quad \ddots \quad \varepsilon-E_k \end{pmatrix} \tag{9}$$

where the V's are the interaction matrix elements with the vibrational continuum, and the W's are the interaction matrix elements with the radiation field. All other matrix elements are zero. The determinant and co-factors were calculated as before. Denoting the vibrational continuum density of states function as $D_0(\varepsilon)$, and similarly $\rho_0(\varepsilon)$ for the radiation field continuum, the final density function for the primary state (see Appendix II) is

$$-\frac{1}{\pi}\,\mathrm{Im}\,[G]_{11} = \frac{D_0(\varepsilon)|V(\varepsilon)|^2+\rho_0(\varepsilon)|W(\varepsilon)|^2}{(\varepsilon-\bar{E}_1)_2+[\pi(D_0(\varepsilon)|V(\varepsilon)|^2+\rho_0(\varepsilon)|W(\varepsilon)|^2)]^2} \tag{10}$$

where now

$$\bar{E}_1=E_1+\mathcal{P}\int \frac{D_0(E')|V(E')|^2}{\varepsilon - E'}dE' +\mathcal{P}\int\frac{\rho_0(E')|W(E')|^2}{\varepsilon - E'}dE'. \tag{11}$$

This expression is merely a generalization of Eq. (8), and results directly from the assumption of non-coupling between continua.

B. Computation of the Line Shape and Decay Function

The approach to calculation of the general line shape using the Green's Function is through the formula derived by Harris [19],

$$\bar{A}'(\varepsilon) = \frac{1}{3}\frac{4\pi\,\varepsilon}{c}\sum_{k=1}^{3} 2\,\mathrm{Im}\langle 0|\mu_k G\,\mu_k|0\rangle \tag{13}$$

where $\bar{A}'$ is the absorption coefficient and is computed as a function of wavenumber ε. The summation is over the three cartesian components of the dipole operator $\underset{\sim}{\mu}$. Our absorption coefficient can be written, assuming only one vector component of $\vec{\mu}$ is active, and that only the discrete state $|1\rangle$ has oscillator strength,

$$\bar{A}' = \frac{8\pi\varepsilon}{3c}\,|\langle 0|\mu|1\rangle|^2\,\mathrm{Im}\langle 1|G|1\rangle$$

$$= \frac{8\pi}{3c}\,\varepsilon\cdot\mu_{01}^2\cdot\frac{\pi|V(\varepsilon)|^2D_0(\varepsilon)}{(\varepsilon-\bar{E}_1)^2+[\pi|V(\varepsilon)|^2D_0(\varepsilon)]^2}. \tag{13}$$

which involves only the G_{11} element of the Green's function. Normally the assumption made is that the product $|V(\varepsilon)|^2 D_0(\varepsilon)$ is a constant. This assumption was made chiefly to give mathematical simplicity to the resulting formulas [5]. However, calculations of $D_0(\varepsilon)$ and the Franck-Condon overlap factor part of $|V(\varepsilon)|^2$ [20] show that both vary approximately exponentially over energy ranges of about a bandwidth. For small molecules, on the other hand, the density function should be almost discrete. The energy dependence of the density-interaction product is also verified in several experimental studies [21-24]. In order to preserve complete generality, we now write

$$|V(\varepsilon)|^2 D_0(\varepsilon) = |V(\bar{E}_1)|^2 D_0(\bar{E}_1) f'(\varepsilon) \tag{14}$$

where $f'(\varepsilon)$ is an as yet unspecified modifying function with $f'(\bar{E}_1) = 1$. This notation will allow for the computation of the line shape in reduced units. $\bar{A}'$ becomes

$$\bar{A}' = \frac{8\pi}{3c} \mu_{01}^2 \frac{1}{(\pi V^2 D_0)} \cdot \varepsilon \cdot \frac{f'(\varepsilon)}{\left[(\varepsilon - \bar{E}_1)^2/(\pi V^2 D_0)^2\right] + [f'(\varepsilon)]^2}$$

where $V^2 D_0 \equiv |V(\bar{E}_1)|^2 D_0(\bar{E}_1)$. We define a reduced energy ξ as,

$$\xi = \frac{\varepsilon - \bar{E}_1}{\pi V^2 D_0} \tag{16}$$

ξ is then energy measured in units of the linewidth, where $\pi V^2 D_0$ is the true line width if $f(\varepsilon) = 1$ for all ε. Finally,

$$\frac{\varepsilon}{\pi V^2 D_0} = \xi + \frac{\overline{E}_1}{\pi V^2 D_0} \simeq \frac{\overline{E}_1}{\pi V^2 D_0} = \text{constant} \tag{17}$$

since $\overline{E}_1 >> \pi V^2 D_0$.

Thus the final expression is

$$\overline{A} = \overline{A}' \cdot \frac{3c}{8\pi \mu_{01}^2} \frac{\pi V^2 D_0}{\overline{E}_1} = \frac{f(\xi)}{\xi^2 + f^2(\xi)} \tag{18}$$

where

$$f(\xi) = f'(\varepsilon). \tag{19}$$

This then gives the line shape upon the assumption of a reasonable $f(\xi)$. The $\overline{A}$ is a reduced absorption coefficient which applies to the shape of any line.

A similar derivation for the case of two coupled but independent continua is also possible and will be used later in the examples. The result comes from Eqs. (10) and (18) and assumes that $\rho_0(\varepsilon)|\, W(\varepsilon)|^2 = W^2\rho_0$ is constant. Then Eq. (16) becomes

$$\overline{A} = \overline{A}' \cdot \frac{3c}{8\pi \mu_{01}^2} \frac{\pi W^2 \rho_0}{\overline{E}_1} = \frac{\dfrac{\pi D_0(\varepsilon)|V(\varepsilon)|^2}{\pi W^2 \rho_0} + 1}{\left(\dfrac{\varepsilon - \overline{E}_1}{\pi W^2 \rho_0}\right)^2 + \left(\dfrac{\pi D_0(\varepsilon)|\, V(\varepsilon)|^2}{\pi W^2 \rho_0} + 1\right)^2} . \tag{20}$$

We also make the assumption that the discrete secondary states are approximated by Gaussian functions (for simplicity only) of a particular

width (ω_i) and position (ξ_i). Thus,

$$\frac{\pi D_0(\varepsilon)|V(\varepsilon)|^2}{\pi\rho_0 W^2} \equiv \delta \sum_i \exp -\left(\frac{\xi - \xi_i}{\omega_i}\right) \qquad (21)$$

where

$$\delta = \frac{\pi V^2 D_0}{\pi W^2 \rho_0}$$

is then the ratio of the line broadening of the primary state due to the interaction with the discrete secondary levels as compared to the broadening due to interaction with the radiation field continuum. The assumption made is that the sum of Gaussians describes the energy dependent product of the density function and the interaction matrix element. For simplicity δ is assumed to be a constant for all coupled levels. The energy is again in reduced units

$$\delta = \frac{\varepsilon - \bar{E}_1}{\pi\rho_0 W^2} \qquad (22)$$

similar to Eq. (16).

C. Time Evolution of the Perturbed State

The approach to the time evolution problem through the Fourier transform of the Green's function was developed by Goldberger and Watson [14a] and Zumino [14b]. The utility of the Green's function is seen here. Not only does it provide a simple and high order way of

doing perturbation theory (sometimes the only way), but it also governs the time evolution of the system. The time evolution of the primary state is given by the probability

$$|(\phi_1,\psi\ (t))|^2 = |\frac{1}{2\pi i}\int_{-\infty}^{+\infty} d\omega e^{-i\omega t} \langle 1|G|1\rangle\ |^2 \qquad (23)$$

where $\psi(t)$ is the complete time dependent wavefunction for the system and $\psi(0) = \phi_1$ corresponding to the preparation of the state by photon absorption into the zero order state ϕ_1. The time evolution of the secondary states is given by

$$|(\phi_i,\psi(t))|^2 = |\frac{1}{2\pi i}\int_{-\infty}^{\infty} d\omega e^{-i\omega t} \langle i|G|1\rangle|^2 \qquad (24)$$

which corresponds to a transition to one of the secondary levels. To get a measure of the total transition, we would want to integrate over the whole set of secondary levels.

As just stated, the Fourier transform of the Green's function gives the time varying overlap integral. Freed and Jortner [25] calculate the probability of finding the molecule in a secondary state, equating the time derivative of Eq. (24) to the observed fluorescence decay. We prefer to calculate the probability of finding the molecule in the primary state with the observed fluorescence decay then being directly proportional to this quantity. (See Ref. [26]).

The Fourier transform in reduced units is found as follows:

$$\xi = \frac{\frac{\omega}{2\pi c} - \bar{E}_1}{\pi V^2 D_0}; \varepsilon = \frac{\upsilon}{c} = \frac{\omega}{2\pi c} \qquad (25)$$

$$d\omega = 2\pi^2 cV^2 D_0 d\xi. \tag{26}$$

The transform becomes

$$\int_{-\infty}^{\infty} d\omega e^{-i\omega t} G_{11} = 2\pi^2 cV^2 D_0 \int_{-\infty}^{\infty} e^{-it(2\pi\xi(c\pi V^2 D_0) + 2\pi c\bar{E}_1)} G_{11} d\xi$$

$$= 2\pi^2 cV^2 D_0 \, e^{-i2\pi c\bar{E}_1 t} \int_{-\infty}^{\infty} e^{-i\xi t'} G_{11} d\xi, \tag{27}$$

where

$$t' = \frac{2\pi}{\frac{1}{\pi cV^2 D_0}} t \tag{28}$$

is time measured in units of 2π times the reciprocal of the line width frequency, or in units of true lifetimes if $f(\xi)$ is constant. The magnitude squared of the above integral then governs the time evolution of the primary state.

The matrix element used in this computation must be the entire matrix element, both real and imaginary parts, unlike the line shape function where only the imaginary part of the Green's function applies. In reduced units the matrix element of concern is

$$G_{11} = \frac{1}{\pi D_0 V^2} \frac{\xi}{\xi^2 + f^2(\xi)} - i \frac{1}{\pi D_0 V^2} \frac{f(\xi)}{\xi^2 + f^2(\xi)}$$

It should be mentioned that the lifetime is technically defined only in terms of an exponential decay whereas almost all examples presented here are nonexponential decays. For this reason we plot the whole decay

curve. The term "lifetime" is used from now on only in a qualitative manner indicating the speed of decay.

III. COMPUTED SPECTRA AND DECAY CURVES

We will now present some examples of line shapes and decay curves that we have chosen to illustrate some of the various spectral perturbations that may occur for nonideal situations. There are obviously a large number of possible examples and only a few can be included here. Each example was chosen to illustrate a particular effect. In real systems, a superposition of these effects may generally be expected. Also, there are other broadening mechanisms, which will come into play in real systems, that we ignore here. All the line shapes correspond to a single vibronic transition in condensed phases or to a single rotational line in a gas phase vibronic transition. One further comment about the examples here is that whenever we refer to an interacting continuum we are in actuality referring to the function that is given by the product $\pi|V(\epsilon)|^2 D_0(\epsilon)$ and not just $D_0(\epsilon)$.

The decay curves were computed using the fast Fourier transform algorithm of Cooley and Tukey [27]. This algorithm takes a finite bandwidth function and converts it into a periodic function. The Fourier series of the periodic function is then computed. The discrete points from this computation are then points in the true Fourier transform of the nonperiodic function. If the original function does not go to zero at the endpoints, errors in the form of ripples in the transform occur. We removed this error as much as possible by multiplying

the Green's function by a "filter" that forced the end points to go smoothly to zero while not affecting the main part of the Green's function near resonance. The jagged appearance of many decay curves is due to the finite point approximation of the algorithm to the continuous transform. Under higher time resolution, the decay curves appear smooth, as they should be.

A. Smooth Density-of-States Function

The first example is the large molecule limit case where the interacting states form a true continuum, see Fig.(1). If the continuum is a constant across the bandwidth, the line shape is a pure Lorentzian function. With a varying continuum, the Lorentzian becomes distorted to a degree depending on how rapidly the continuum varies. We allowed the continuum to vary exponentially. This particular form of the energy dependence is not critical for the general conclusions drawn here. For a moderately varying continuum, such as with an exponent of 0.1 per linewidth, the Lorentzian becomes asymmetric with greater intensity on the lower energy side than on the higher energy side of the resonance. The peak also shifts slightly to higher energy, although this is not readily detected in the figure. For slightly higher exponents, 0.5 per linewidth, the same effect continues. The distortions of the symmetric Lorentzian are not overly noticeable on inspection. A moment analysis of the line would possibly reveal the distortion more easily. In the cases where the continuum is rapidly varying, exponents of 1.0 and 5.0 per linewidth, the line continues to shift its peak slightly to higher energy, but at the same time sharpens considerably and increases in peak

FIGURE 1 (Uniform Density)

Uniform density of states varying exponentially. All line shapes are plotted on the same scale. The exponential coefficients are from top to bottom, 0.0, 0.1, 0.5, 1.0, 5.0.

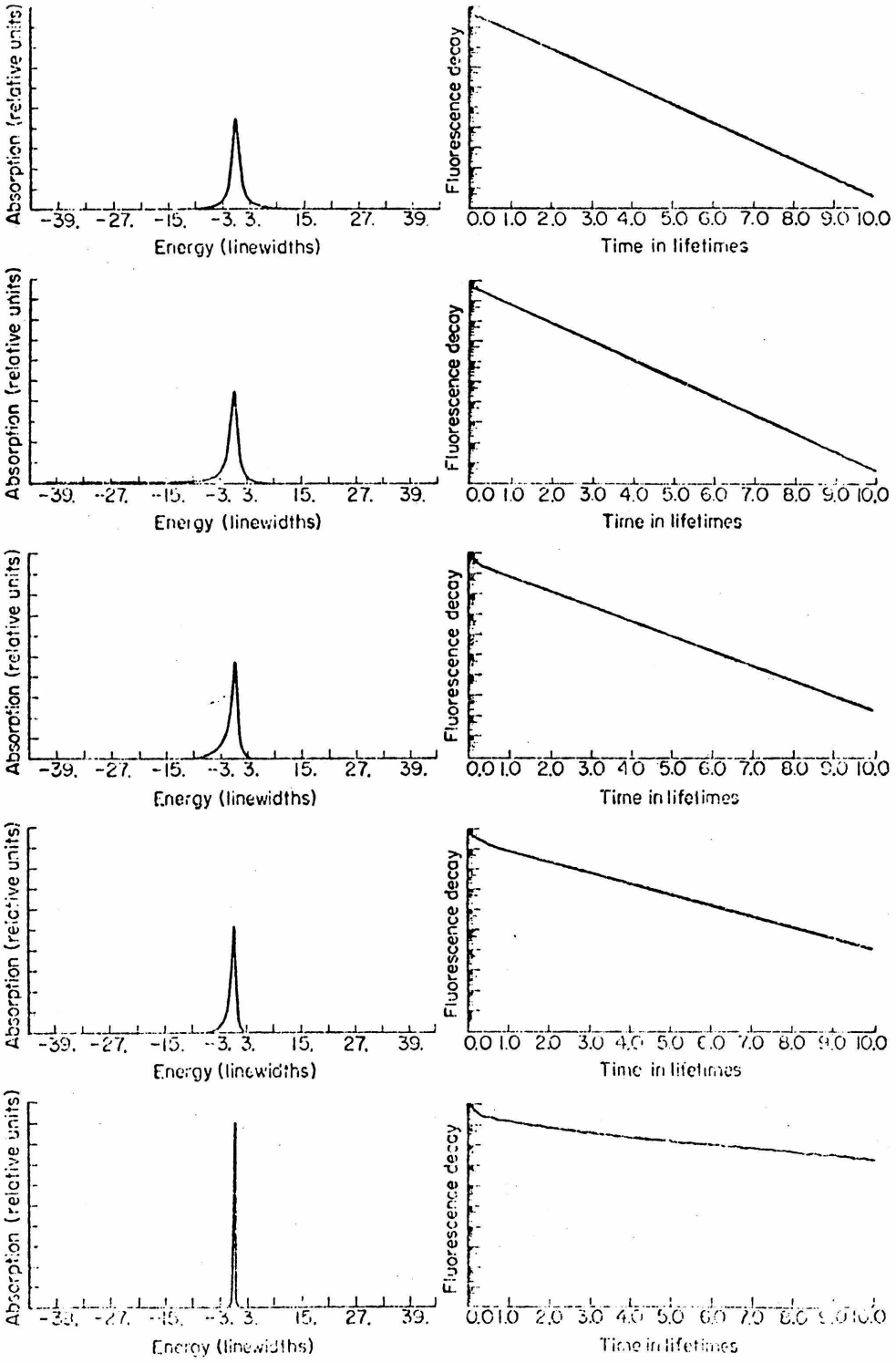
Absorption (relative units)
-39. -27. -15. -3. 3. 15. 27. 39.
Energy (linewidths)
Fluorescence decay
0.0 1.0 2.0 3.0 4.0 5.0 6.0 7.0 8.0 9.0 10.0
Time in lifetimes
(a)
(b)
(c)
(d)
(e)

intensity. We do not know if such rapidly varying continua exist in nature, so verifying this prediction may prove impossible.

The decay curves also follow the expected pattern of longer lifetime corresponding to narrower bandwidth. The decay curve corresponding to the pure Lorentzian shows exponential behavior over almost the entire time period except for very short times. The rise preceeding the decay can only be observed when the exciting pulse is a delta function in time. For a pulse of a finite width of time, this effect is washed out [28]. The rise is due to the limits of integration imposed by the finite bandwidth. If the limits could be infinite, then the decay would be exponential at all times. Asymmetry in the absorption spectrum manifests itself as a curvature (in a log plot) at short times. At longer times the curve becomes linear (exponential) in the log plot. The stronger the asymmetry, the longer the curvature lasts. The deviation from exponential decay due to a varying continuum is not striking and care would have to be taken to observe it in real systems.

B. Discrete Secondary Levels

The rest of the examples involve a number of relatively discrete secondary levels that have both a variable position and width, superimposed on, and noninteracting with, a constant, smooth continuum as described in Eqs. (20) and (21).

The continuum can be regarded as the radiation field continuum governing radiative decay or any other interacting continuum. The secondary discrete levels obtain their width either from interaction

with the radiation field, interaction with other continua if possible, or from collisions with other molecules which can be regarded as effectively broadening out the vibrational levels.

We now consider three cases obtained by variations of the parameters, δ, ω_i, and ξ_i.

1. Variable Spacing of Couples Levels

For this example (Fig. 2) we chose ω_i=0.5 linewidths and δ=50. The spectra show many spurious peaks due to the coupled levels. At the position of each coupled level there appears a doublet peak. Sometimes the doublet is not resolved if the width of the coupled level is too small, or if the coupling strength is too small and the coupled level too far from resonance.

This doublet structure is clearly seen in Fig. 2. The large splitting at the position of the primary state is due to there being a coupled level exactly in resonance with it. The symmetric appearance of the profile of the spurious peaks is due to the constancy of δ for all coupled levels and the symmetric placement of the levels. If this were not so, there would be no simple profile and the peaks would vary in intensity and splitting. The examples of variable δ will display this point a little more.

The doublet exactly at resonance is due to the plus and minus combinations of the two degenerate states. For exact resonance the intensity distribution is symmetric as shown here. When the secondary state is slightly off resonance, the intensity is asymmetric [28]. The doublets that occur far from resonance are due to a more subtle effect.

FIGURE 2 (Variable Spacing)

Discrete density of states with $w_i = 0.5$ and $\delta = 50.0$. The line shapes are on the same scale. The level spacing is, from top to bottom, 10.0, 5.0, 2.0.

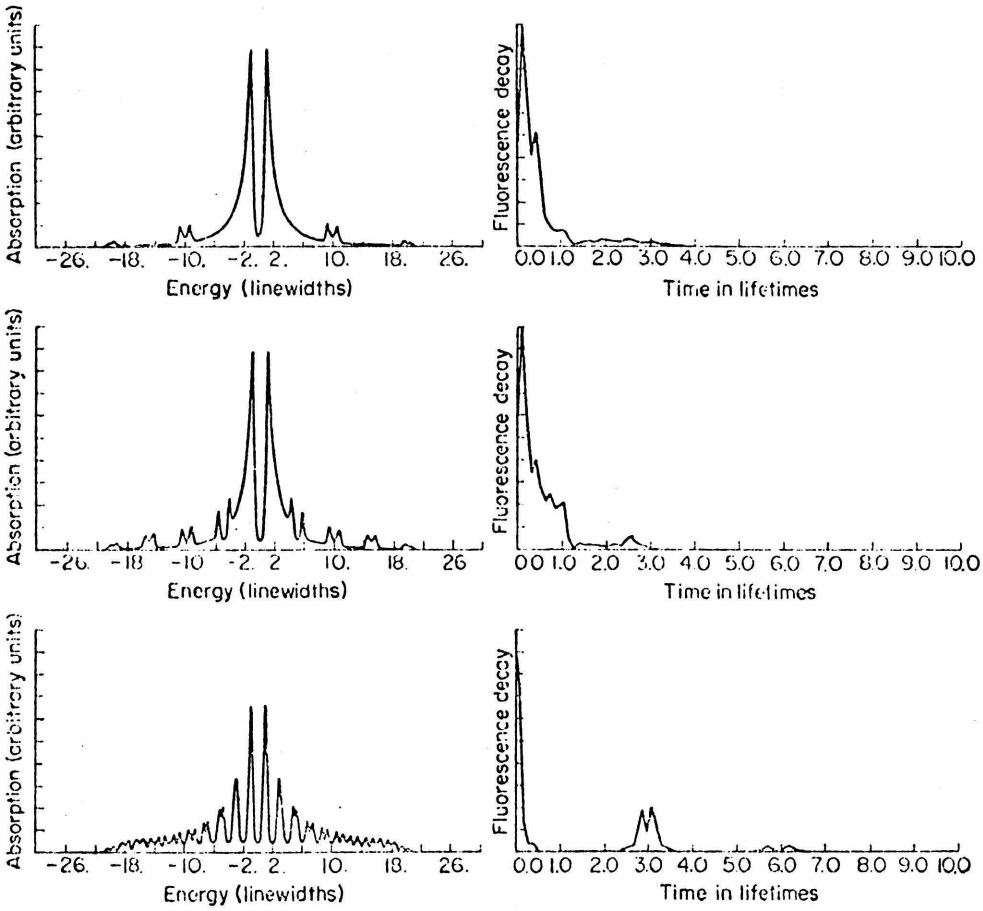
Absorption (arbitrary units)
-26. -18. -10. -2. 2. 10. 18. 26.
Energy (linewidths)
Fluorescence decay
0.0 1.0 2.0 3.0 4.0 5.0 6.0 7.0 8.0 9.0 10.0
Time in lifetimes
(a)
Absorption (arbitrary units)
-26. -18 -10 -2. 2 10. 18. 26
Energy (linewidths)
Fluorescence decay
0.0 1.0 2.0 3.0 4.0 5.0 6.0 7.0 8.0 9.0 10.0
Time in lifetimes
(b)
Absorption (arbitrary units)
-26. -18. -10. -2. 2. 10. 18. 26.
Energy (linewidths)
Fluorescence decay
0.0 1.0 2.0 3.0 4.0 5.0 6.0 7.0 8.0 9.0 10.0
Time in lifetimes
(c)

The nature of the broadened state is necessary to understand this. Any broadened level is not really a single state but consists of superposition of a large number of discrete (or at least very narrow) energy levels. We can mix the secondary and primary states by a stepwise perturbation approach. In first order the primary level mixes with each component of the broadened secondary level giving each one oscillator strength. The shape of the spectrum should reflect simply the energy distribution of the interacting secondary state. Now, however, these first-order states can mix through indirect interaction via the primary state. Since they are almost degenerate states, these second- and higher-order interactions are nonnegligible. These higher-order interactions result in a redistribution of the first order intensity within the broadened secondary level. The levels near the center gain very little intensity whereas those on the wings gain proportionately more. The net result is a proportionate increase in the intensity of the wings with respect to the center. Thus, a "hole" is burned in the center of the broadened secondary level. The extent of this hole burning is dependent on the coupling strength and distance from resonance, which determine the interaction magnitude, and on the width of the secondary level, which determines the magnitude of the splitting of the two components of the doublet.

The decay curves are now highly nonexponential and show quantum beat effects (See Ref. [3] for some discussion of this phenomenon). The actual structure of the decay curve is complicated by the presence of several coupled levels at different spacing. The first two decay curves are dominated by the structure very near resonance. Calculations with

only this one level present show that the first three peaks in the upper decay curve, and the first, second, and fourth peaks in the second decay curve are due to this major doublet in the absorption spectrum. The third decay curve is quite different from the first two, corresponding to a much more radical spectral perturbation. The initial rise in the fluorescence followed by the decay will be discussed in a future paper. The decay curves are not simple because they are a superposition of many recurrence phenomena from the many coupled levels.

2. Variable Coupling Strength (Fig. 3)

One would expect the coupling strength parameter to determine how the intensity of the primary state is distributed between the discrete secondary states and the secondary continuum. To a certain extent the calculated shapes confirm this. The intensity of the central doublet does decrease slightly on increase of δ. More intensity is shunted to the outlying coupled levels as the coupling strength is increased. The progression from single lines to double lines is clearly shown as the coupling strength increases. Even at the lowest coupling strength, the peaks at +5.0 and -5.0 are beginning to show the effects of doublet resolution as the single peaks are flattened on top. The decay curves are dominated by the central doublet.

The position of the beats is now independent of the coupling strength, but the height of each beat is related to the coupling strength ratio. The shape of the curve changes little for times less than ~ 0.5 lifetimes. Beyond this, as the coupling strength increases, the beats become stronger. This is related to the fact that the levels

FIGURE 3 (Variable Coupling Strength)

Discrete density of states with $w_i = 0.5$ and the levels are spaced 5.0 energy units apart. The line shapes are on the same scale. The coupling parameter, δ, is, from top to bottom, 5.0, 10.0, 50.0, 100.0.

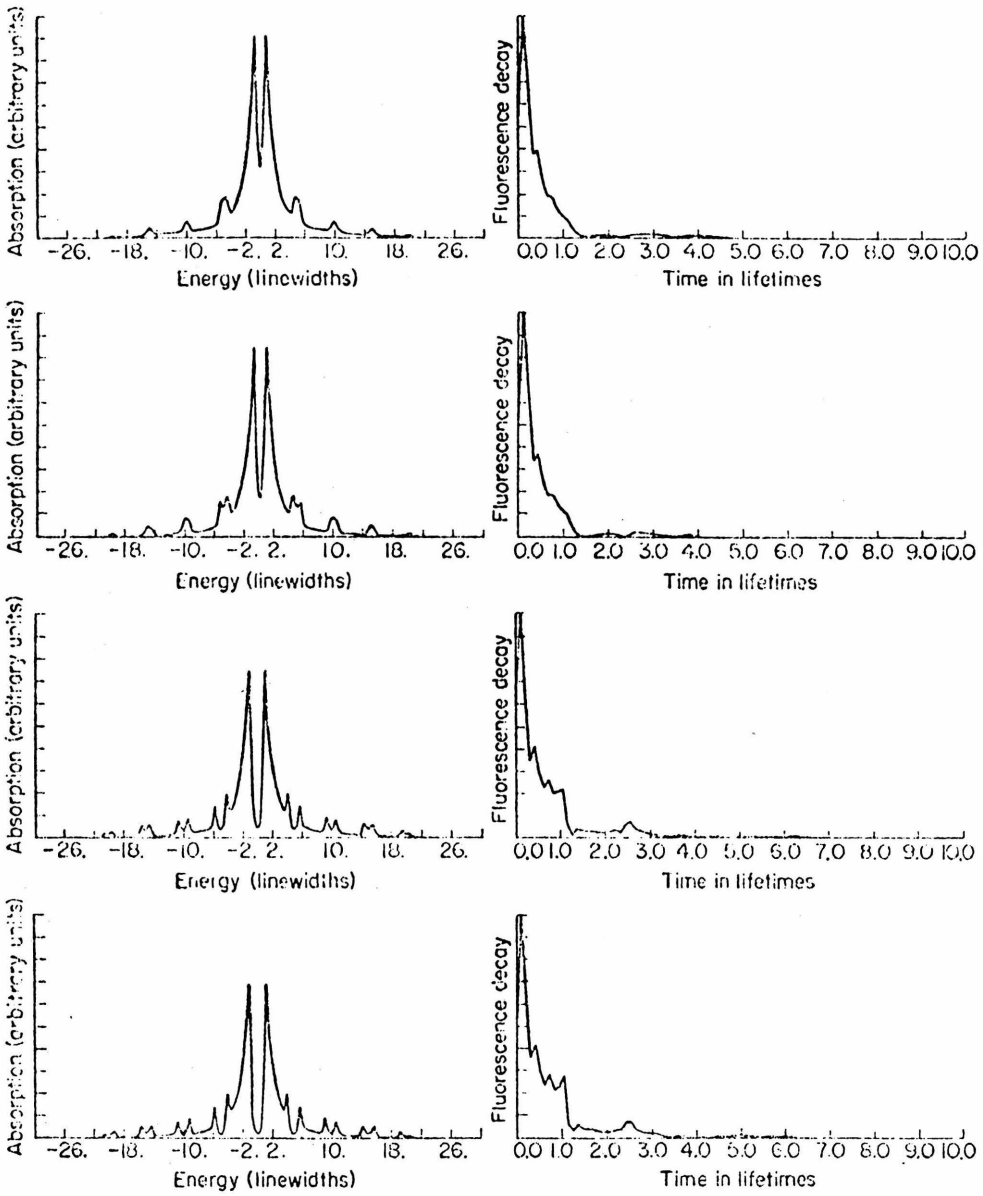
Absorption (arbitrary units)
-26. -18. -10. -2. 2. 10. 18. 26.
Energy (linewidths)
Fluorescence decay
0.0 1.0 2.0 3.0 4.0 5.0 6.0 7.0 8.0 9.0 10.0
Time in lifetimes

(a)

(b)

(c)

(d)

further from the resonance position gain more absorption intensity. Thus, the dominance of the central doublet on the decay curve is lessened as its intensity becomes relatively smaller.

3. Variable Width of the Coupled Levels (Fig. 4)

For this case $\delta = 10$ and the spacing is equal to 1.0 linewidths. For very narrow coupled levels (ω_i = 0.1 linewidths), the doublet structure described previously does not appear resolved. A singlet appears at the position of each coupled level. The most prominent feature is the strong doublet (again due to the coupled level at exact resonance) at the position of the primary level. For a slightly greater width [ω_i=0.5 linewidths, which, with a spacing of one linewidth, makes the $\pi|V(\varepsilon)|^2 D_0(\varepsilon)$ product almost constant], there is a dramatic decrease in the intensity of the central peak due to broadening. For an ω_i=1.0 linewidth, the spectrum is featureless and very broad. The decay curves merely reflect the changes in the spectrum along the lines discussed earlier. For the broadest spectrum, the decay is almost too fast for the time resolution employed here.

IV. SUMMARY

We have investigated in this paper the various types of spectral perturbations resulting from interactions leading to radiationless transitions. We have shown that a nonuniform interaction continuum manifests itself in a perturbation on the spectral line shape as described previously in the examples. These perturbations range from

FIGURE 4 (Variable Width)

Discrete density of states with δ = 10.0 and the level spacing equal to 1.0. The line shapes are on the same scale. The width of the coupled levels is, from top to bottom, 0.1, 0.5, 1.0.

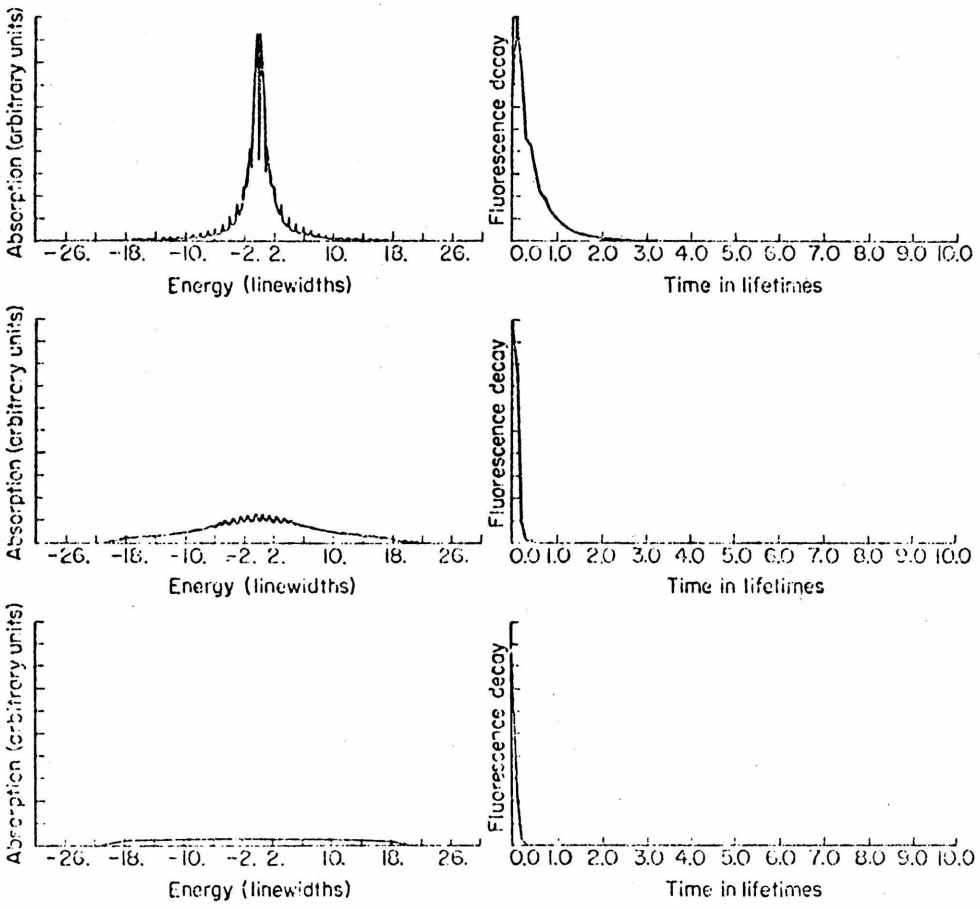
Absorption (arbitrary units)
-26. -18. -10. -2. 2. 10. 18. 26.
Energy (linewidths)
Fluorescence decay
0.0 1.0 2.0 3.0 4.0 5.0 6.0 7.0 8.0 9.0 10.0
Time in lifetimes
(a)
Absorption (arbitrary units)
-26. -18. -10. -2. 2. 10. 18. 26.
Energy (linewidths)
Fluorescence decay
0.0 1.0 2.0 3.0 4.0 5.0 6.0 7.0 8.0 9.0 10.0
Time in lifetimes
(b)
Absorption (arbitrary units)
-26. -18. -10. -2. 2. 10. 18. 26.
Energy (linewidths)
Fluorescence decay
0.0 1.0 2.0 3.0 4.0 5.0 6.0 7.0 8.0 9.0 10.0
Time in lifetimes
(c)

making a pure Lorentzian asymmetric to introducing either singlet or doublet peaks into the spectrum at positions corresponding to the positions of the secondary levels. The magnitude and type of perturbation depend on the parameters describing the interacting continuum.

We have also shown how the line shape is intimately related to the decay curve through the process of Fourier transformation. The various perturbations of the spectrum are also manifest in the decay curve as was shown in the examples. The ideal exponential decay can be greatly distorted depending on the perturbation. The appearance of a beat decay occurs when the interacting continuum is resolved into relatively discrete states.

A later paper will deal with the effect on the decay curve of varying the temporal and energy bandwidth characteristics of the exciting light.

APPENDIX I

The determinant is evaluated by performing column operations on the matrix. Multiply the i-th column by $+V_{i1}/(\varepsilon-E_i)$ and add to the first column. The resulting determinant is,

$$|\underset{\sim}{G_0^{-1}}-\underset{\sim}{V}| = \begin{vmatrix} \varepsilon-E_1-\sum_{i\neq 1}\frac{|V_{1i}|^2}{\varepsilon-E_i} & \cdots & -V_{1i} & \cdots \\ & \ddots & & \\ & & \varepsilon-E_i & \\ & & & \ddots \end{vmatrix}$$

$$= \prod_{\text{all } i}(\varepsilon-E_i)\left[1-\frac{1}{\varepsilon-E_1}\sum_{j\neq 1}\frac{|V_{1k}|^2}{\varepsilon-E_j}\right]$$

where the sums and products are taken over all the coupled states. The cofactors are,

$$[\text{cof } \underset{\sim}{G}]_{11} = \prod_i \frac{\varepsilon-E_i}{\varepsilon-E_1}$$

$$[\text{cof } \underset{\sim}{G}]_{ii} = \prod_j \frac{\varepsilon-E_j}{\varepsilon-E_i}\left[1-\frac{1}{\varepsilon-E_1}\sum_{k\neq 1,i}\frac{|V_{1k}|^2}{\varepsilon-E_k}\right]$$

Since we need only the trace of the matrix, the only elements we need calculate are the diagonal elements. Thus,

$$[\underset{\sim}{G}]_{11} = \prod_i \frac{\varepsilon-E_i}{\varepsilon-E_1} \Bigg/ \prod_i (\varepsilon-E_i) \left[1 - \frac{1}{\varepsilon-E_1} \sum_{k\neq 1} \frac{|V_{1k}|^2}{\varepsilon-E_k} \right]$$

$$= \left[\varepsilon-E_1 - \sum_{k\neq 1} \frac{|V_{1k}|^2}{\varepsilon-E_k} \right]^{-1}$$

$$[\underset{\sim}{G}]_{ii} = \frac{1}{\varepsilon-E_i} \left\{ \left(\varepsilon - E_1 - \sum_{k\neq 1,i} \frac{|V_{1k}|^2}{\varepsilon-E_k} \right) \right\} \Bigg/ \left(\varepsilon - E_1 - \sum_{k\neq 1} \frac{|V_{1k}|^2}{\varepsilon-E_k} \right)$$

The trace is then,

$$\text{tr } \underset{\sim}{G} = \left[1 + \sum_{i\neq 1} \frac{1}{\varepsilon-E_i} \left(\varepsilon - E_1 - \sum_{k\neq 1,i} \frac{|V_{1k}|^2}{\varepsilon-E_k} \right) \right] \Bigg/ \left(\varepsilon - E_1 - \sum_{k\neq 1} \frac{|V_{1k}|^2}{\varepsilon-E_k} \right)$$

Transforming from a sum over discrete, coupled states to an integral over a quasicontinuum of states whose density is given by $D_0(\varepsilon)$, the trace becomes

$$\text{tr } \underset{\sim}{G} = \frac{1 + (\varepsilon-E_1) \int \frac{D_0(E')}{\varepsilon-E'} dE' - \int \int_{E'\neq E''} \frac{D_0(E')D_0(E'')|V(E'')|^2}{\varepsilon-E'} dE'dE''}{\varepsilon - E_1 - \int \frac{D_0(E')|V(E')|^2}{\varepsilon-E'} dE'}$$

APPENDIX II

The determinants and cofactors are evaluated as in Appendix I. The result for the determinant is

$$|\underset{\sim}{G_0^{-1}} - \underset{\sim}{V}| = M \left[1 - \frac{1}{\varepsilon - E_1} \sum_{\substack{\text{both} \\ \text{cont.} \\ i \neq 1}} \frac{|\Omega_{1i}|^2}{\varepsilon - E_i} \right]$$

and the cofactors are given by

$$[\text{cof } \underset{\sim}{G}]_{11} = M/(\varepsilon - E_1)$$

$$[\text{cof } \underset{\sim}{G}]_{11} = \frac{M}{\varepsilon - E_i} - \frac{M}{(\varepsilon - E_1)(\varepsilon - E_i)} \sum_{\substack{\text{both} \\ \text{cont.} \\ k \neq i}} \frac{|\Omega_{1k}|^2}{\varepsilon - E_k}$$

Where the following symbols have been used,

$\Omega_{1i} = V_{1i}$ or W_{1i} depending on which continua one is in

$M = \prod_i (\varepsilon - E_i)$ where i ranges over both continua

The diagonal elements are then

$$[\underset{\sim}{G}]_{11} = \left(\varepsilon - E_1 - \sum_{\substack{\text{both} \\ \text{cont.} \\ i \neq 1}} \frac{|\Omega_{1i}|^2}{\varepsilon - E_i} \right)^{-1}$$

$$[\underset{\sim}{G}]_{ii} = \frac{1}{\varepsilon - E_i} \left\{ \left(\varepsilon - E_1 - \sum_{\substack{\text{both} \\ \text{cont.} \\ k \neq 1, i}} \frac{|\Omega_{1k}|^2}{\varepsilon - E_k} \right) \Bigg/ \left(\varepsilon - E_1 - \sum_{\substack{\text{both} \\ \text{cont.} \\ k \neq 1}} \frac{|\Omega_{1k}|^2}{\varepsilon - E_k} \right) \right\}$$

nally the trace is,

$$\left[\varepsilon-E_1-\sum_{\substack{\text{both}\\ \text{cont.}\\ i\neq 1}}\frac{|\Omega_{1i}|^2}{\varepsilon-E_i}\right]^{-1}\left[1+\sum_{\substack{\text{both}\\ \text{cont.}\\ i\neq 1}}\frac{1}{\varepsilon-E_i}\left[\varepsilon-E_1\cdot\sum_{\substack{\text{both}\\ \text{cont.}\\ k\neq 1,i}}\frac{|\Omega_{1k}|^2}{\varepsilon-E_k}\right]\right]$$

make the tranformation to the continuum form. The denominator

$$\Xi_1-\int\underbrace{\frac{D_0(E')|V(E')|^2}{\varepsilon-E'}dE'}_{\mathcal{P}_1(\varepsilon)}-\mathcal{P}\int\underbrace{\frac{\rho_0(E')|W(E')|^2}{\varepsilon-E'}dE'}_{\mathcal{P}_2(\varepsilon)}$$

$$+i\pi(D_0(\varepsilon)|V(\varepsilon)|^2+\rho_0(\varepsilon)|W(\varepsilon)|^2)$$

nerator consists of a number of terms. Evaluating only the first

ıich concerns the primary levels, we obtain

$$\langle 1|G|1\rangle=\frac{1}{\varepsilon-\bar{E}_1-i\pi D_0(\varepsilon)|V(\varepsilon)|^2+i\pi\rho_0(\varepsilon)|W(\varepsilon)|^2}$$

$$\bar{E}_1=E_1-\mathcal{P}_1(\varepsilon)-\mathcal{P}_2(\varepsilon)$$

REFERENCES

[1] (a) Robinson, G. W., 1961, J. Mol. Spectry., 6, 58.

(b) Robinson, G. W., and Frosch, R. P., 1962, J. Chem Phys., 37, 1962.

(c) Robinson, G. W., and Frosch, R. P., 1963, J. Chem Phys., 38, 1197.

[2] Henry, B. R., and Kasha, M., 1968, Ann. Rev. Phys. Chem., 19, 161.

[3] Jortner, J., Rice, S. A., and Hochstrasser, R. M., 1969, Adv. in Photochemistry, 7, 149.

[4] (a) Schlag, E. W., Schneider, S. , and Fischer, S. F., 1971, Ann. Rev. Phys. Chem., 22, 465.

(b) Freed, K. F., "The Theory of Radiationless Processes in Polyatomic Molecules," (Preprint).

[5] Heller, D. F., Freed, K. F., and Gelbart, W. M., 1972, J. Chem. Phys., 56, 2309.

[6] Robinson, G. W., "Molecular Electronic Radiationless Transitions," Excited States, Vol. I, ed. by Lim, E. C. (Academic Press) (in press).

[7] Fano, U., 1961, Phys. Rev., 124, 1866.

[8] (a) Bixon, M., and Jortner, J., 1968, J. Chem. Phys., 48, 715.

(b) Bixon, M., and Jortner, J., 1968, J. Chem. Phys., 50, 3284.

(c) Bixon, M., and Jortner, J., 1969, J. Chem. Phys., 50, 4061.

[9] (a) Scharf, B., 1970, Chem. Phys. Letters, 5, 456.

(b) ibid., p. 459.

[10] Byrne, J. P., and Ross, I. G., 1971, Australian J. Chem., 24, 1107.

[11] (a) Hochstrasser, R. M., and Marzzacco, C., 1968, J. Chem. Phys., 49, 971.

(b) Hochstrasser, R. M., and Noe, L. J., 1970, J. Chem. Phys., 50, 1684.

(c) Hochstrasser, R. M., and Dym, S., 1970, J. Chem. Phys., 51, 2448.

(d) Hochstrasser, R. M., 1968, Acc. Chem. Res., 1, 226.

[12] Kasha, M., Henry, B. R., and Rhodes, W., 1969, Proc. Nat'l Acad. Sci. U.S., 63, 31.

[13] (a) Rhodes, W., 1969, J. Chem. Phys., 50, 2885.

(b) Rhodes, W., (preprint).

[14] (a) Goldberger, M. L., and Watson, K. M., 1964, Collision Theory (J. Wiley and Sons, Inc.), Chap. 8.

(b) Zumino, B., 1961, Lectures on Field Theory in Many Body Problems, ed by Caianello, F. R., (Academic Press), p. 37.

[15] (a) Yonezawa, F., 1964, Progress of Theoretical Physics, 31, 357.

(b) Yonezawa, F., and Matsubara, 1966, Progress of Theoretical Physics, 35, 357.

(c) Goodings, D. A., and Mozer, B., 1964, Phys. Rev., 36, A1093.

(d) Onodera, Y., and Yonezawa, F., 1968, J. Phys. Soc. Japan, 24, 341.

[16] Hong, Hwei-Kwan, and Robinson, G. W., 1970, J. Chem. Phys., 52, 825.

[17] Nitzan, A., and Jortner, J., 1971, J. Chem. Phys., 55, 1355.

[18] Irving, J., and Mullineux, N., 1959, Mathematics in Physics and Engineering (Academic Press), p. 519.

[19] Harris, R. A., 1963, J. Chem. Phys., 39, 978.

[20] Burland, D. M., 1969, Ph.D. Thesis, California Institute of Technology.

[21] (a) Schlag, E. W., and von Weyssenhoff, N., 1969, J. Chem. Phys., 51, 2508.

(b) von Weyssenhoff, N., and Kraus, F., 1971, J. Chem. Phys., 54, 2387.

[22] (a) Parmentar, C. S., and Schuyler, M. W., 1970, J. Chem. Phys., 52, 5366.

(b) Ware, W., Selinger, B., Parmentar, C. S., and Schuyler, M. W., 1970, Chem. Phys. Letters, 6, 342.

(c) Selinger, B., and Ware, W., 1970, J. Chem. Phys., 53, 3160.

[23] Spears, K. G., and Rice, S. A., 1971, J. Chem. Phys., 55, 5561.

[24] Wessel, J., 1971, Ph.D. Thesis, U. of Chicago.

[25] Freed, K. F. , and Jortner, J., 1970, J. Chem. Phys., 52, 6272.

[26] See Bergland, G. D., July, 1969, IEEE Spectrum, p. 41.

[27] Chock, D. P., Jortner, J., and Rice, S. A., 1968, J. Chem. Phys., 49, 610.

[28] C. A. Langhoff, unpublished results.

PART 3

THE ENERGY SHIFT TERM AND ITS EFFECT ON THE ABSORPTION LINE SHAPE

I. INTRODUCTION

In applying the Green's function to various perturbation problems, a term always arises which is called the energy shift or level displacement operator. It is given by the formula,

$$\text{Energy Shift} = \mathcal{P} \int \frac{\pi |V(\varepsilon)|^2 D_0(\varepsilon)}{\varepsilon - E_0} d\varepsilon \qquad (1)$$

where E_0 is the zero order energy of the shifted state, $D_0(\lambda)$ is the density of states with which E_0 interacts and $|V(\lambda)|^2$ is the strength of the interaction. Heitler presents a discussion of this term when the interacting states are the radiation field [1]. Once the density and interaction strengths are known, the new energy of the state is found by solving the following equation for ε,

$$\varepsilon - E_0 - \mathcal{P} \int \frac{\pi |V(\varepsilon)|^2 D_0(\varepsilon)}{\varepsilon - E_0} d\lambda = 0 \qquad (2)$$

Generally, the equation must be solved iteratively and a solution is generally difficult to find. The solution of this equation and its properties was briefly discussed on page 27. There it was shown that as the limit to a continuous set of states was reached, the number of eigenvalues becomes infinite, and are infinitely close together, i.e. a continuum as expected. The level shift operator really does not "shift" levels around in this situation. If, however, the weighted density function has structure (i.e. peaks), the peaks will be shifted

around much along the same lines as the delta function states are shifted. The spectra fitting procedure used by the authors in another paper [2] is in effect a way of finding a solution to Eq. (2) by an iterative trial and error method.

If one wishes to compute the line shape of a homogeneously broadened molecular resonance (See Refs. [2]-[5]), the energy shift is frequently ignored because of the difficulty of computation and also because it is generally believed to not contribute significantly to the line shape. We will show here that this neglect of the energy shift is permissable in some cases, but that in other situations the energy shift plays a dominant role in determining the actual line shape. These latter cases are those where the secondary levels [6] are discrete.

Some other discussions of the energy shifts in different contexts have appeared in the literature. The situation where the secondary level density is bounded below results in the possibility of the formation of new molecular states [7].

II. LINE SHAPES AND THE ENERGY SHIFT TERM

All calculations of homogeneously broadened line shapes up to this time [1] have used the following formula,

$$\alpha(\varepsilon) = \frac{\pi|V(\varepsilon)|^2 D_0(\varepsilon)}{(\varepsilon-\overline{E}_0)^2+(\pi|V(\varepsilon)|^2 D_0(\varepsilon))^2} \qquad (3)$$

where the symbols used are

ε - energy variable

$D_0(\varepsilon)$ - density of secondary states

$V(\varepsilon)$ - interaction matrix element of primary and secondary states

$\alpha(\varepsilon)$ - absorption coefficient multiplied by a constant proportionality factor

$\bar{E}_0$ - shifted primary state energy.

$\bar{E}_0$ is treated as a constant in the above line shape. For the situation where $\pi|V(\varepsilon)|^2 D_0(\varepsilon)$ = constant, the line is Lorentzian and the energy shift $R_a(\varepsilon)$

$$R_a(\varepsilon) = \mathcal{P} \int \frac{\pi|V(E)|^2 D_0(E)}{\varepsilon - E} \, dE$$

is exactly zero. This is strictly the only case where the neglect of energy shift is valid. In situations where the $\pi|V(\varepsilon)|^2 D_0(\varepsilon)$ term depends on energy one must use a slightly modified form for the line shape function,

$$\alpha(\varepsilon) = \frac{\pi|V(\varepsilon)|^2 D_0(\varepsilon)}{(\varepsilon - \bar{E}_0(\varepsilon))^2 + (\pi(V(\varepsilon)|^2 D_0(\varepsilon))^2} \qquad (4a)$$

$$\bar{E}_0(\varepsilon) = E_0 - R_0(\varepsilon) \qquad (4b)$$

where the $\bar{E}_0(\varepsilon)$ energy dependent term replaces the constant $\bar{E}_0$.

As in the previous paper [3], this line shape function can be computed in relative units. In our calculations for each point of the

spectrum, we must first calculate the two parts of the principal value integral Eq. (1), take the sum of these two and then insert this into the line shape function. The figures that we calculate here have parameters which are essentially identical to those presented in Ref. [3], where the energy dependence of the shift term is ignored. The details of calculation are the same as in Ref. [2].

The first case (Fig.(1)) deals with situations where the secondary level density is smooth, but increasing in magnitude with increasing energy. This increase in Ref. [3] was exponential but in the present calculations it is linear. All that is of concern is what general trends seem to develop, not the relevance of a specific energy dependence. The first thing to be noticed is that the sharpening effect observed by ignoring the energy shift is not present when the energy shift is correctly included. The function of the energy shift to move the resonance position is clearly seen. Although there was an energy shift observed in Ref. [3], it was very small. In fact, from the figures there, no energy shift is readily detectable. This is an indication that the magnitude of splittings calculated by deleting the energy shift will be much too small. The slope of the density of secondary levels does have an effect on the line shape as well as on the resonance position. Increasingly sloped densities result in broader lines. The lines still appear to be Lorentzian functions or close approximations.

One problem not clearly evident from the drawing is that the spectra near the ends of the calculated interval show a gradual upturn.

FIGURE 1 (Variable Smooth Density)

The density is a linear function of energy with the slopes from top to bottom 0.0 (a pure Lorentzian), 0.5, 1.0, 5.0 respectively.

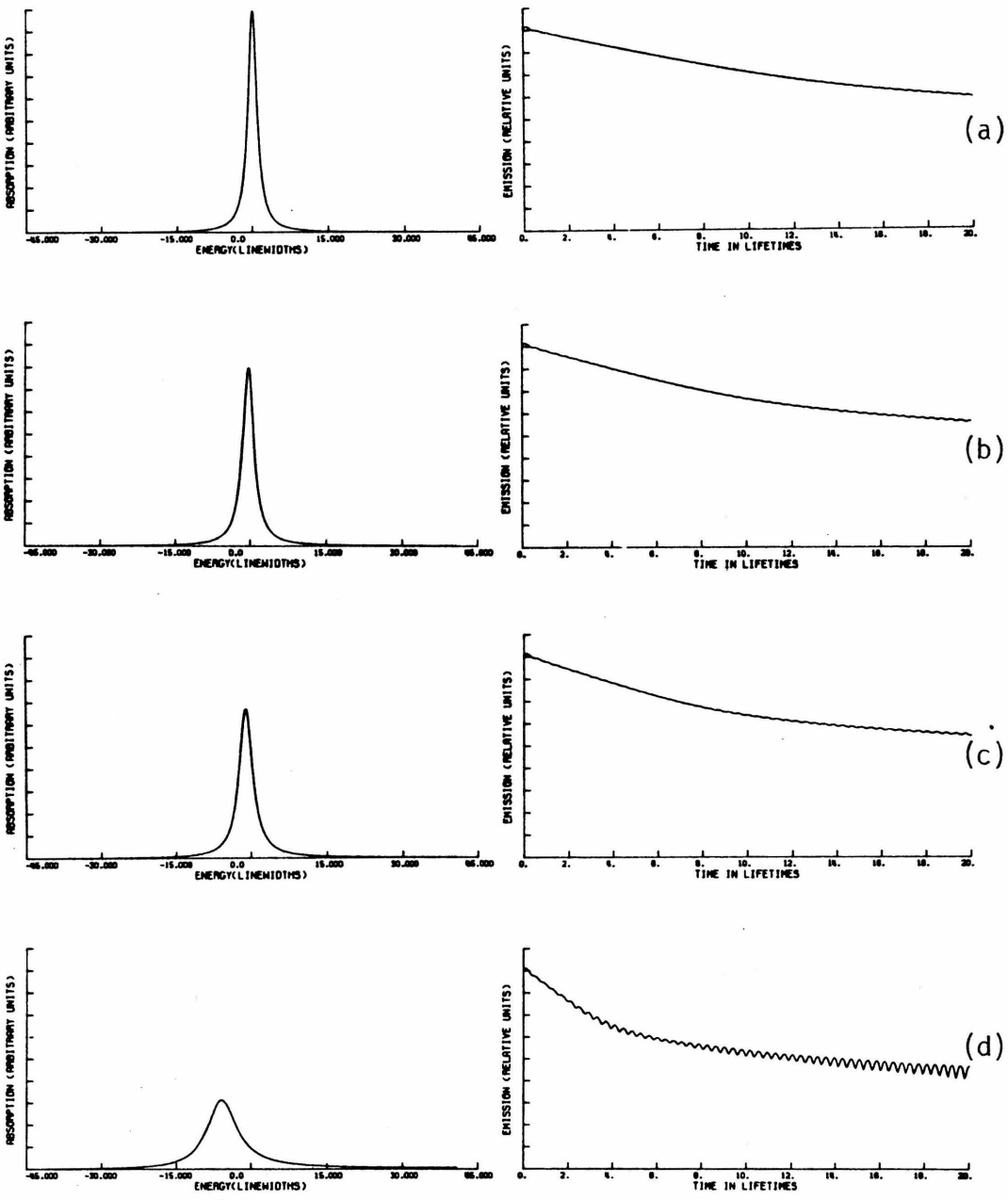
ABSORPTION (ARBITRARY UNITS)
ENERGY(LINEWIDTHS)
EMISSION (RELATIVE UNITS)
TIME IN LIFETIMES
(a)
(b)
(c)
(d)

This is noticeable in some later figures. This effect is not real and is due to the artificial termination of the secondary level density there. Although not noticeable in the spectra, the time decay curve results are very sensitive to this effect. The ripples that appear on the decay curves are due to this effect. Even the filter function discussed in Ref. [3] is unable to remove them. Thus, no serious notice should be taken of these ripples as they are a calculational artifact. The only point to notice about the decay curves is that they reflect the broadening change in the corresponding spectrum by shortening their decay times. The decays do show deviations from exponential behavior, but the deviation is not radical. Only a small curvature can be seen. Again ripples in the curve are due to the interval end point effect mentioned above and are not significant.

The following figures all deal with the situation where the secondary state density is line like. These are the situations where one expects to see a multiplet spectrum and a quantum beat decay. The first example of this group illustrates the effect of a variable spacing between secondary levels (Fig. 2). There are some general features which should be noticed. First, the secondary level in resonance with the primary level gives rise to three, not two, peaks in the spectrum. This is in contrast to the doublet formed if the energy shift is ignored [3]. However, the doublets formed off resonance in the neglected energy shift spectra are now doublets only at much higher coupling strengths. The general trend that we see is that the levels are more closely spaced, the primary line distributes itself in a broader general envelope of sharp lines. This means that

FIGURE 2 (Variable Spacing)

The widths of all levels is 0.5 ξ and the coupling strength is 5.0 ξ. Top to bottom, the number of levels is 7, 13, and 31, and the spacing between levels is 10.0, 5.0, and 2.0.

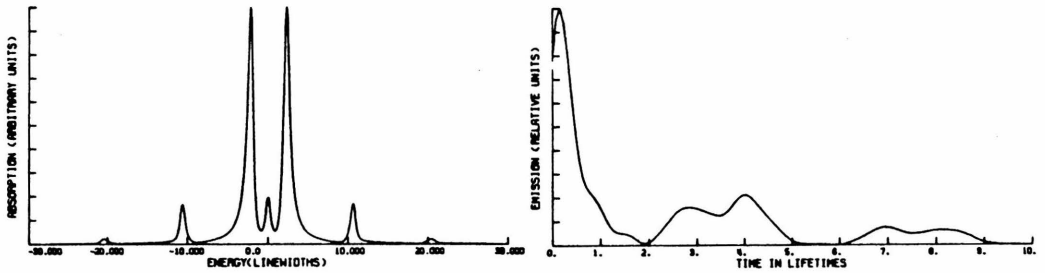
ABSORPTION (ARBITRARY UNITS)
ENERGY(LINEWIDTHS)
EMISSION (RELATIVE UNITS)
TIME IN LIFETIMES

(a)

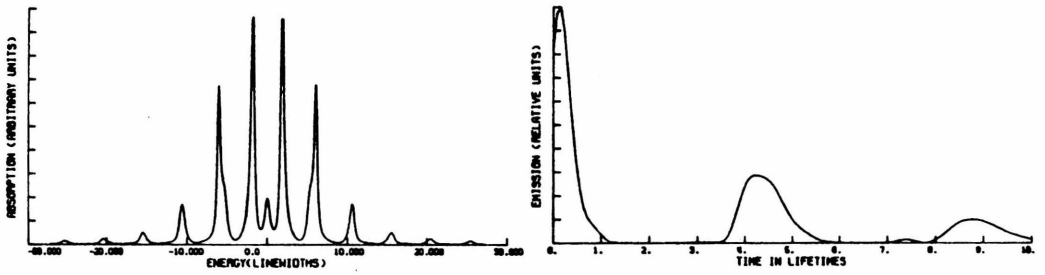
ABSORPTION (ARBITRARY UNITS)
ENERGY(LINEWIDTHS)
EMISSION (RELATIVE UNITS)
TIME IN LIFETIMES

(b)

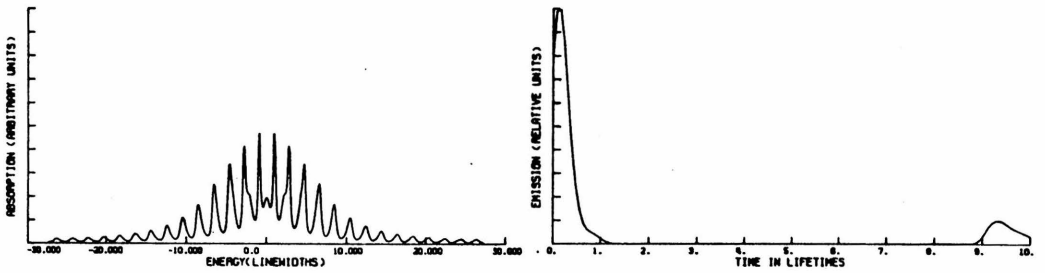
ABSORPTION (ARBITRARY UNITS)
ENERGY(LINEWIDTHS)
EMISSION (RELATIVE UNITS)
TIME IN LIFETIMES

(c)

we are approaching the statistical limit situation [8].

The decay curves are quite complicated as were those for the neglected energy shift case. The occurrence of beats is observed to be approximately inversely related to the spacing of the lines in the spectrum. The similarity of the first two decay curves is due to the dominating effect of the central triplet on the Fourier transform of the Green's function. The third decay curve is much different from the first two because the central triplet structure is now much less dominant.

Figure (3) illustrates the effect of a variable coupling strength. It is in this figure that one of the most important differences between spectra calculated with and without the energy shift appears clearly. In Ref. [3] the secondary levels off resonance give rise to new lines in the spectrum. For very weak [9] coupling, the lines are singlets. When the coupling strength is increased, the height of the line increases up to a certain point which is only a fraction of the intensity of the central peak. Increasing the coupling beyond that causes a splitting which gives rise to a doublet. The intensity of each component never exceeds a certain level. When the energy shift is correctly included, the height of the off resonance peak is now much greater and can be equal or greater than the central peak. Doublets are produced, but at relatively higher coupling strengths than before. Moreover the two components of the doublets are now highly assymmetric in intensity, the component furthest away from resonance being most intense.

FIGURE 3 (Variable Strength)

There are 13 coupled levels in each spectrum. They begin at -30.0 ξ and are spaced 5.0 ξ apart and have a width of 0.5 ξ. The coupling strength is, top to bottom, 1.0, 5.0, 10.0, and 20.0 ξ respectively.

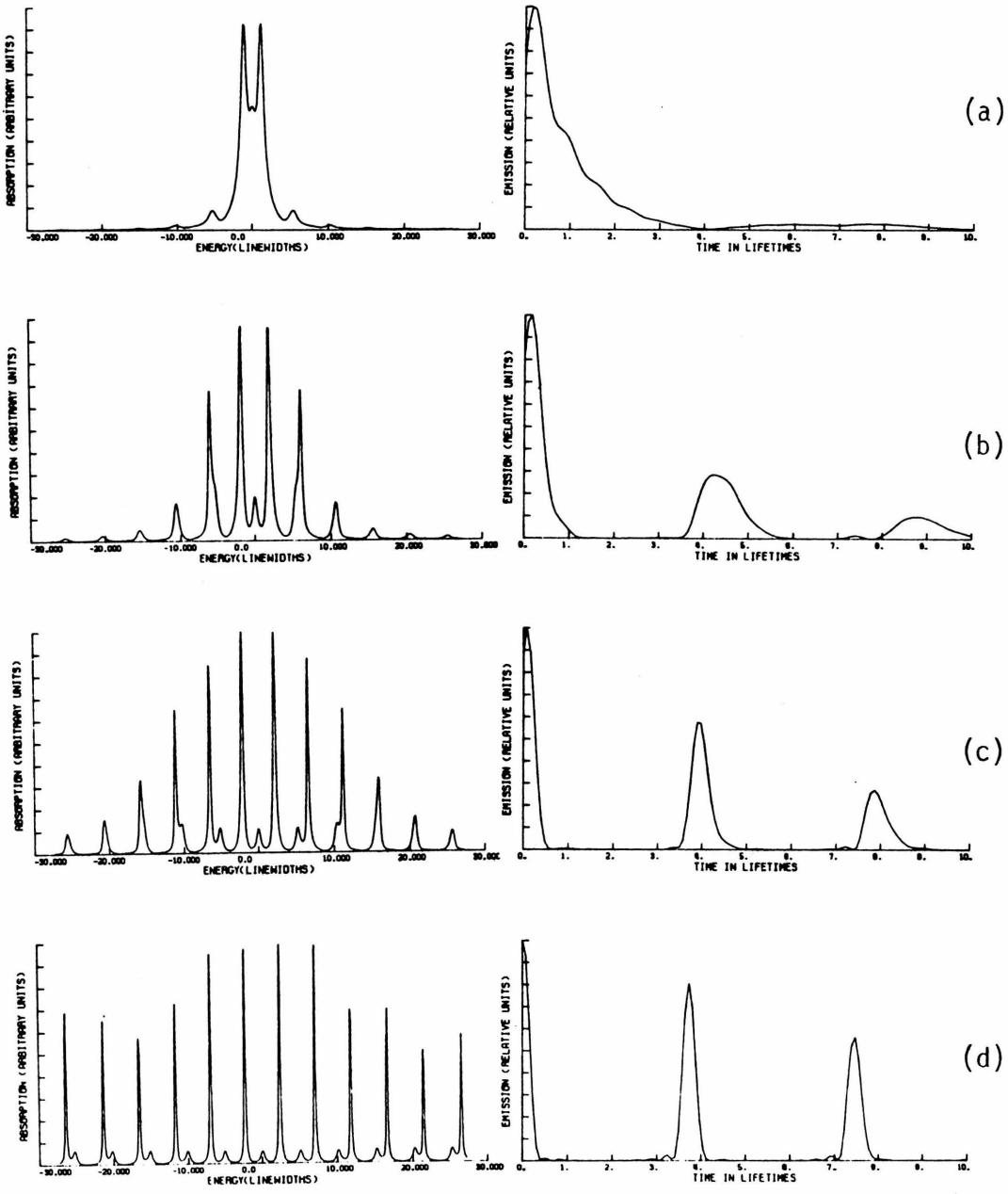
ABSORPTION (ARBITRARY UNITS)
ENERGY(LINEWIDTHS)
EMISSION (RELATIVE UNITS)
TIME IN LIFETIMES
(a)
(b)
(c)
(d)

FIGURE 4 (Variable Width)

There are 61 coupled levels in each spectrum beginning at -30.0 ξ and separated by 1.0 ξ and each has a coupling strength of 5.0 ξ. The widths are, top to bottom, 0.1, 0.3, and 1.0 respectively.

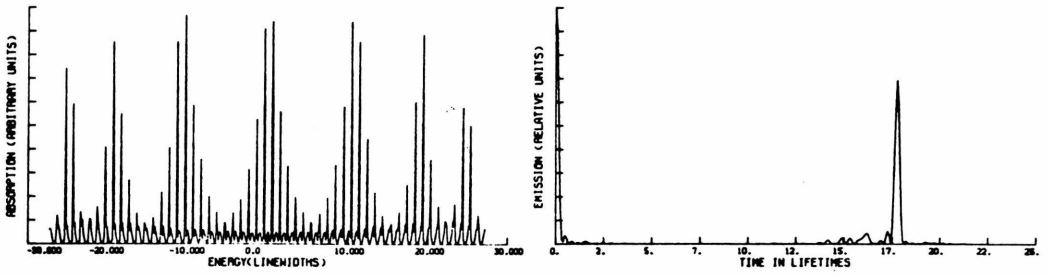
ABSORPTION (ARBITRARY UNITS)
ENERGY(LINEWIDTHS)
EMISSION (RELATIVE UNITS)
TIME IN LIFETIMES

(a)

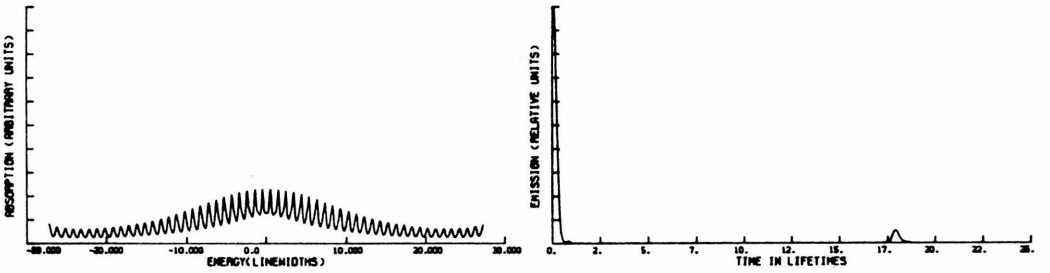
ABSORPTION (ARBITRARY UNITS)
ENERGY(LINEWIDTHS)
EMISSION (RELATIVE UNITS)
TIME IN LIFETIMES

(b)

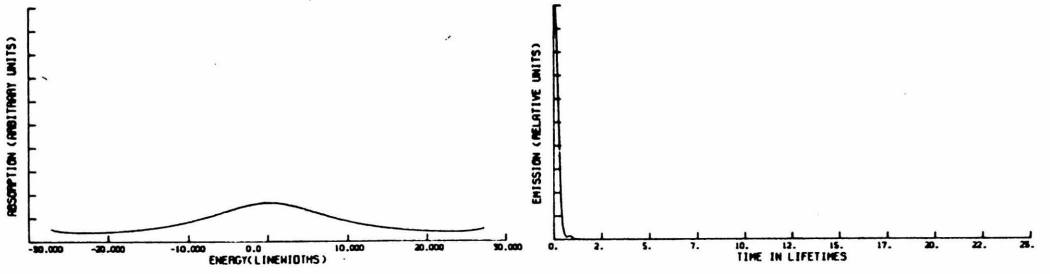
ABSORPTION (ARBITRARY UNITS)
ENERGY(LINEWIDTHS)
EMISSION (RELATIVE UNITS)
TIME IN LIFETIMES

(c)

The statement that many extra lines would appear in such a perturbed spectrum (if coupling strengths are high enough) is strongly reinforced. Little semblance of the original Lorentzian would be expected to be evident. Assignment of such a spectrum when the levels are not as symmetrically spaced as here would clearly be impossible according to standard spectroscopic methods.

The decay curves reflect quite clearly the spectral modifications. Beginning with a nearly non-beat decay, they progress to a very sharply beated decay for the final spectrum. It is noticeable that the position of the beats changes only very little. This occurs because the position of the peaks in the spectrum change very little. The decay curve resembling the Fourier transform of the spectrum is clearly illustrated here (See Ref. [10] for a more exact understanding of the Fourier transform process).

The final figure illustrates the transition from a discrete to a continuous secondary state spectrum. This is accomplished by fixing the positions and strengths of the secondary states and then increasing the widths. All levels have the same coupling strength. The first spectrum in this figure shows clearly how the high order perturbation technique used here distributes the intensity. The first order theory would predict a spectrum resembling the second spectrum. But, as is seen, when the secondary states are discrete enough, the second and higher order terms can play a dominant role in the intensity distribution. The doublets again appear as expected. The

upturned ends in the last spectrum are due to the artificial termination of the calculation at the end of the interval and are not physically real.

The pattern of the decay curves follows directly from the spectrum. The beat magnitude is dependent on the dominance of the sharp structure in the spectrum. Where there is no structure in the spectrum, the decay is smooth and related to the spectral breath.

III. CONCLUSION

We have shown here the energy shift operator can be an important term in calculating the line shape of a homogeneously broadened molecular resonance. When the interacting states are discrete, or line-like, the energy shift may be the dominant term in the line shape function. Calculations of the line shape function neglecting the energy shift in these situation will be definitely wrong, even though the experimental line shape may be reproduced. For situations where the interacting states are only slowly varying the energy shift term is much less important. Thus, for a really correct calculation of the line shape function, the energy shift term should be included.

REFERENCES

[1] Heitler, W., 1954, The Quantum Theory of Radiation (Oxford U. Press), § 16 and § 34.

[2] Langhoff, C. A., and Robinson, G. W., (in preparation).

[3] Langhoff, C. A., and Robinson, G. W., 1973, Mol. Phys., (in press).

[4] (a) Sharf, B., and Silbey, R., 1970, Chem. Phys. Lett., 5, 456.

(b) Ibid., 1970, Chem. Phys. Lett., 5, 459.

[5] Fano, U., 1961, Phys. Rev. A., 124, 1866.

[6] We employ the standard model of radiationless transition theory which has, in zero-order, a primary state carrying all the oscillator strength interacting with a set of secondary states which are continuous.

[7] Gelbart, W. M., and Jortner, J., 1971, J. Chem. Phys., 54, 2070.

[8] Bixon, M., and Jortner, J., 1968, J. Chem. Phys., 48, 715.

[9] The magnitude of the coupling depends on the distance the level is from resonance because of the energy denominator.

[10] Langhoff, C. A., and Robinson, G. W., (in preparation).

PART 4

THE OCCURRENCE AND OBSERVATION OF NONEXPONENTIAL DECAYS

I. INTRODUCTION

An almost universal model of electronic radiationless transitions in polyatomic molecules has in zero order a discrete state, which carries all the oscillator strength, interacting with a quasi-continuum of states. In the ideal case where the interacting continuum is a constant over an energy range of one or more bandwidths, the line shape is predicted to be Lorentzian. If broad band excitation is used, resulting in the entire Lorentzian line being excited uniformly, then the emission is predicted to be an exponential decay [1].

Now we ask the question, what happens if the exciting light source has a bandwidth smaller than that of our broadened level such that only part of the band is excited. The article by Kasha, et al., [2], deals specifically with this question in a qualitative way. Their chief concern was to describe the nature of the initial state upon absorption of a photon. Rhodes [3] has applied density matrix methods to this problem and has formalized the results of Kasha, et al. The conclusion of these papers is that the bandwidth of the exciting light is important in determining the nature of the initial excited state. Since the emission properties will depend on the initial state, they will also depend on the bandwidth of excitation.

Previously [4], we have discussed the effect of non-constant coupled continua on the line shape and corresponding emission decay curves for some model systems. In this paper we study the decay curves in more detail including the effect of finite excitation bandwidth.

Finite bandwidth excitation also has a finite time duration. We show how the Green's function method automatically takes this into account.

Since there is an experimental problem in obtaining the minimum time width (related to the bandwidth by the uncertainty principle) of the exciting pulse, we also compute some decay curves where the time width of the pulse is wider than its minimum time width. This is intended to give the experimentalist a better idea of the conditions necessary to observe quantum beat and other nonexponential decays.

II. THEORY

A. Basic Assumptions

We use the standard zero order model with one discrete state (primary state) which carries all the oscillator strength and a quasi-continuum of states (secondary states) coupled to the primary state but carrying no oscillator strength. In the sense of Nitzan and Jortner [5], we assume that the primary state is isolated so the effect of other states carrying oscillator strength is negligible. Since all oscillator strength is derived from the primary state, all new states are indistinguishable in the sense of Ref. [1]. Assuming that an appropriate choice of zero order states has been made, we use the techniques of reference [4] and compute an absorption lineshape.

We make some further assumptions concerning experimental

conditions to which these results relate. The "experiment" is presumably either done in the gas phase under isolated molecule conditions, or in a very dilute mixed crystal where the host is presumed to be inert and any exciton effects may be ignored. In the former situation we are then talking about rovibronic states, in the latter about vibronic states. Discussion about the assumptions made about the exciting light characteristics is in the next section.

B. The Exciting Light

Most previous studies have employed the so-called broad band approximation [1] (See also Ref. [6]). Thus, by implicit assumption the exciting pulse is a delta function in time. This is so because of the uncertainty principle. The Fourier transform process assures us that the energy - bandwidth uncertainty principle is automatically accounted for in computing our decay curves. This is easily proved using the convolution theorem. For the case of a finite bandwidth exciting pulse, we modify the true Green's function by multiplying it by the band shape of the exciting pulse. Let us call this excitation function E(x). Then the amplitude of the time decay of this excited state is

$$\int_{-\infty}^{+\infty} e^{-i2\pi xt} \cdot G(x) \cdot E(x)\, dx = \mathfrak{F}[G(x)E(x)] \qquad (1)$$

By the convolution theorem, this transform of a product is a convolution of the transforms of each individual function in the product.

$$\mathcal{F}[G(x)\cdot E(x)] = \int_{-\infty}^{t} \bar{E}(t')\bar{G}(t-t')\,dt' \tag{2}$$

The upper limit of integration is established by the fact that our Green's function is causal, or retarded. We have used the notation

$$\bar{E}(t) = \int_{-\infty}^{\infty} e^{-i2\pi ft} E(f)df = \mathcal{F}[E(f)]$$

$$\bar{G}(t) = \int_{-\infty}^{\infty} e^{-i2\pi ft} G(f)df = \mathcal{F}[G(f)] \tag{3}$$

Thus, we see that by using a finite band of exciting light, we automatically include the finite time width that is implied by the uncertainty principle because of our use of the Fourier transform to calculate the time evolution.

In practical situations one seldom is able to obtain the minimum time duration that the uncertainty principle implies given a particular frequency bandwidth. The only source which can possibly achieve the minimum time duration is the mode locked laser. Flash lamps and even pulsed or Q-switched lasers do not approach the minimum time. In the mode locked laser the phases of all the emitters (modes) are fixed at a definite value because of the strong radiation field. Thus, the

emitters can interfere with each other giving rise to the short duration pulse. In other types of sources the phases of the emitters (or modes) are randomly distributed. There is no interference between emitters because they are not coupled to one another as in the mode locked laser. Thus, if used without any modifications, the results calculated by the methods described above and in reference [4] are not applicable to most conventional experiments.

In order to find the proper modification to bring our minimum uncertainty results in line with conventional experiments, it is important that a number of points are made clear. The first point to consider is that the Fourier transform of the Green's function gives one the time evolution of a "single" molecule after it has absorbed a "single" photon. These results are given in terms of probabilities which are presumably interpretable in terms of experiments involving many "single" molecules. Also, the Fourier transform of the exciting pulse energy band shape gives again a probability distribution of photons with time. Without any modifications the results of our calculations give the results for the best possible experiment limited only by the uncertainty principle. When the photon statistics are not the ideal minimum, we must modify our decay curves to take this nonideality into account. This modification again takes the form of a convolution. We presume that we can form a real life pulse from the minimum uncertainty pulse by adding together a number of minimum pulses each displaced slightly in time. We define a function D(t) which does this

displacement-addition process. Then, our observed emission decay $D_0(t)$ is given by the following convolution

$$D_0(t) = \int_0^t D(t-\lambda)\, \mathcal{F}_G(\lambda)\, d\lambda \qquad (4)$$

where we used the abbreviation

$$\mathcal{F}_g(\lambda) = \int_{-\infty}^{\infty} e^{-i2\pi x\lambda} \cdot E(x) \cdot G(x) dx \qquad (5)$$

After we present some model calculations using the minimum uncertainty pulse, we will present a few results using the above convolution procedure with a model D(t). These results are given in Section III D.

C. Nature of Excited State

The excited state which is initially prepared is definitely not a zero order state in the narrow band excitation case [2]. Our perturbation treatment has mixed the primary and secondary states of zero order into a new set of eigenfunctions which we shall call molecular eigenstates. Note that these "molecular" eigenstates also include the radiation field states even though we do not explicitly say so. What we have in effect done is couple the primary state to two sets of secondary states, the molecular continuum and the radiation field continuum. (See Ref. [7] for a more complete discussion.) These are true molecular eigenstates only in the sense that the zero order

Hamiltonian H_0 plus the interaction term V completely describe the molecule. A band in an absorption spectrum then corresponds to a superposition of a large number of these molecular eigenstates.

Now that we have generated our molecular eigenstates, the importance of the exciting bandwidth is seen. The exciting light acts as the selector of, or in Rhode's terminology [3], as a projection operator on the molecular eigenstates. The molecular eigenstates which participate in the observed resonance fluorescence are in part determined by the experimentalist. If he uses a broad band of excitation, then he excites all the molecular eigenstates generated by the interaction of the primary and secondary states. This is then equivalent to exciting the zero order primary state followed by radiationless "transition" to the secondary states [2] since the superposition of all the molecular eigenstates gives back the zero order states. This provides justification for the approximation that one band corresponds to one state, but only for this type of excitation. When we narrow the exciting band so that only a fraction of the generated molecular eigenstates are excited, their superposition does not give the zero order states. Any further discussion of the dynamics of this excited state must use the molecular eigenfunctions, not the zero order functions. Thus, when we refer to a state henceforth, we mean one of these molecular eigenstates unless otherwise specifically mentioned.

D. Nature of the Emission Process

Once the selected molecular eigenstates have been formed by the excitation process (which we still are assuming is a delta function in time), they begin to evolve in time. The time evolution of a single molecular eigenstate $|j\rangle$ is governed by the exponential factor $e^{-iE_j\hbar^{-1}t}$ where E_j is the energy of state $|j\rangle$. The time evolution of the total eigenstate is the sum over all the excited molecular eigenstates

$$\psi_{tot}(t) = \sum_{\substack{\text{Mol.}\\\text{Eig.}}} e^{-iE_j\hbar^{-1}t}|j\rangle. \tag{6}$$

The emission decay curve is then given by the expression $|\langle\rho|\psi_{tot}(t)\rangle|^2$ where $|\rho\rangle$ is the zero order primary state. For the cases with which we deal where there are an infinite number of eigenstates, this sum becomes a Fourier transform. Also, as shown in Ref. [4], the exponential operator can be changed into a Green's function with the final expression for the emission decay curve given by

$$|\langle\rho|\psi_{tot}(t)\rangle|^2 = \left|\frac{1}{2\pi i}\int_{-\infty}^{\infty} e^{-iE_j\hbar^{-1}t}G_{pp}(E')dE'\right|^2 \tag{7}$$

where G_{pp} is the diagonal element of the Green's function matrix corresponding to the primary state. Thus, Fourier transform process actually calculates the direct time evolution of the excited molecular eigenstates plus the interference terms between the molecular eigenstates. It is these interference terms which give the emission

decay its shape. One can get a qualitative idea of the decay of a particular absorption band by doing a rough Fourier transform mentally. If the spectrum has two main peaks, for example, one would expect a relative maximum in the decay curve for a time t such that $e^{-iE_j\hbar^{-1}t}$ has maxima coinciding with the maxima of the absorption spectrum. Also, all the higher harmonics of this particular time should be local maxima in the decay curve. This of course results in a beat decay as expected. More complicated features of the decay curves can be understood in this way.

It should be noted that in Eq. (7) both the real and imaginary parts of the Green's function are transformed. This is to be contrasted with the absorption coefficient formula [4] where only the imaginary part of G_{pp} is used. An alternative reasoning can be used to obtain the time evolution process. We expand each stationary state $|j\rangle$ in our zero order basis set,

$$|\gamma\rangle = C_{\gamma p}|p\rangle + \int d\lambda \rho(\lambda) c_\gamma(\lambda)|\lambda\rangle \tag{8}$$

We can then calculate the spontaneous emission probability (transition moment squared) as a function of time. Assuming that the exciting band is uniform, we get

$$\begin{aligned} |\langle 0|\underset{\sim}{\mu}\cdot\hat{\underset{\sim}{\varepsilon}}|\Psi(t)\rangle|^2 &= \int d\gamma |\langle 0|\underset{\sim}{\mu}\cdot\hat{\underset{\sim}{\varepsilon}}|\gamma\rangle|^2 e^{-i\gamma\hbar^{-1}t} \\ &= |\langle 0|\underset{\sim}{\mu}\cdot\hat{\underset{\sim}{\varepsilon}}|p\rangle|^2 \int d\gamma |c_{\gamma p}|^2 e^{-i\gamma\hbar^{-1}t} \end{aligned} \tag{9}$$

We have assumed that

$$|\Psi(0)> = \int d\gamma c_{\gamma p}|p> \tag{10}$$

Now the term $|c_{\gamma p}|^2$ represents the density of the primary state as a function of energy, thus

$$|c_{\gamma p}|^2 = -\frac{1}{\pi} \text{Im } G_{pp} \tag{11}$$

It appears that from this analysis one need only transform the imaginary part of the Green's function. On the other hand, the derivation of Eq. (7) is rigorous [8].

This apparent dilemma is resolved by understanding the physical nature of the real part of the Green's function. The classical problem of a driven, damped harmonic oscillator is very similar to the resonance fluorescence problem except for the assumption of an harmonic potential. The solution has been worked out many times (see Refs. [9] and [10]). The response of the system consists of an in-phase or so-called coherent response and a 90° out-of-phase (quadrature) or incoherent response. This is analagous to the real and imaginary parts of the Green's function. The net response is thus out of phase with the driving force with a phase angle given by the arctangent of the out-of-phase divided by the in-phase components. This latter property has some interesting consequences (see Section III E). When

one moves far away from resonance, the imaginary part of the response (and thus Im G_{pp}) goes to zero and one is left with only the real part. One can easily show that in this case the real part correctly gives the dispersion formula for scattering by virtual states [10]. This is the key point. The Green's function formalism thus gives not only the true absorption re-emission component of resonant fluorescence, but also the scattered light.

In truth, the above statement is not rigorously correct. The scattering near a resonance is not the normal virtual scattering used to derive dispersion formulas. It is in fact intermingled and coupled to the "absorption re-emission". Experimentally the two processes are inseparable. The power of the Green's function method is evident here. It allows us to unify the real experimental situation with the theoretical model by including all components of detectable light emission.

E. Effect of Excitation Bandwidth on Time Evolution

There are two effects which a finite exciting bandwidth has on our process. The emission decay curve, as we saw in Section B, is automatically a convolution of the time band shape of the exciting pulse and the time evolution of the Green's function. As was pointed out, this is the best experiment that one can do. Any use of time delta functions with finite bandwidth exciting sources in theoretical treatments bear only a small resemblance to what can be done in the laboratory and results thereof should be carefully used.

Secondly, as was pointed out in Section D., the bandwidth selects which eigenstates are to be excited. Obviously, the emission decay curve is greatly affected by this selection process since it is determined by the interference between the evolving excited states. Thus, when we excite a Lorentzian band with a broad band of exciting light such that all of the states are excited, the interference between these evolving states gives an exponential decay. If the bandwidth only selects part of the Lorentzian band, the resulting decay is of necessity nonexponential. The results of our model calculations show this quite clearly. Thus, this selection process is at the discretion of the experimentalist and he should be able to control the type of emission decay curve he wants, within the confines of the molecular Hamiltonian, by choosing the exciting bandwidth properly. Conversely, to observe nonexponential decays, he must carefully choose his exciting bandwidth to be able to observe them.

III. RESULTS

A. Details of the Calculations

In order to try to understand in more detail the decay curves corresponding to a particular spectrum (i.e., a Green's function), we restrict ourselves to the situation where there is only one discrete coupled level. There is also a constant coupled set of states which is necessary to take into account the radiation field states and any other

coupled continuum of levels that may be present. We use the relative units of reference [4] where all energies are given relative to the line width due to the constant coupled levels alone (the term $\pi W\rho^2$ in [4]). Time is measured in units relative to the lifetime of the state due to coupling with the constant density of sets. In some cases the constant density set of levels is the radiation field, so the units are measured relative to the radiative lifetime. For the most part we restrict ourselves to the minimum uncertainty-principle-width pulse discussed above. Finally, we calculate some decay curves with a nonminimum time duration pulse to see what effect this experimental situation has on the observation of nonexponential decays.

We use two different mathematical band shapes for our finite bandwidth pulses. The first is a simple Gaussian of varying width and position which is called henceforth a GA pulse. The second is the function describing the spectral output of a single order of a diffraction grating [11] which is henceforth denoted as a DG pulse. This expression is

$$\frac{\sin^2 \pi\frac{(x-x_0)}{W_1}}{W \sin^2 \frac{\pi(x-x_0)}{x_{BW}}} \tag{12}$$

where x is the energy variable, x_0 the center position of the exciting band, W its half-width (measured to the first zero), and x_{BW} is the bandwidth of the computed absorption spectrum. These two different

types of pulses are used to show what the differences are for different shaped pulses. Also, the Gaussian pulse should approximate the output of a mode locked laser, whereas the diffraction grating pulse should approximate those experiments utilizing a flash lamp (or other thermal source) and a monochromator for wavelength selection. Although there are differences in the details of the decays, the general conclusions for both types of bandshape are the same.

Since we compute the Fourier transform of the real and imaginary parts of the Green's function separately, we must properly recombine the real and imagainary parts of the transforms of each part in order to get the correct decay function. First the transforms of the real and imaginary parts of G are denoted by,

$$a^R_t + ib^R_t = \int_{-\infty}^{\infty} G_R(f)\, e^{-i\pi ft}\, df \qquad (13a)$$

$$a^I_t + ib^I_t = \int_{-\infty}^{\infty} G_I(f)\, e^{-i\pi ft}\, df \qquad (13b)$$

where $G = G_R - iG_I$ and the a's and b's are functions of t. This is correct for t>0. For t<0, the correct transforms are the complex conjugates (easily seen by replacing t by -t on the right hand side of Eq. (5)) of the above transforms. Proceeding for t>0,

$$|\mathcal{F}_g(t)|^2 = |\, a^R_t + ib^R_t - i(a^I_t + ib^I_t)|^2$$

$$= |a_t^R + b_t^I + i(b_t^R - a_t^I)|^2 = (a_t^R + b_t^I)^2 + (b_t^R - a_t^I)^2 \quad (14)$$

Notice that the minus sign indicates that there is some interference between the real and imaginary parts. For $t<0$,

$$|\mathfrak{F}_g(t)|^2 = |a_t^R - ib_t^R - i(a_t^I - ib_t^I)|^2 \quad (15)$$

$$= (a_t^R - b_t^I)^2 + (b_t^R + a_t^I)^2$$

The only difference between the two time regions is a difference in sign as indicated. This means we can compute the entire response function of the system to an excitation pulse which has a finite time duration. The zero of time in this scale corresponds to the maximum in the excitation function. Note we still have a causal Green's function. Negative time has meaning because our excitation function mathematically extends to plus and minus infinity. Thus, we can actually detect fluorescence before time zero.

One further note on the way the decay curves are plotted is in order. The maximum of each curve is assigned the arbitrary value of one. This allows for a convenient evaluation of the shape of different curves, but gives no indication of the relative magnitude of emitted light. To get a feeling for the latter, we have calculated the integrated area under the curves and collected these together with the maximum value in Table 1. This fact should be ever present in the

reader's mind when viewing the plots.

B. Constant Density of States

1. Exciting Band on Resonance, Variable Width

This case is illustrated in Fig. (1) where a Gaussian excitation pulse is employed. Because of the simplicity of this particular case, an analytical Fourier transform can be obtained. The Green's function is given by

$$G(f) = \frac{f}{f^2+a^2} - i\,\frac{a}{f^2+a^2} = \frac{1}{f+ia} \tag{16}$$

f is the frequency or energy variable and a is the (constant) linewidth ($a = \pi V^2 D_0$) [4]. The excitation function is given by

$$E(f) = e^{-f^2/b^2} \tag{17}$$

with b being the width parameter. Thus the Fourier transform, which is the decay function $\mathfrak{F}_g(t)$, is

$$\mathfrak{F}_g(t) = \int_{-\infty}^{\infty} \frac{e^{-f^2/b^2}}{f+ia}\, e^{-2\pi ft}\, df \tag{18}$$

By the convolution theorem this integral is a convolution of the Fourier transforms of each member of the product. These transforms are,

$$\bar{G}(t) = \int_{-\infty}^{\infty} e^{-i2\pi ft} G(f)df = \frac{1}{2\pi i} e^{-2\pi at}, \quad t \geq 0 \tag{19a}$$

$$\bar{E}(t) = \int_{-\infty}^{\infty} e^{-i2\pi ft} \cdot e^{-f^2/b^2} df = b\sqrt{\pi}\, e^{-\pi^2 b^2 t^2} \tag{19b}$$

Thus, the convolution is

$$\mathcal{F}_g(t) = C \int_{-\infty}^{\infty} \bar{E}(t')\bar{G}(t-t')dt' \tag{20a}$$

$$= C \int_{-\infty}^{t} \bar{E}(t')\bar{G}(t-t')dt' \tag{20b}$$

C is a constant factor and the upper limit in Eq. (20b) is due to $\bar{G}(t)$ being a causal, or retarded Green's function whose value is 0 if $t<0$. Putting in Eqs. (19a) and (19b) into Eq. (20b),

$$\mathcal{F}_g(t) = Ce^{-2\pi at} \int_{-\infty}^{t} e^{-\pi^2 b^2 t'^2 + 2\pi at'} dt' \tag{21a}$$

$$= Ce^{-2\pi at} \int_{-\infty}^{t} e^{+(\frac{a}{b})^2} e^{-(\pi bt' - \frac{a}{b})^2} dt' \tag{21b}$$

We now transform the integration variable. Let

$$\begin{aligned} t' &= t'' + \frac{a}{b^2} \\ dt' &= dt'' \end{aligned} \tag{22}$$

$$\mathcal{F}_g(t) = Ce^{+(\frac{a}{b})^2} e^{-2\pi at} \int_{-\infty}^{t-\frac{a}{b^2}} e^{-\pi bt''^2} dt'' \qquad (23)$$

The integral is closely related to the error function. Thus,

$$\int_{-\infty}^{t-a/b^2} e^{-\pi^2 b^2 t''^2} dt'' = \int_{-\infty}^{0} e^{-\pi bt''^2} dt'' + \int_{0}^{t-a/b^2} e^{-\pi bt''^2} dt'' \qquad (24a)$$

$$= \frac{1}{2}\sqrt{\frac{1}{b}} + \int_{0}^{t-a/b^2} e^{-\pi bt''^2} dt'' \qquad (24b)$$

When $t < a/b$, the upper limit of the integral is negative. This means the whole integral is negative since the integrand is positive definite, but the direction of the integration is negative. Thus, for times less than a/b^2, the amplitude of the decay has the form,

$$\mathcal{F}_g(t) = C' e^{-2\pi at} (C'' - C'''(t)) \qquad (25)$$

where C', C'' are constants and $C'''(t)$ is a decreasing positive function of t. The net effect of this added term is to displace the maximum in the decay curve from time t = 0 to some later time. The response to $\bar{E}(t)$ is then time delayed with respect to the excitation pulse for the particular $\bar{E}(t)$ chosen. The physical reasons for this time delay will be discussed in a later section.

As t gets large, the function $C'''(t)$ varies less rapidly than for short times. This effectively means $C'''(t)$ can be approximated by

a constant and the decay becomes exponential. This statement is only true if one views the decay curve over a limited time range. Over a very long time the decay is not purely exponential.

We now turn to the numerically calculated spectra, Fig.(1). They verify clearly the above analytical results. The time delay is present in all cases and follows the pattern that one would expect. As the width of the Gaussian excitation function increases, the magnitude of the delay decreases. In the limit of an infinitely wide excitation, i.e., an excitation which is a delta function in time, the time delay is small but nonzero. In practice this limit is, of course, never reached. Numerically, the band must be finite even without using an excitation function. So, in reality, the true excitation function is the Gaussian multiplied by a top hat rectangular function. When the top hat is much wider than the Gaussian in energy space, the time duration is much shorter than that of the Gaussian and can be ignored.

The degree of exponentiality in the decay curves is shown clearly in log plots of the above decay curves Fig., (3). None of the decay curves are purely exponential over the entire decay. From roughly 3.0 to 16.0 lifetimes the decay curves for all but the narrowest band case are quite linear. At longer times there is a gentle upward curvature. The curvature in the narrowest band case results from the relatively long time delay present there. As concerns the very long time part of the curves, the intensity of emitted light is down by roughly three orders of magnitude. This means that unless the

FIGURE 1 (Variable Width, Constant Density)

In all figures in this paper the spectrum is shown as a dashed line and the excitation function is shown as a solid line. The spectrum is a pure Lorentzian. The excitation band is a Gaussian with widths, top to bottom, 1.0, 2.0, 5.0, and 10.0 ξ, and position always on resonance.

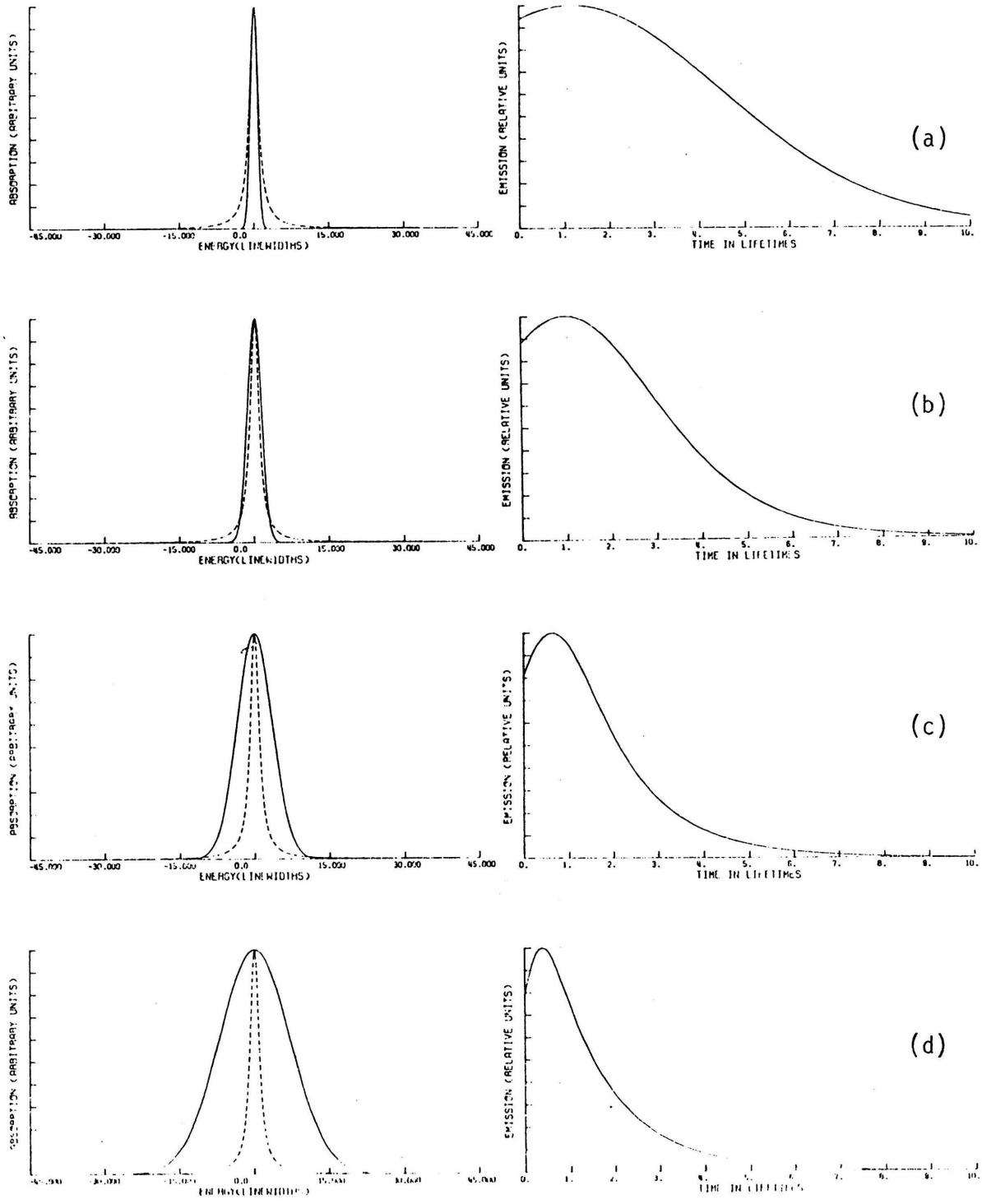
ABSORPTION (ARBITRARY UNITS)
-45.000
-30.000
-15.000
0.0
15.000
30.000
45.000
ENERGY(LINEWIDTHS)
EMISSION (RELATIVE UNITS)
0.
1.
2.
3.
4.
5.
6.
7.
8.
9.
10.
TIME IN LIFETIMES
(a)
(b)
(c)
(d)

initial intensity is great, noise may obscure an accurate determination of this part of the curve. Also, inhomogeneous effects such as collisions between molecules or collision with the walls, effects not included in this model, would distort the curves from the shapes calculated here for long times.

For even smaller bandwidths than used here, one would expect that the deviations from exponentiality would be greater. However, one factor to consider is that the smaller the bandwidth, the longer the time duration of the pulse. Then the meaning of a lifetime experiment becomes obscure since the experiment is measuring the time duration of the pulse as much as the response of the molecular system to the pulse. The limit to keep in mind, which illustrates the difficulty, is the case of a delta-function-in-energy excitation. This means that the time duration of the excitation is infinite. Obviously, no lifetime can be measured.

2. Constant Energy Bandwidth of Excitation, Variable Position

The linear plots, Fig. (2), of the decay curves do not show a marked effect due to variable position. The time delay decreases as the excitation band moves off resonance and disappears completely in Fig. (3d). The decay curves, especially Figs. (3a) and (3d) look like Gaussian functions, but this is difficult to state with the limited time range of these plots. Fig. (3b) is a logarithmic plot of the

FIGURE 2 (Variable Position, GA, Constant Density)

The spectrum is a pure Lorentzian. The Gaussian excitation bandwidth is 1.0 ξ and the positions are, top to bottom, 1.0, 2.0, 3.0, and 5.0 ξ respectively.

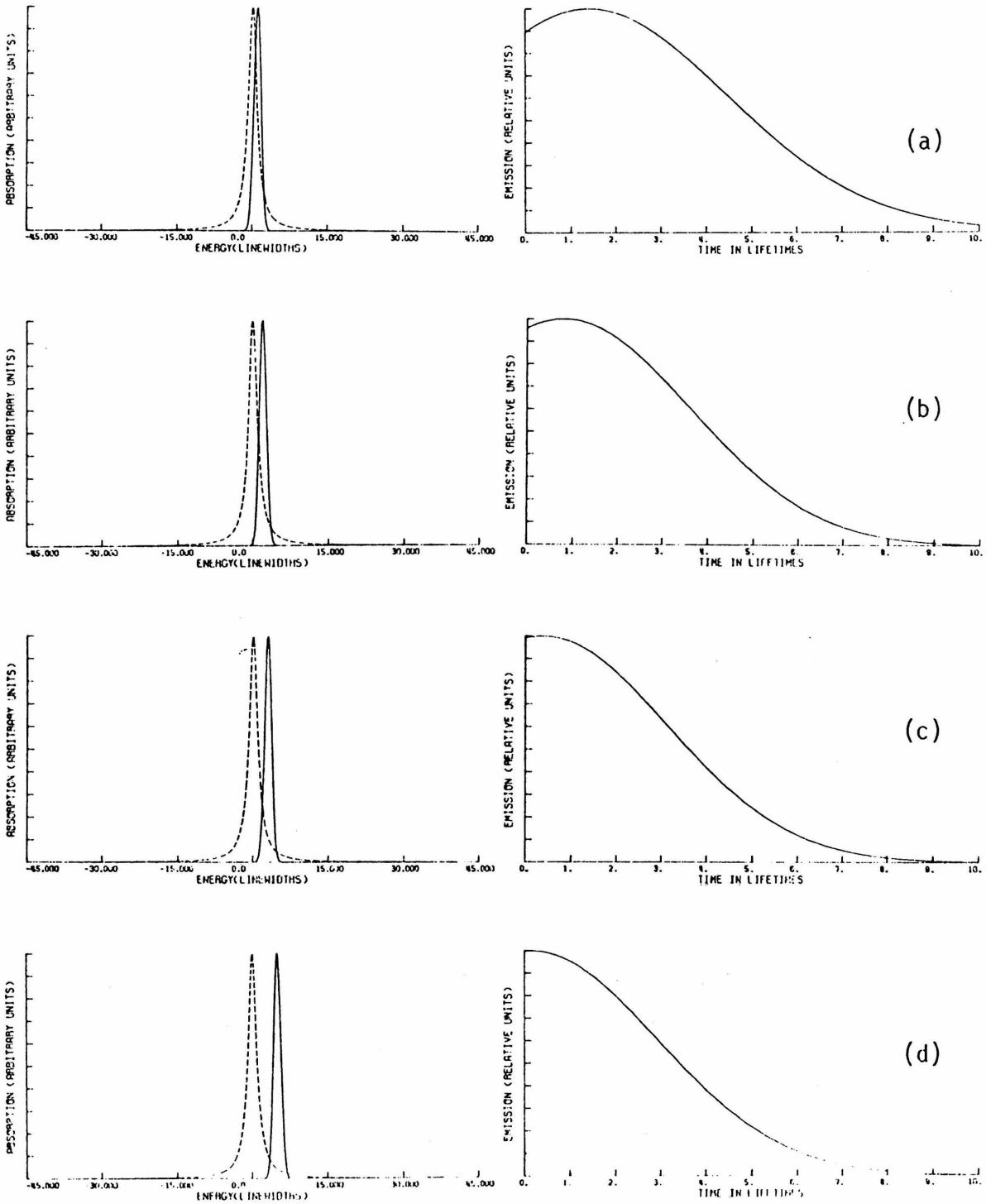
ABSORPTION (ARBITRARY UNITS)
-45.000
-30.000
-15.000
0.0
15.000
30.000
45.000
ENERGY(LINEWIDTHS)
EMISSION (RELATIVE UNITS)
0.
1.
2.
3.
4.
5.
6.
7.
8.
9.
10.
TIME IN LIFETIMES
(a)
(b)
(c)
(d)

decay curves of Fig. (2) on a longer time scale. It reveals much more about the form of the decay curves than the linear plots. The last two plots show that the decay curve is essentially a Gaussian curve over 6-7 orders of magnitude. The first decay curve shows possibly a mixture of Gaussian and exponential decay curves. The curve starts to tail off like a Gaussian at around 12 lifetimes, but then it begins to straighten out and look more like a straight line exponential decay. It never becomes a straight line as a pure exponential should, but the decay curves in Fig. (3a) are not really straight lines either, and they should be very close to exponentials.

The interesting decay curve is the second one of Fig. (3b). The curve seems to show a beat at around 14-15 lifetimes. What has happened here is that the "effective" spectrum, i.e., the product of the excitation function and the true spectrum, has two peaks. One is the resonance peak of the spectrum which is multiplied by a small number due to the small value of the excitation function at that energy. The second is the point where the excitation function is a maximum. Thus, an "artificial" beat decay pattern has been created by the experimentalist in choosing his excitation function. One should note that the magnitude of the beat is small and in a real experiment may not be detectable. The log plots also give an indication of the intensity and relative yield of emission (see also Table 1). The expected pattern which is that less intensity in absorption results in less emission intensity is seen to be obeyed.

FIGURE 3 (Log Plots of Emission)

On the left hand side are the logarithmic plots of the decay curves of Fig. 1 to longer times. On the right hand side are the logarithmic plots of Fig. 2.

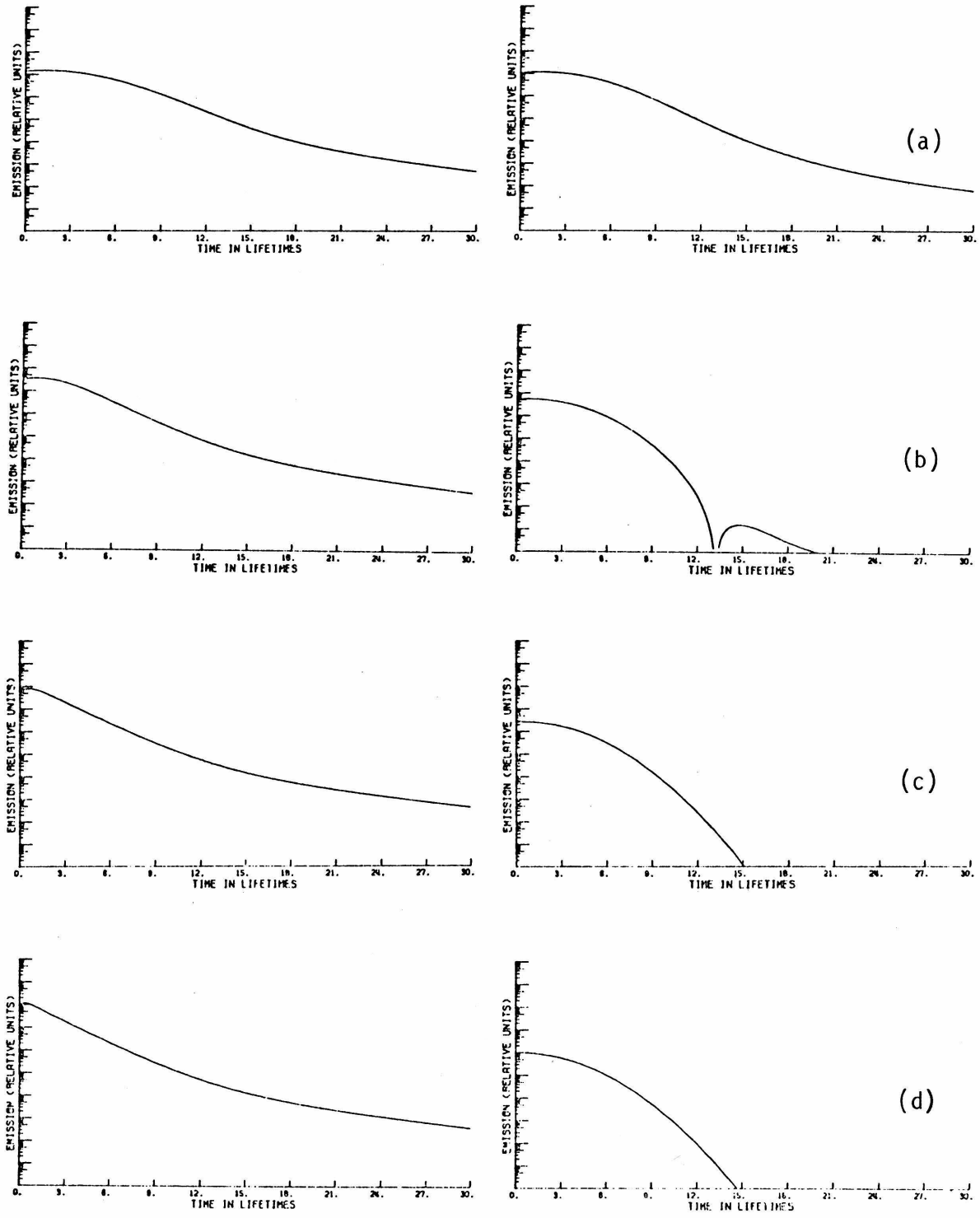
EMISSION (RELATIVE UNITS)
TIME IN LIFETIMES
0. 3. 6. 9. 12. 15. 18. 21. 24. 27. 30.
(a)
(b)
(c)
(d)

C. Line-Like Coupled Densities

1. Single Coupled Level at Resonance; Excitation on Resonance, Variable Width

The situations where there is one coupled level on resonance are not amenable to analytical solution. Thus, we rely solely on the numerical results. For all spectra dealt with here, the coupled level parameters are as follows: position = 0.0, width = 0.5 linewidths, coupling strength = 20.0 linewidths. This results in the splitting pattern depicted in Figs. (4) and (5). The doublet is the expected pattern from second order perturbation theory. The small peak comes from the higher order terms in the expansion of the Green's function [4]. The decay curves are dominated by the doublet in most cases.

Turning to the decay curves, we use both the DG pulse and the GA pulse. The spectrum of our present case is one in which a beat decay would be expected to occur. For excitation bandwidths narrow enough so that the two peaks of the doublet are only weakly excited, the beats may be missing or very weak. This is indeed the observed situation and is especially apparent with the GA pulse plots, Fig. (4). In Figs.(4c) and (4d) the beats in the decay are very strong because in these cases the doublet is strongly and uniformly excited. One can easily see that the beat positions do not change very much because the positions of the spectral peaks remain fixed. A detailed viewing of the plots however shows that the beats do shift very slightly closer

FIGURE 4 (Variable Width, GA, Level in Resonance)

There is one coupled level with position at 0.0 ξ, width of 0.5 ξ, and coupling strength of 20.0 ξ. The excitation band position is 0.0 ξ, and the widths are, top to bottom, 0.5, 2.0, 5.0, 10.0.

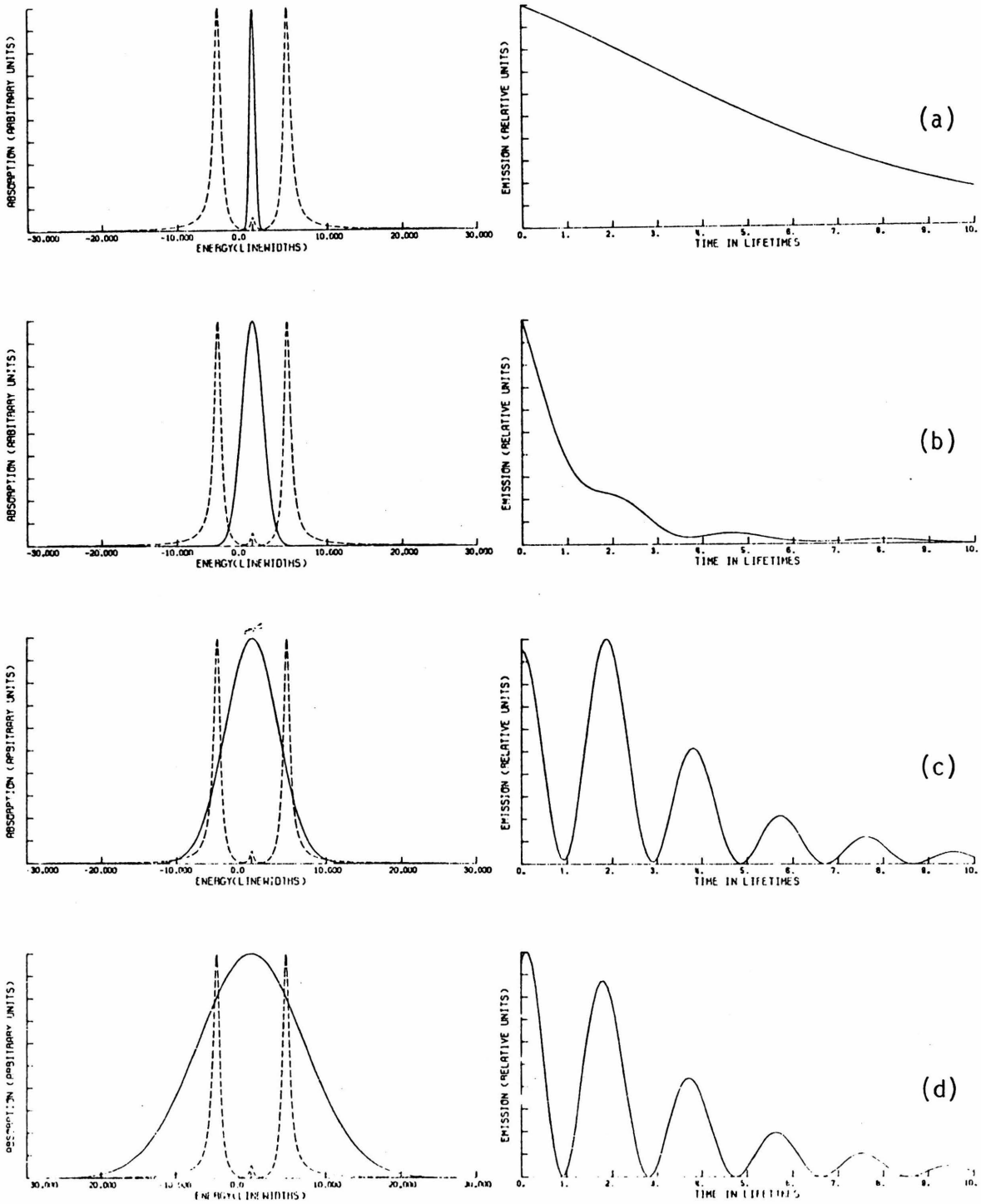
ABSORPTION (ARBITRARY UNITS)
ENERGY(LINEWIDTHS)
EMISSION (RELATIVE UNITS)
TIME IN LIFETIMES
(a)
(b)
(c)
(d)

with increasing bandwidth. This is due to the excitation function "effectively" shifting the peaks slightly. One curious feature is that in Fig. (4c) the second beat is higher than the first. The most reasonable explanation of this seems to be that the time delay observed with the constant density case comes into play and reduces the first beat relative to the second. See Section III E for a further discussion.

The DG pulse plots resemble the G pulse plots except for a few details. One must remember that when the width parameters for the DG pulse (first zero) and the G pulse (1/e of maximum) are equal, the main peak of the two functions is not roughly the same width. Thus, for example, Fig. (5d) resembles Fig. (4c) more than Fig. (4d). This should be clear from the plots of spectrum and excitation function. There are some extra peaks in Figs. (5a) and (5b) and even (5c) as compared to Fig. (5d), the latter of which should be mostly the spectrum determined decay curve. These are due to the side peaks in the excitation function itself. Actually, as indicated in Table 1, these beats are very weak compared to those due to the spectrum. Thus, in Fig. (5c) the extra peaks are very weak and in Fig. (5d) they are missing completely. The lack of really strong beats in Fig. (5c) is due to the coincidental position of the first zero of the excitation pulse and the two peaks of the doublet.

Table 1 gives the value of the maximum of the decay function and the integrated areas under the decay curve. This gives one an indication of the emitted intensity for each decay curve since, as mentioned in

FIGURE 5 (Variable Width, DG, Level in Resonance)

Same spectrum as Fig. 4. The position of the excitation band is 0.0 ξ and the widths are, top to bottom, 0.5, 2.0, 5.0, and 10.0.

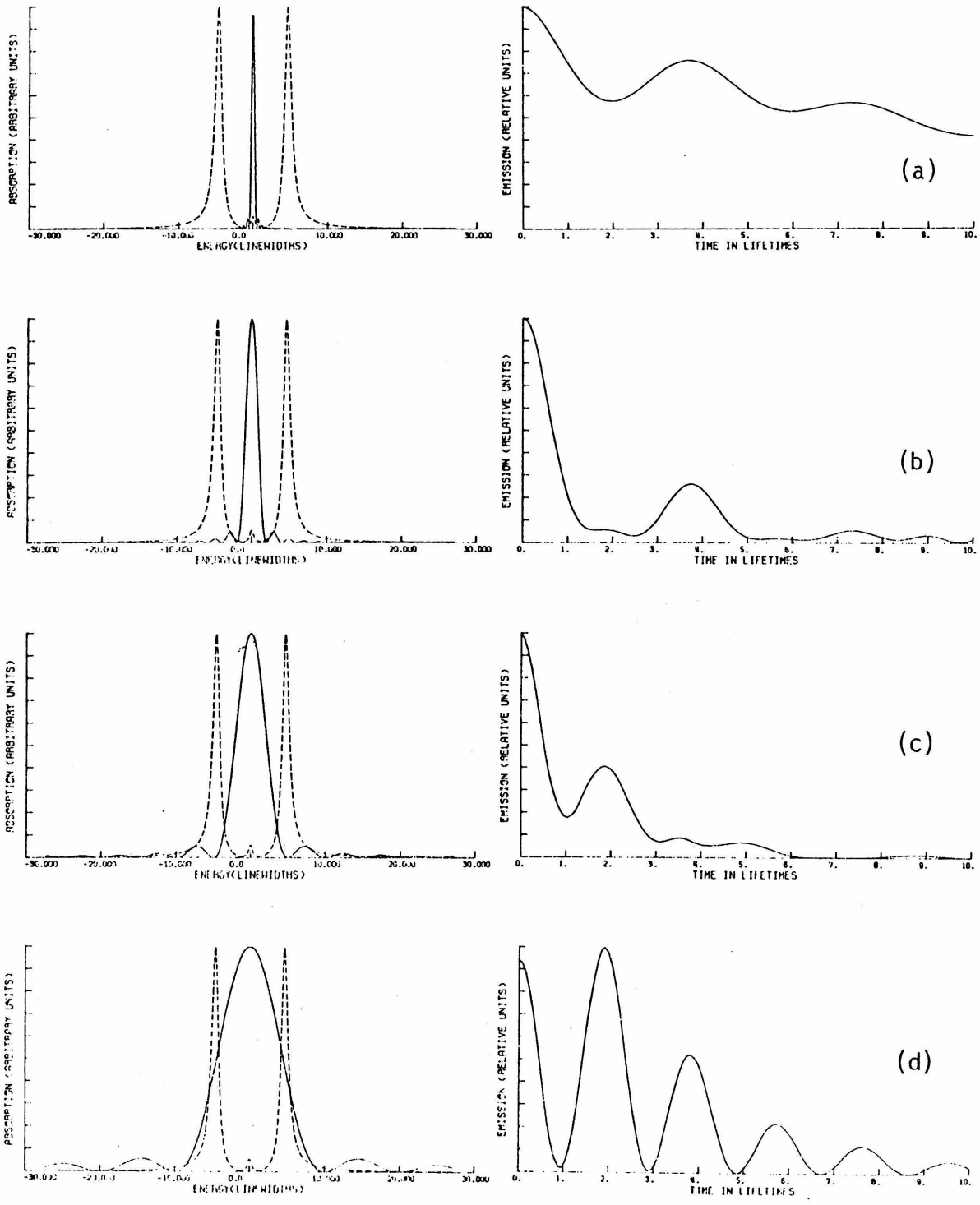
ABSORPTION (ARBITRARY UNITS)
-30.000
-20.000
-10.000
0.0
10.000
20.000
30.000
ENERGY(LINEWIDTHS)
EMISSION (RELATIVE UNITS)
0.
1.
2.
3.
4.
5.
6.
7.
8.
9.
10.
TIME IN LIFETIMES
(a)
(b)
(c)
(d)

Section III A, no feeling for this can be obtained from the plotted decay curves.

2. Single Coupled Level in Resonance, Constant Width and Variable Position.

For this series of plots we plot only the GA pulse curves. They are illustrated in Fig. (6). The most interesting feature of this series is the dependence of beat appearance on the excitation of both peaks of the doublet spectrum. This was mentioned previously, but is made very clear in these decay curves. The intensity of the beats diminishes quite markedly as the excitation band moves to the right thereby exciting primarily the peak on the right. The last decay curve shows no beats at all resembling the decay curves of Fig. (1). The maxima and integrated intensities show no unusual features. For this particular case it turns out that they are all of the same order of magnitude. One final comment on the time delay observed here is that one only sees a measurable delay when the excitation band is centered or is close to a large peak in the spectrum. See Section III E for a more complete discussion.

3. Single Coupled Level Off Resonance, Constant Position, Variable Width

The spectrum, Fig. (7), here shows again a triplet structure as did the spectrum when the coupled level was in resonance with the primary level.

FIGURE 6 (Variable Position, GA, Level in Resonance)

The spectrum is the same as Fig. 4. The excitation band has a width of 1.0 and the positions are, top to bottom, 2.0, 4.0, 6.0, and 8.0 respectively.

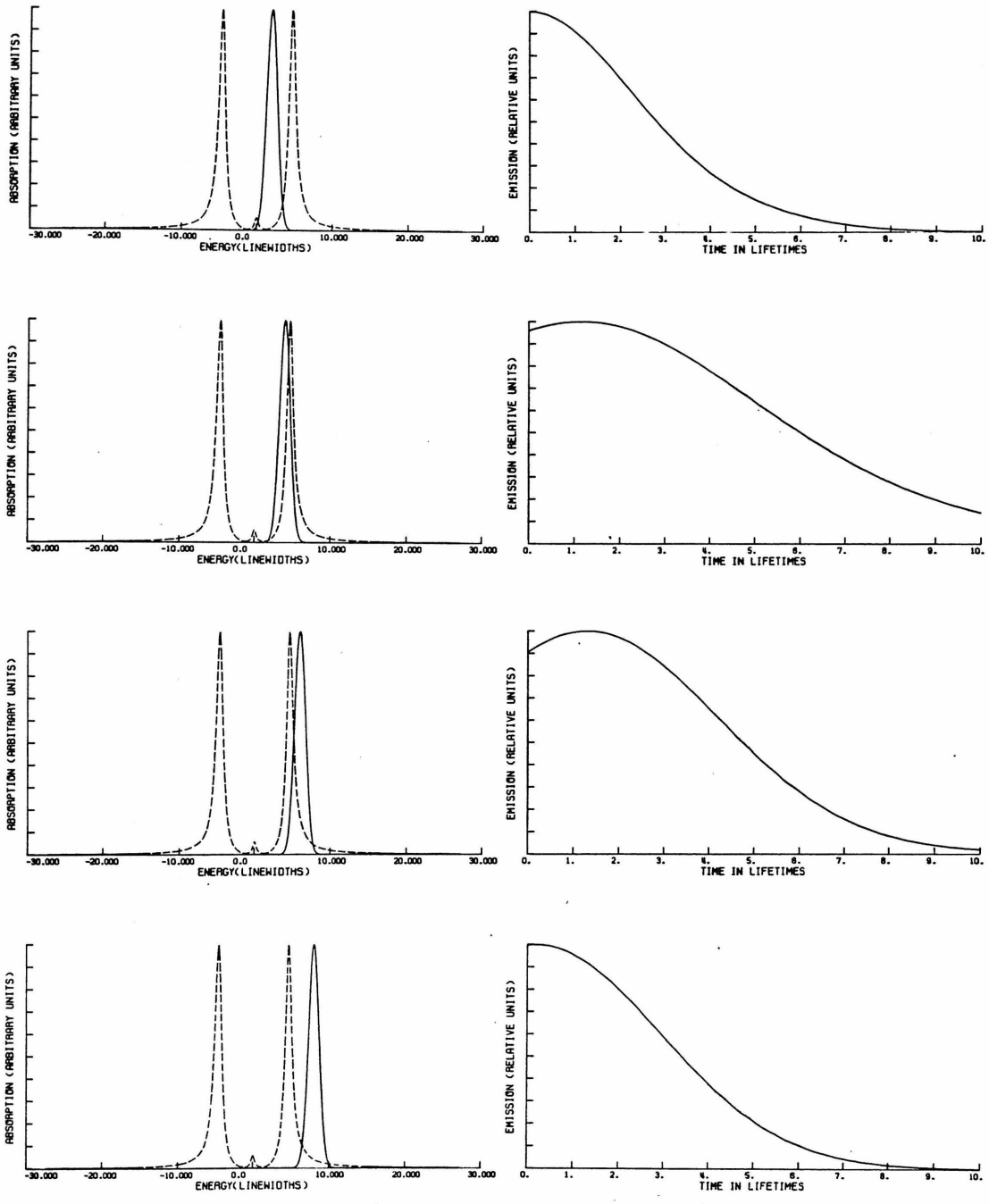
ABSORPTION (ARBITRARY UNITS)
-30.000
-20.000
-10.000
0.0
10.000
20.000
30.000
ENERGY(LINEWIDTHS)
EMISSION (RELATIVE UNITS)
0.
1.
2.
3.
4.
5.
6.
7.
8.
9.
10.
TIME IN LIFETIMES

FIGURE 7 (Variable Width, DG, Level Off Resonance)

The single coupled level is at 5.0 ξ, its width is 0.5 ξ, and its coupling strength is 10.0 ξ. The DG excitation band is positioned at 0.0 ξ and has widths, top to bottom, 2.0, 5.0, 10.0, and 20.0 .

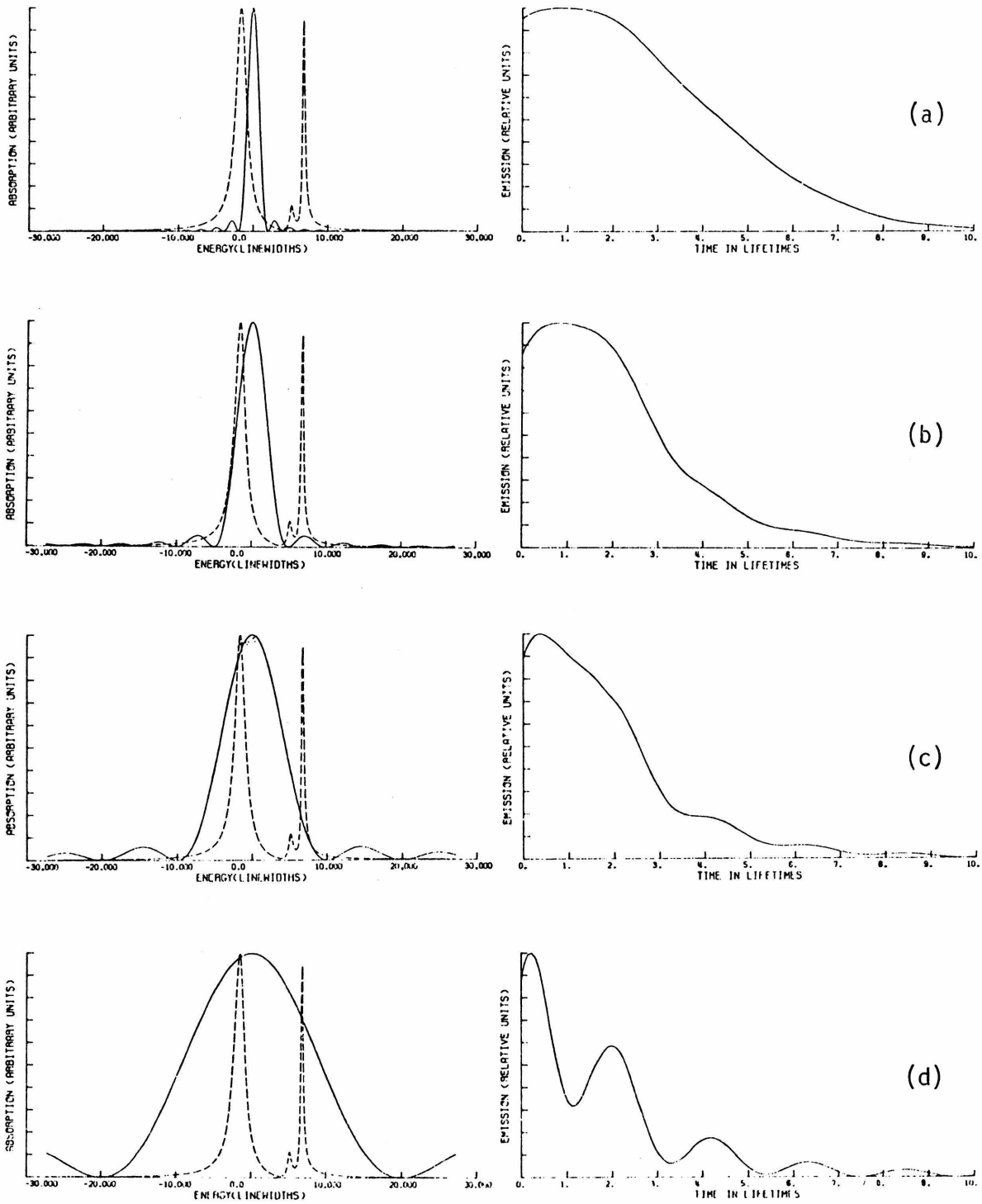
ABSORPTION (ARBITRARY UNITS)
-30.000
-20.000
-10.000
0.0
10.000
20.000
30.000
ENERGY(LINEWIDTHS)
EMISSION (RELATIVE UNITS)
0.
1.
2.
3.
4.
5.
6.
7.
8.
9.
10.
TIME IN LIFETIMES
(a)
(b)
(c)
(d)

The two major peaks are of about equal peak intensity, the level close to resonance being the broader line. It is these two lines that one would expect to appear using simple second order perturbation theory. The two levels, one at 0.0 and the other at 5.0 on our energy scale, interact and repel each other. One would calculate that these two levels should lie at the energies -3.1 and 8.1 on our energy scale using the interaction strength of 10.0. They do lie very close to these points. Thus, simple perturbation theory explains the major aspects of the spectrum. However, one can only rationalize the third peak using the higher interaction order terms. This third peak lies very close to the zero order coupled level position. If the coupling strength would be weaker, the third peak would not appear. The coupled level would then give rise to a line shape resembling the Fano line shape [12]. Only when the coupling strength is above a certain level does the single line split into a doublet. See Ref. [4].

The calculated decay curves reflect most of the trends which have been previously noted in the foregoing discussion. The very weak beat structure appearing in Figs. (7a) and (7b) is most likely due to the side bands of the excitation function with a little assistance from the spectrum. In Fig. (7c), the spectrum is being excited more uniformly and the beats are getting stronger. Finally, in Fig. (7d) we see strong beat structure as both major peaks are strongly excited. The maxima and integrated intensity all increase as the bandwidth increases. They are all of the same order of magnitude (Table 1).

4. Single Coupled Level Off Resonance, Variable Position, Constant Width

Again, the decay curves for this case, Fig. (8), are understood by the same principles outlined before. To get beats, both peaks must be excited, Fig. (8b). Otherwise one sees merely a monotonic decay, Figs. (8a), (8c), (8d). From a close inspection of the spectra and excitation function for Fig. (8c) and (8d), one would guess that beats due to the weak third peak and the strong peak should appear. In fact they are present, but they do not occur within the 10.0 lifetimes of the plotted decay curves. Also, they are very weak because of the difference in the size of the two peaks excited and are almost unresolvable. Integrated intensities and maxima obey their relationship noted earlier with the magnitude of excited absorption intensity.

D. Nonminimum Time Excitation Pulses

The results to be presented here are based on the discussion in the latter part of Section II A (Eqs. (4) and (5)). The D(t) used in these calculations is defined as follows:

$$\begin{array}{ll} 0.0 & t<\tau_1 \\ 1.0 & \tau_1 \leq t<\tau_2 \\ \dfrac{t}{\tau_2} & \tau_2<t\leq 0 \\ 0.0 & t>0 \end{array} \qquad (26)$$

This crudely approximates a real excitation pulse which can be relatively long compared to the decay time, but has a short cutoff compared to the decay time. Naively, one might expect to be able to

FIGURE 8 (Variable Position, DG, Level Off Resonance

The spectrum is the same as Fig. 7. The DG excitation width is 1.0 ξ, and its position is, top to bottom, 0.0, 2.5, 5.0, and 7.5 ξ respectively.

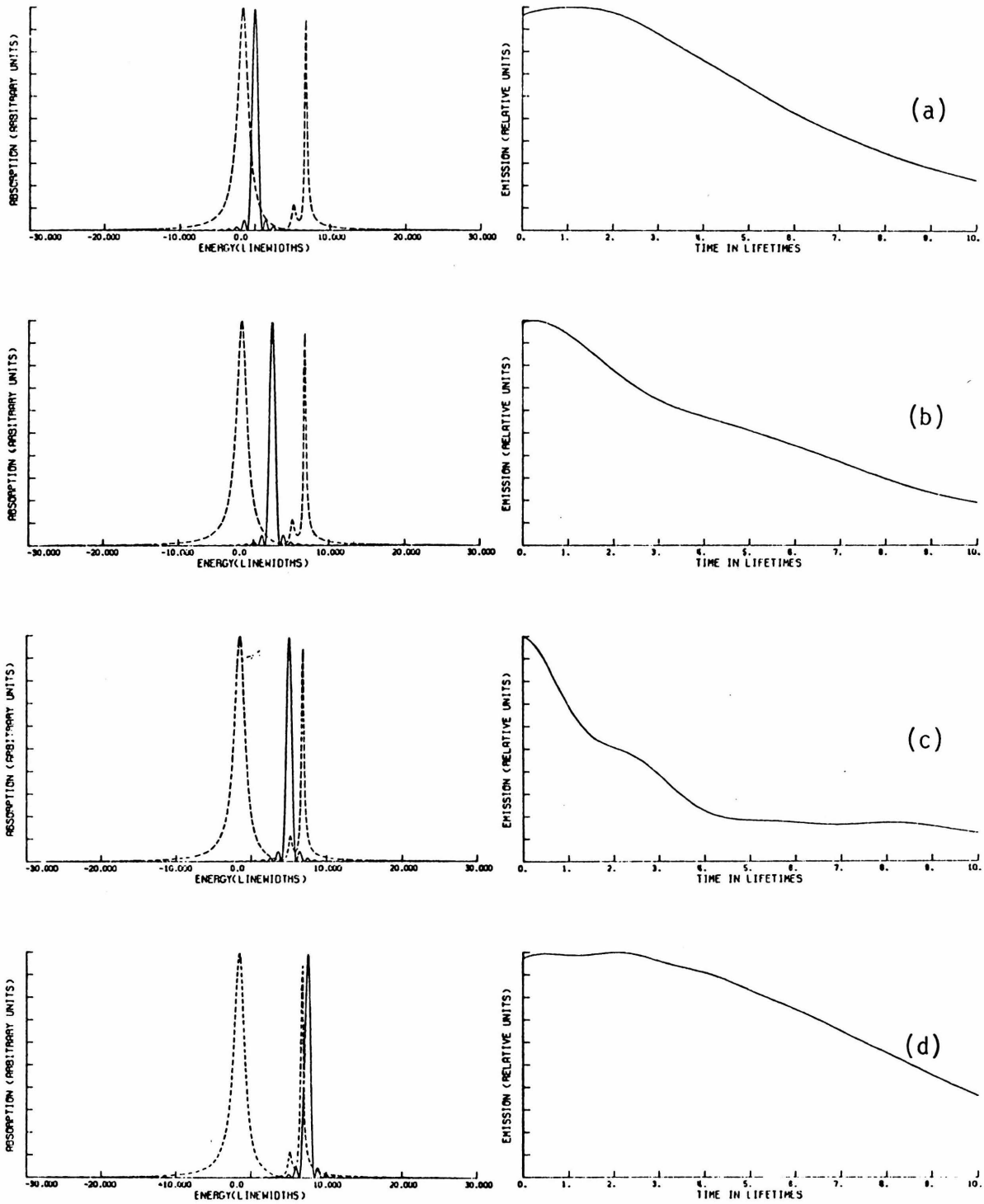
ABSORPTION (ARBITRARY UNITS)
-30.000
-20.000
-10.000
0.0
10.000
20.000
30.000
ENERGY(LINEWIDTHS)
EMISSION (RELATIVE UNITS)
0.
1.
2.
3.
4.
5.
6.
7.
8.
9.
10.
TIME IN LIFETIMES
(a)
(b)
(c)
(d)

view the decay time because of the sharp cutoff. One can certainly get results out of such an experiment, but, as we show here, they are not necessarily the results one desires. Before beginning it should be noted that the above definition of D(t) introduces a slight shift in the time scale of the plots. Thus, sometimes beats may appear to be moving as the parameters of D(t) change. This is due solely to the particular definition of D(t) and the manner in which the convolution was computed, and is not physically real. The above D(t) was chosen to make computations as simple as possible.

Before proceeding to the actual plots, one important point regarding the units of time will be made. The units used, as noted before, are from Ref. [4]. There, time is measured in the reciprocal linewidth frequency due to interaction only with the radiation field. Thus, time is measured in units of the "radiative lifetime" which is different from the natural or observed lifetime. When both coupled continua are constant in density and coupling strength (i.e., the statistical limit), the units are not very important. The decays are generally exponential and a nonuncertainty minimum pulse does not distort this. However, when the molecular density is discrete, there is a subtle change which is significant. In these cases, the radiative bandwidth can be much larger than it appears from the absorption spectrum [7]. Then the time scale (i.e., the unit lifetime) is much shorter than one would expect from the linewidths observed in

the spectrum. The observed linewidths are due to the widths of the secondary coupled levels only, not to the radiative width of the primary level. The latter quantity is obtained only by fitting the observed spectrum to the lineshape formula [4].

The net result is that the possibility of observing nonexponential decays is crucially dependent on the knowledge of this primary radiative width, at least for the case where an incoherent or thermal light source is used. Thus, if one observes an exponential lifetime for such a system to be A seconds, and if the primary state radiative lifetime is say A/5 seconds then a pulse duration even as long as 0.5A will obscure most nonexponentiality in the decay curve. This is what we shall show in the following figures. Of course, if one uses an ideal uncertainty-minimum pulse, the above discussion does not apply. Then all one need do, as shown in the previous decay curves, is to make one's excitation band excite the multiple peaks in the spectrum. Beats will then be observed.

The plots on the left of Fig. (9) are the curve of Fig. (1d) with various D(t). The parameters are given in the figure. Very little change is noticed in the shape of the curves. This is because the curves are mostly exponential over this time range and the convolution process does not change this. The time delay seems to disappear, but it really is still present since the zero of the time scale should actually be farther to the left. The time delay is smeared out and is made more difficult to observe.

FIGURE 9 (Variable Time)

The left hand side uses the emission curve of Fig. 1d with τ_1 having the values, top to bottom, 0.075, 0.3, 0.54, 1.54 lifetimes, and τ_2 = 0.075, 0.23, 0.46, 0.46 lifetimes respectively. The right hand side uses the emission curve from Fig. 7d. τ_1 and τ_2 are as follows, top to bottom: τ_1 = 0.075, 0.3, 0.54, 1.54 lifetimes, and τ_2 = 0.075, 0.23, 0.46, 0.46 lifetimes respectively.

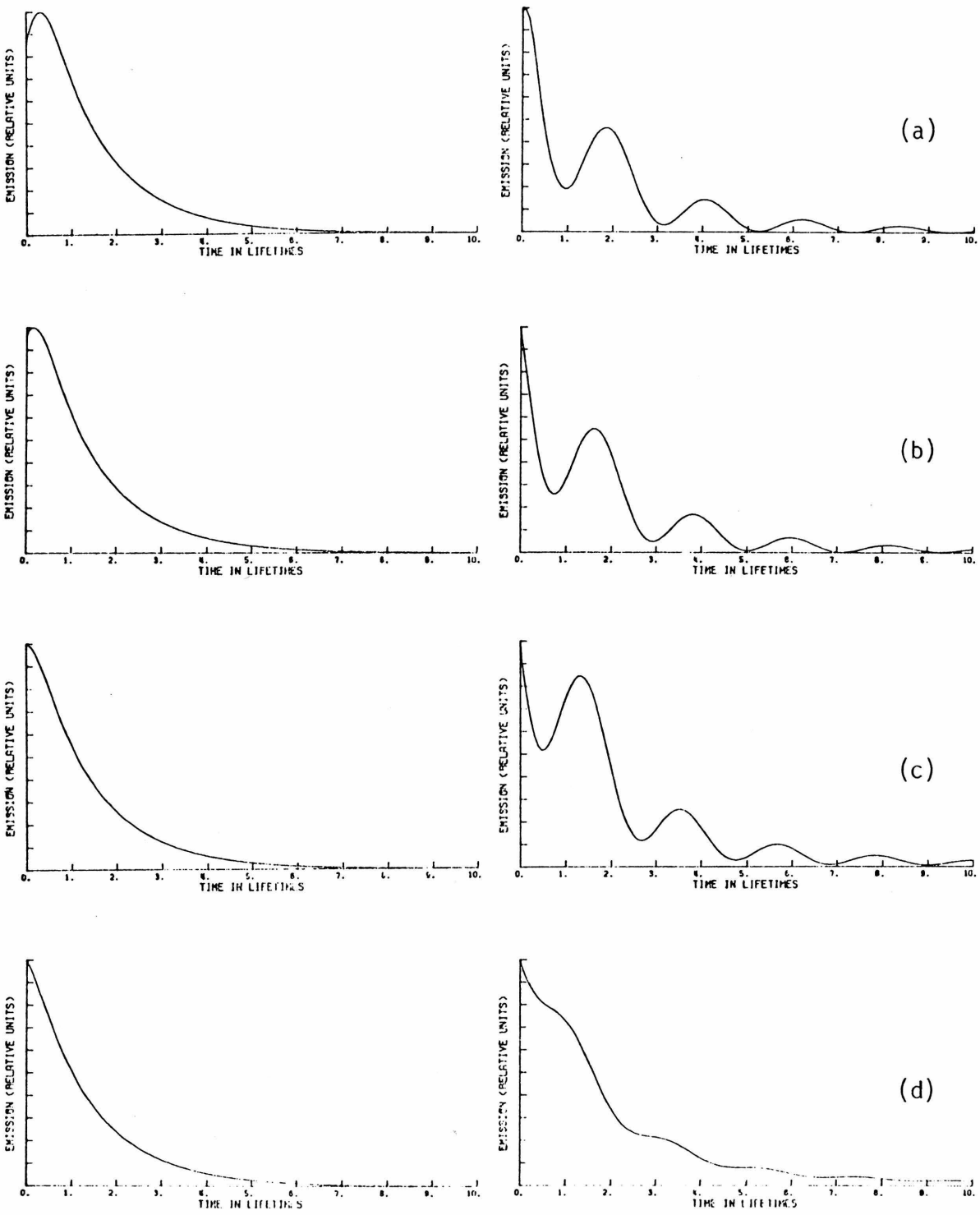
EMISSION (RELATIVE UNITS)
TIME IN LIFETIMES
(a)
(b)
(c)
(d)

The right hand side of Fig. (8) shows how pronounced an effect a nonuncertainty-minimum pulse has on a beat decay. This decay curve comes from Fig. (7d). The first three decay curves show strong beat structure. However, as the pulse width reaches two lifetimes, the beat structure is almost gone. If one had noise to contend with, the final curve may itself look like a perfectly smooth decay.

One further note about nonuncertainty minimum pulses is concerned with the integrated intensities and intensity maxima of the decay curves. The wider the pulse width, the larger both of these quantities will be. Thus, one will not get an accurate measure of the absolute quantum yield by integrating the emission decay curve under these situations. Relative yields might be measured, but they are subject to a number of errors such as scattered light, constancy of D(t) from one experiment to another and the artificial determination of the zero of the time scale [13]. Quantum yield measurements are more accurately done using long time light pulses as discussed by Nitzan and Jortner [6].

E. Initial Rise in Fluorescence

In several of the spectra-decay curve plots presented above, there has been a noticeable initial rise in the fluorescence intensity. This is certainly not expected from the simple models which give rise to exponential or cosinusoidal modulated exponentials [14]. We will

now explore in detail the physical reasons for the occurrence of this phenomenon and comment on its significance.

There are several experimental factors which result in the appearance of the initial rise. From a survey of the decay curves contained in this paper, several of these factors can be observed. The first is that the excitation band must be centered around significant absorption intensity in the spectrum. See Fig. (2) for an example of this. Secondly, the width of the excitation band is related inversely to the rate at which the fluorescence rises. With a wide excitation bandwidth, the rise is rapid; with a narrow excitation bandwidth, the rise is slower. See Fig. (1) for an example.

The first of these observations is related to the question of the meaning of the real and imaginary parts of the Green's function and their transforms. As was previously shown, the real part corresponds to the in phase response and the imaginary part to the out of phase response of the molecule to the electromagnetic field. When both parts of the Green's function are non-zero, the response of the molecule has a time lag due to the non-zero phase angle of the response.

This is a fairly well-known phenomenon in the theory of scattering [15]. The reasoning is as follows: the initial state of the system at $t = -\infty$ consists of an incident wave packet (superposition of plane waves) and the molecule in its ground state. The final state of the system at $t = +\infty$ is a scattered wave plus the molecule in its

ground state. Now, as shown above, the scattered wave acquires a phase change in being scattered by the molecule due to a resonance. Following the treatment of Bohm [15] one can write the phase of the scattered wave as

$$\phi(p) = p\cdot\frac{x}{\hbar} - E\cdot\frac{t}{\hbar} \tag{27}$$

where p is the momentum, x the position, t the time and π the phase of the scattered wave. Taking the derivative with respect to p, setting this equal to zero and solving for x,

$$x = -(\frac{\partial E}{\partial p})t - \hbar(\frac{\partial \phi}{\partial p}) = -\frac{p}{M}t - \hbar\frac{\partial \phi}{\partial p} = -vt - \hbar\frac{\partial \phi}{\partial p} \tag{28}$$

using the fact that $E = p^2/2m$ and $p = mv$. Thus, for a given position, x_0, the time delay in reaching x_0 compared to an unscattered wave is,

$$\Delta t_0 = \frac{\hbar}{v_0}(\frac{\partial \phi}{\partial p}) \tag{29}$$

Thus, we see that the time delay is a perfectly natural result from the theory of resonant scattering.

Goldberger and Watson [16] provide an additional discussion of the delay phenomenon based on Wigner's original concept of the lifetime of the scattering event. Physically, the time delay is viewed as the time that the photon takes to undergo a series of "scatters" off the resonance. The "series of scatters" is described diagramatically by the expansion of the Green's function [4]. This

process is similar to the one dimensional scattering of a wave packet off a square well potential [17]. As the wave packet reaches the well, it tends to rebound back and forth in the well before moving on. The photon wave packet does exactly the same thing in the "well" of the molecular resonance.

With this understanding, we can easily understand the two observations made earlier on the occurrence of the time delay. The phase angle of the response is given by

$$\phi(\varepsilon) = \tan^{-1}\left(\frac{\mathrm{ImG}(\varepsilon)}{\mathrm{ReG}(\varepsilon)}\right) \tag{30}$$

for a particular energy ε. The excitation function will select a range of energies over which one could compute an average π. If, in this range, the imaginary part is small with respect to the real part, the phase angle is small and the time delay short. The opposite is also obviously true. Since the absorption spectrum is proportional to ImG, peaks correspond to large values of ImG. ReG does not vary as rapidly or as much as ImG, so the peaks indicate a region of large phase shift and thus large time delay.

The second observation relating the width of the excitation pulse to the rate of rise is explained simply by a consideration of the uncertainty principle. Wide bandwidth excitation has a short time duration and thereby a quicker rise. Thus, the rise to the maximum in the decay curve is quicker. The delay times are different for

different width pulses since the average phase angle will change slightly. Thus, the first and second observations are intermingled. With a slightly wider band, the rise to maximum is faster, but the phase angle is slightly smaller and the time delay is thus a little shorter. See Figs. (1) and (2) for examples.

F. Positive and Negative Time Plots

Fig. (10) displays some example decay curves for both positive and negative times. The curves on the left of the Fig. (10) are those of Fig. (1). The progression is toward a wider bandwidth-narrower time pulse as one moves down the figure. The top curve shows very little effect of the actual decay in this time range since the excitation pulse time duration is roughly as long as the decay time. Only by going to longer times can one get a measure of the decay process. As the pulse duration becomes shorter, the curves become more asymmetric and move toward the limit of a delta function pulse followed by a long emission decay.

The right hand side of Fig. (10) displays the right hand side of Fig. (9). The dramatic loss of resolution of a beat decay is seen in the last curve. The apparent shift in time is due to the way D(t) was defined as discussed previously. It is interesting to note that the beats also appear before time zero.

With these curves we can see that there is a new way to do emission decay experiments. One merely starts the detection apparatus

FIGURE 10 (Full Time)

The left hand side shows the same curves as Fig. 1. The right hand side shows the right hand side of Fig. 9.

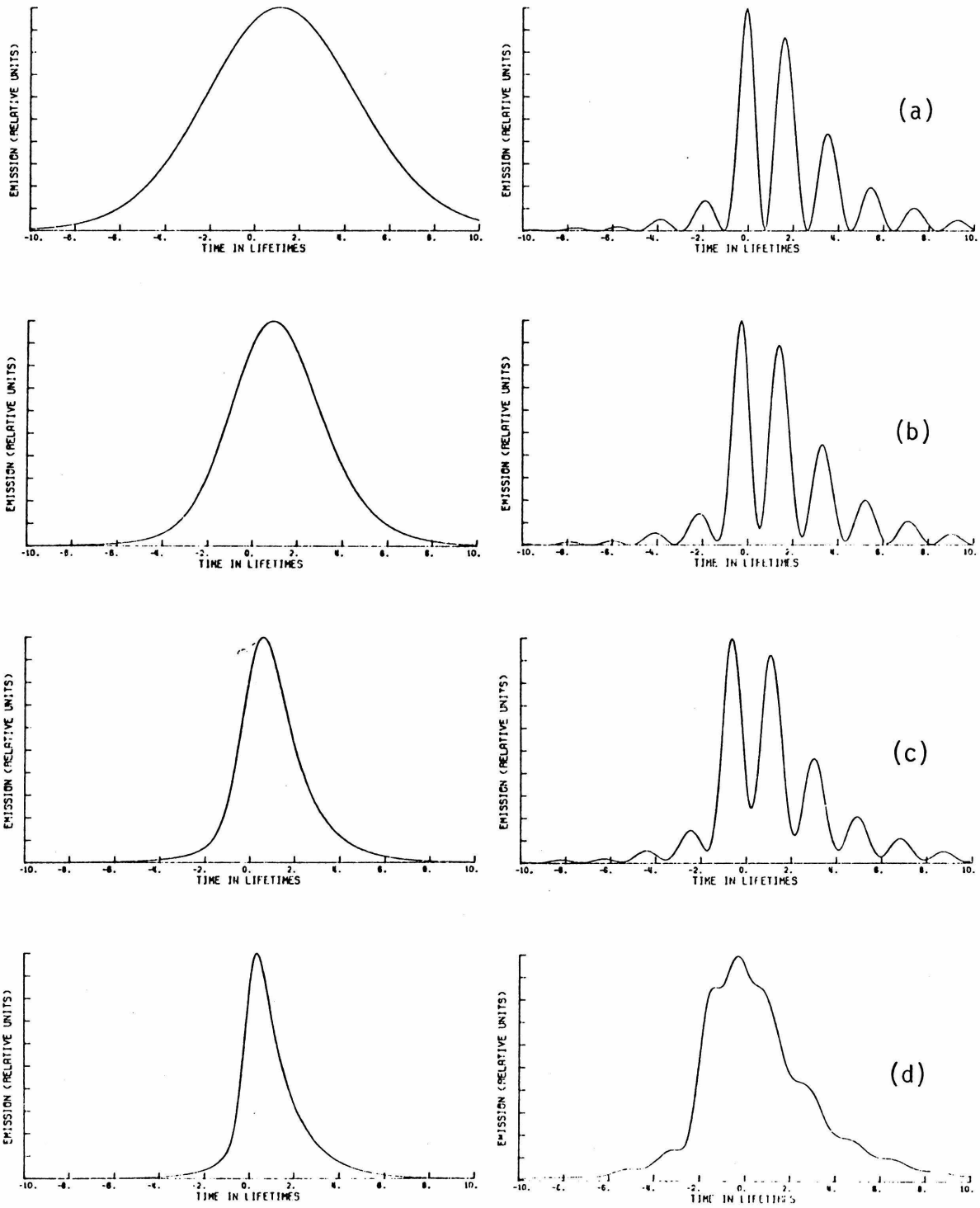
EMISSION (RELATIVE UNITS)
TIME IN LIFETIMES
(a)
(b)
(c)
(d)

before the pulse arrives at the sample and measures the entire pulse of emitted light. This removes the problem of deciding (artificially at best) where the excitation pulse stops and the decay starts. With our method of treating the decay problem, the distinction between resonance "scattering" and resonance "absorption-emission" is removed as it is in any real experiment. To get the true "molecular" decay function, one must deconvolute the finite pulse shape from the decay function.

IV. SUMMARY

This paper deals with the application of the Green's function technique to the study of resonance fluorescence from molecular resonances. In particular we apply the technique to the situation where the excitation bandwidth is finite and both the position and bandwidth are variable. For statistical limit cases where the product of secondary level density and interaction matrix element are constant, the resulting decays, upon using the above excitation band, are nonexponential in general, but in most cases are approximately exponential decays. For situations like the intermediate case where the secondary level density is "line-like", the possibility of a quantum beat decay occurs. It was shown that the observation of these beats is critically dependent on the experimentalist's choice of exciting light conditions. In particular he must choose his excitation

bandwidth and position properly, and, if using a nonuncertainty principle light pulse, he must regulate the time duration of the pulse in order to be able to see the beats.

Theoretically, we have shown that the Green's function method describes both scattered and absorbed re-emitted light which are of necessity experimentally indistinguishable. The presence of both real and imaginary parts of the Green's function results in their being a phase change or time delay in the response of the system to the light pulse. This is seen experimentally by a time delay in the emitted light as compared to the "free flight time" of light over the same distance. In addition, we have shown that the effect of using a finite bandwidth excitation is trivially accounted for in the Green's function method by multiplying the Green's function by the excitation function. The finite time duration of such a pulse is automatically accounted for in the Fourier transform process. We can also by this method compute the magnitude of emitted light from times before the maximum of the pulse arrives until long after it has arrived giving a complete picture of the time response of the system.

TABLE 1

		Maximum of Decay Curve[a]	Integrated Intensity[a]
Figure 1	(a)	0.150	0.802[b] (0.8148[c])
	(b)	0.360	1.316[b] (1.321[c])
	(c)	0.798	1.925[b] (1.929[c])
	(d)	1.188	2.226[b] (2.231[c])
Figure 2	(a)	0.1173	0.6150[c]
	(b)	0.0551	0.2333[c]
	(c)	0.0270	0.1022[c]
	(d)	0.0099	0.0357[c]
Figure 3	See Figs. 1 and 2 above.		
Figure 4	(a)	0.000079	0.00021[b]
	(b)	0.001587	0.00099[b]
	(c)	0.1674	0.1911[b]
	(d)	0.6983	0.7199[b]
Figure 5	(a)	0.000043	0.000129[b]
	(b)	0.00058	0.000357[b]
	(c)	0.0058	0.003659[b]
	(d)	0.2088	0.2366[b]

TABLE 1 (continued)

		Maximum of Decay Curve[a]	Integrated Intensity[a]
Figure 6	(a)	0.00013	0.00020[b]
	(b)	0.04273	0.13090[b]
	(c)	0.04748	0.11630[b]
	(d)	0.00958	0.01725[b]
Figure 7	(a)	0.05699	0.1309[b]
	(b)	0.2989	0.5081[b]
	(c)	0.5547	0.7690[b]
	(d)	1.031	0.9760[b]
Figure 8	(a)	0.01419	0.04503[b]
	(b)	0.00176	0.00466[b]
	(c)	0.00052	0.00082[b]
	(d)	0.00880	0.03362[b]

[a] The units are undimensioned but all are on the same scale. Absolute values mean nothing; only relative values have meaning.

[b] These integrated intensities are only for the portion of the decay curve which is plotted.

[c] These integrated intensities represent the entire decay curve including the portion not plotted.

REFERENCES

[1] Bixon, M., and Jortner, J., 1968, J. Chem. Phys., 48, 715.

[2] Kasha, M., Henry, B. R., and Rhodes, W., 1969, Proc. Nat'l Acad. Sci. U. S., 63, 31.

[3] (a) Rhodes, W., 1969, J. Chem. Phys., 50, 2885.

(b) Rhodes, W., 1971, Chem. Phys. Lett., 11, 179.

[4] Langhoff, C. A., and Robinson, G. W., 1973, Mol. Phys. (in press).

[5] Nitzan, A., and Jortner, J., 1972, Chem. Phys. Lett., 14, 177.

[6] Nitzan, A., and Jortner, J., 1972, J. Chem. Phys., 57, 2870.

[7] Langhoff, C. A., and Robinson, G. W., (in preparation)

[8] Zumino, B., 1961, in Lectures on Field Theory and the Many-Body Problem, E. R. Caianello, ed. (Academic Press), p. 37.

[9] Braddick, H. J. J., 1965, Vibrations, Waves, and Diffraction, (McGraw-Hill).

[10] Heitler, W., 1954, The Quantum Theory of Radiation (Oxford U. Press).

[11] Born, M., and Wolf, E., 1965, Principles of Optics (Pergamon Press), pp. 401-407.

[12] Fano, U., 1961, Phys. Rev., 124, 1866.

[13] Spears, K. G., and Rice, S. A., 1971, J. Chem. Phys., 53, 3160.

[14] (a) Robinson, G. W., and Frosch, R. P., 1962, J. Chem Phys., 37, 1962.

(b) Ibid., 1963, J. Chem. Phys., 38, 1187.

[15] Bohm, D., 1951, Quantum Theory (Prentice-Hall), pp. 257-261.

[16] Goldberger, M. L., and Watson, K. M., 1964, Collision Theory, (Wiley & Sons.)

[17] Schiff, L. I., 1968, Quantum Mechanics (McGraw-Hill), 108-109.

PART 5

THE INTERMEDIATE ENERGY GAP CASE AND THE SECOND SINGLET OF NAPHTHALENE IN DILUTE MIXED CRYSTALS

I. INTRODUCTION

Hoping to resolve a question concerning the assignments of the first two electronic transitions in naphthalene, in 1954 D. S. McClure investigated the spectrum of naphthalene in a durene host crystal [1]. The naphthalene goes into the crystal structure substitutionally and should closely approximate the oriented gas model. There are several advantages to this technique. First, the complication of rotational band structure is removed. Secondly, sequence structure, which is pronounced in gas phase naphthalene spectra [2], can be eliminated by going to liquid hydrogen or helium temperatures. Thirdly, polarizations of different electronic transitions can be isolated and overlapping transitions separated according to their polarization. McClure did find the correct assignments of the two singlets by being able to separate the two transitions by polarization.

A new problem arose, however, when he viewed the spectrum in the region of the second singlet. Instead of seeing a set of normally spaced vibronic transitions which would be assignable in terms of a harmonic oscillator with possibly anharmonic corrections, the lines were irregularly spaced and were described as a "forest of lines". This entangled spectrum was attributed to vibronic perturbations, but no quantitative explanation was offered. The key point to remember about this system is the small energy gap

($\sim$ 3000 cm^{-1}) between the first and second singlets. If the lower state interacts with the upper state, then the density of levels is so low in the region of resonance with the upper state that the spectrum would not be broadened as in the statistical limit [3], but would be split into numerous lines.

Some other examples of this type of splitting have recently been observed. The system quinoxalene in durene apparently shows the same effect [4]. Similar spectra have been observed for phenathrene in durene [5] and pyrene in biphenyl and fluorene [6]. Interestingly, there have also been reports on some anomalous emission properties in the region of the second singlet of naphthalene [7] and the pyrene derivative 3, 4 benzpyrene [8].. Also, some anomalous emission properties of benzophenone have been reported [9]. The emission in this case is from the first singlet which interacts with a very close ($\sim$ 2000 cm^{-1} separation) triplet level. These examples are also most likely closely related to the well known anomalous spectra of NO_2, SO_2, and CS_2 [10]. Thus, it is beginning to appear that these vibronically entangled systems are somewhat more common than was at first realized. The case of naphthalene is the most carefully documented and analyzed case yet reported. We will later analyze this case in greater detail. Before we proceed to do this, we will present a general discussion of the vibronically tangled electronic states and their emission properties.

II. GENERAL THEORY OF VIBRONICALLY TANGLED SYSTEMS

The first real theoretical discussion of vibronically tangled systems was presented by Douglas [10]. His arguments are mostly qualitative and are based on some results connecting the oscillator strength (which is proportional to the integrated intensity) of an absorption band to the lifetime of the state giving rise to absorption [11]. Douglas was principally interested in explaining the emission lifetimes observed in NO_2, SO_2, and CS_2. In these molecules, the lifetime is longer than estimates obtained from the oscillator strength of the transitions. His idea was that a set of zero order states could be postulated in which only one carried oscillator strength and all states interact by vibronic perturbations. The result is in Douglas's words, "The perturbations therefore have the effect of producing a spectrum in which there are a large number of weak lines instead of the expected smaller number of strong lines and the lifetime is correspondingly shorter." Bixon and Jortner [12] have formalized Douglas' arguments based on a model in which the levels carrying no oscillator strength are described by a "ladder" of equally spaced levels. Later, Nitzan and Jortner [13] used somewhat more rigorous mathematics and a more general consideration of the coupled levels to reaffirm the earlier results. All of these models are based on the premise that the lifetime of a state is related to the oscillator strength of the

transition. We will now examine this basic idea somewhat more thoroughly and show that it is not generally true.

Let us consider the following simple example: we are given an atomic energy level which carries oscillator strength from the ground state. There is no molecular continuum with which it can interact, only the radiation field continuum is present. When the line shape is calculated, it turns out to be the familiar Lorentzian. The absorption coefficient (or cross section) is equal to the following expression [14],

$$\frac{w^3}{2\pi\hbar c^3} |\langle g|\mu|E_0\rangle|^2 \cdot \frac{\gamma}{(\varepsilon-E_0)^2+(\pi\gamma)^2} \tag{1}$$

where $|g\rangle$ is the ground state, $|E_0\rangle$ the excited state, ε the energy variable, and γ is the width which is equal to

$$\gamma = \frac{w^3}{2\pi\hbar c^3} |\langle a|\mu|E_0\rangle|^2 \tag{2}$$

This, of course, means that the state obeys an exponential decay law with a lifetime equal to $\hbar\gamma^{-1}$. Since the Lorentzian is normalized, integration over the Lorentzian part of the line shape gives unity. Thus, the integrated intensity is proportional only to the transition dipole moment. Note also that the width of the level is proportional to the same quantity. Thus, by the uncertainty principle, the lifetime is inversely related to the width of the level which is in turn directly proportional to the oscillator

strength. This is the explanation of Mulliken's relationship [11]. If the transition moment is increased, the integrated intensity is increased. Also, the line is broadened and the lifetime is shortened. Thus, we see that the oscillator strength-lifetime relationship is obeyed here. We would expect the above model to hold for most low lying, nonpredissociated diatomic excited states also since the only interacting states here are the radiation field states. However, these are the only situations where the relationship would be expected to hold true. For polyatomics in general, the relationship is not valid as we shall show.

If one now amends the simple model by introducing a set of molecular quasi-continuum states, then any relationship between lifetime and oscillator strength is destroyed. In this case, the familiar statistical limit [3], the integrated absorption remains the same, but the linewidth is increased and the lifetime is shortened. Thus, the lifetime is dependent only on the shape of the line, not its integrated area. This is the interpretation that the authors have been advocating recently [15]. The problem that Douglas failed to realize is that, for polyatomics, the observed lifetime is a combination of several "component lifetimes" (or rates [16]). The oscillator strength gives us a measure of the radiative component. If there are "nonradiative" processes competing with emission, the observed lifetime reflects this competition and must change accordingly.

Now if we allow the molecular continuum to have structure, i.e., be line-like, we then arrive back at the situation where we started this discussion. These are the cases which Douglas [10] originally discussed. We see that the lifetime-oscillator strength relationship is not valid for the molecules Douglas discussed. The lifetime is not dependent only on the oscillator strength, but rather on the shape of the line. When a simple Lorentzian line is split up into a number of narrower lines by interaction with a line-like continuum, the lifetime must depend on the width of the narrower lines in the spectrum, not the net integrated intensity or oscillator strength. Since decay curves will not in general be exponential, we use the term lifetime somewhat loosely to describe the rapidity of the decay [15a].

Take the following limit of the Douglas model where the number of coupled levels is allowed to become very large. According to Douglas-Bixon-Jortner argument, the lifetime should get very long. However, this situation is approaching the statistical limit where the lifetime is known to be shortened. This limit illustrates the basic inconsistency of the treatment given by Douglas and Bixon and Jortner.

Based on our model calculations previously reported [15], we can illustrate some of these ideas. In the spectra shown in Fig. (1), we have one coupled level positioned at +5.0 linewidths. We vary the width of this level and excite it with a Gaussian pulse as shown. Then we look at the lifetime of the emission. Fig. (1a)

FIGURE 1

The spectra are shown as dashed lines, the excitation band as a solid line.

(a) Pure Lorentzian, Gaussian excitation with width 20.0 ξ, and position 0.0 ξ.

(b) The coupled level parameters are position = 5.0 ξ, width = 3.0 ξ, and interaction strength = 30.0. The Gaussian excitation band is positioned at 7.0 ξ, and has width 2.0 .

(c) Same spectrum as (b); excitation parameters are position = 0.0 ξ, width = 20.0 ξ.

(d) The coupled level parameters are position = 5.0 ξ, width = 1.0 ξ, interaction strength = 10.0 ξ. Excitation parameters are position = 7.0 ξ, width = 5.0 ξ.

(e) The spectrum is the same as (d); excitation parameters are position = 0.0, width = 20.0.

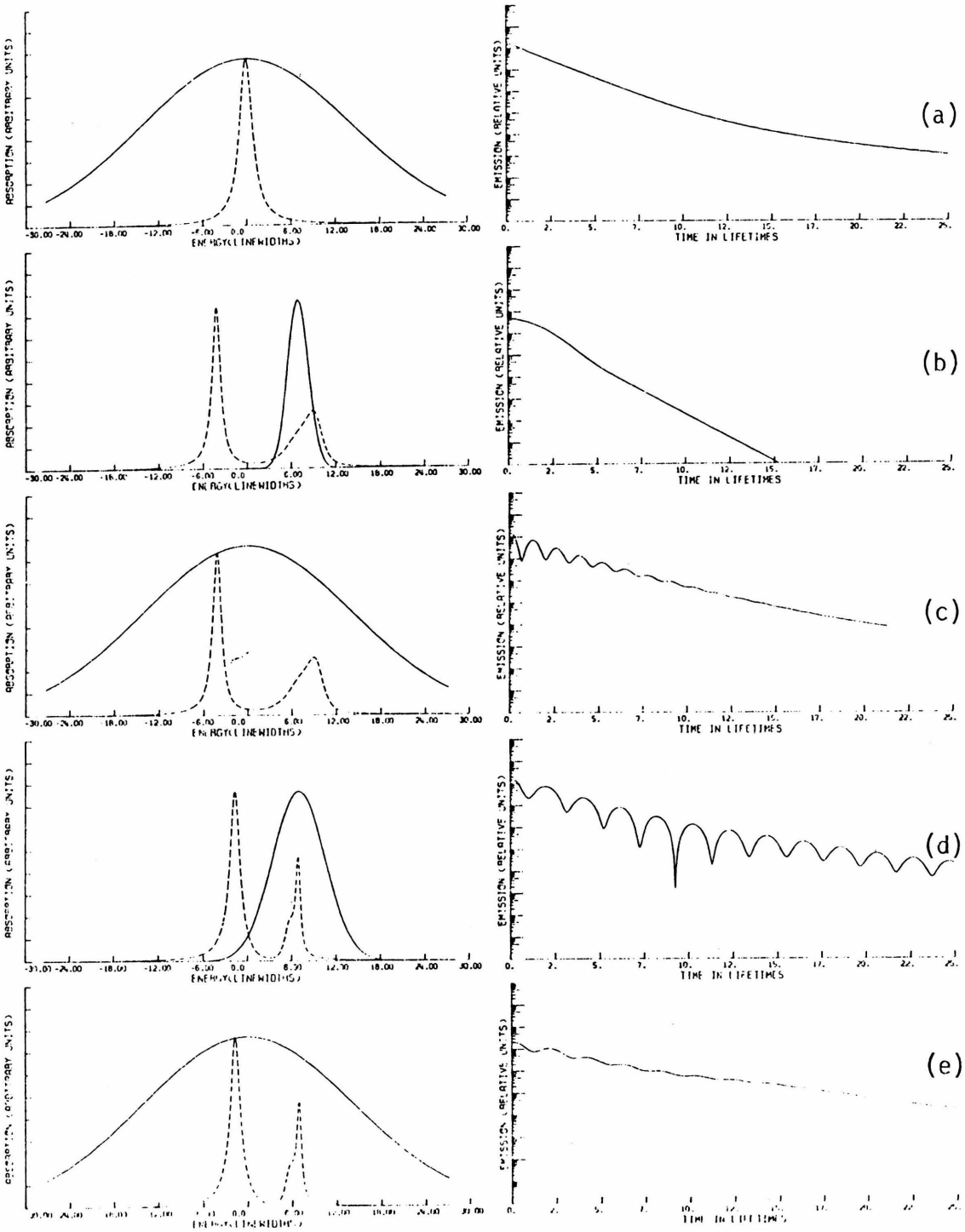
(a)
(b)
(c)
(d)
(e)
TIME IN LIFETIMES

is the plot of a pure Lorentzian with its corresponding decay curve. In Fig. (1b) the coupled level is wider (3.0 lifetimes) than the primary line, and the emission decay is thus faster than the pure Lorentzian. This level has only a fraction of the integrated intensity of the pure Lorentzian, but has a shorter lifetime. This is the opposite of the prediction by the "dilution of oscillator strength" theory. In Fig. (1d) the coupled level is the same width as the pure Lorentzian and has a slightly longer lifetime than the original primary state. Fig. (1c) and Fig. (1d) are plots of the excitation of the entire state. These are much different from the excitation of the isolated coupled level for now the primary peak is excited strongly. Thus, the lifetime here will be slightly longer than the original zero-order primary lifetime because the primary peak has been narrowed. Thus, we see that it is the shape of the resonance which determines the emission decay characteristics, not the integrated intensity of the spectrum. The latter only governs the radiative component of the lifetime and ignores contributions from intramolecular radiationless transitions.

III. THE NAPHTHALENE SECOND SINGLET SPECTRUM-THEORY

We will here only be concerned with the origin region of the second signlet and the totally symmetric additions to the origin.

Wessel [17] has treated, in addition, the low energy portion of the spectrum corresponding to the first singlet absorption which is vibronically induced by the second singlet. We will only be concerned with the c´ polarized (short molecular axis) absorption. In this polarization, which is apparently very pure, the first singlet ($^1B_{3u}$) has no oscillator strength and the second singlet ($^1B_{2u}$) has its oscillator strength only along this polarization. Any lines appearing must be due to intensity originating in the second singlet. In the gas phase, of course, both polarizations are mixed. In terms of model systems, the traditional canonical model [15] seems to be a very good representation for this system. See Refs. [1] and [17] for more detailed explanations of the experimental conditions and techniques.

A. Wessel's Treatment

We will now briefly explain Wessel's spectral fitting procedure so that we may compare it to our procedure later. The first approximation which Wessel makes is to assume that both zero order and final states have no width. Thus, he will compute a spike function for a state whose height is proportional to the integrated intensity of the corresponding peak in the spectrum. The position of the spike should be either at the maximum of a single spectral peak or the intensity centroid of a multiple peak. With this approximation he sets up a finite dimensional matrix of the

following form:

$$\begin{pmatrix} H(1,1)\cdots H(1,i)\cdots \\ \vdots \quad \ddots \quad \vdots \\ H(i,1) \quad\quad H(i,i) \\ \vdots \quad \ddots \quad \vdots \\ \end{pmatrix} \tag{3}$$

where only the first column, first row, and diagonal are nonzero. The diagonal elements are the energies of the zero order states with H(1,1) being the position of the $^1B_{2u}$ origin. The H(1,i)'s are the interaction energies between zero order states $|1\rangle$ ($^1B_{2u}$ origin) and $|i\rangle$ (higher vibronic level of $^1B_{3u}$). One then has to diagonalize the above matrix and find the eigenvalues. The eigenvalues then give the perturbed energy levels. By changing the various matrix elements in a trial and error procedure, the observed spectrum is fit by iteration. We will perform the same calculation, but we have allowed our zero order states to have width. Thus, we generate a true fit to the spectrum, not to just peak positions and integrated intensities.

One thing that must be done when using this method is to separate out "lattice" intensity from the $^1B_{3u}$ vibronically borrowed intensity. By lattice intensity we mean phonon combination bands associated with a vibronic transition. Thus, in a solid one may see a transition due to excitation of a pure molecular vibronic state, and also to the pure vibronic state plus one or more phonons.

The idea is the same as having symmetric normal mode additions to an origin band in the gas phase. Generally, these phonon "addition bands" are broad and lie to the high energy side of a vibronic transition. Wessel attempts to eliminate any contribution of this phonon intensity by drawing a baseline which touches the valleys in his spectrum. This eliminates supposedly the broad underlying intensity attributed to the phonon bands. While this seems perfectly reasonable, no one can say with certainty where the baseline should be drawn. If it is in error, the integrated intensities will be in error making the calculated results also in error. We do not feel that this procedure results in gross errors by any means, but it is an uncertainty in the calculation [19]. We use a different procedure which takes the phonon states into account. Thus, we do not have to do the type of baseline subtraction Wessel did.

In order to simplify the calculations, Wessel assumed that only the $^1B_{2u}$ origin contributes intensity. This neglects the possible contributions from the symmetric mode additions to the origin. We will do the same. This should not produce any serious errors in the calculated spectrum. First, we shall only be interested in the resonance region where contributions from other intensity sources should be minimal. Secondly, the $^1B_{2u}$ origin does carry about 70 percent more intensity than any symmetric addition peak, so it should be the major contributor to borrowed intensity anyway,

especially near resonance. Thirdly, if one does the multiple intensity source problem [20], it can be shown that one can mimic the multiple-source spectrum by a one-source spectrum, especially in a resonance region, or far away from all intensity sources. Thus, we should be able to calculate a spectrum which fits the observed spectrum.

By measuring the intensity of the $b_{1g}(8)$ mode of $^1B_{3u}$ (this is the lowest frequency mode which can borrow intensity), and by estimating the changes which occur in Franck-Condon overlap factors, Wessel estimated what the intensities of symmetric additions to the b_{1g} modes should be. In comparing these with the calculated intensities from the diagonalization, there are certain lines which appear to have abnormally low intensities. This he attributes to cancellation of the borrowed intensity from the $^1B_{2u}$ origin because of interference with the symmetric additions to the $^1B_{2u}$ origin. One can still calculate a correct spectrum, however. Once parameters are obtained, one may go back and compare the calculated intensities with the computed Franck-Condon envelope. If the two intensities disagree, appeal can then be made to the moment interference model. Thus, we see that the calculated parameters from the spectral fit are really the correct ones. It is then a question as to whether they are consistent with Franck-Condon overlap factors. Since this happens for only a few lines, this approximation is further reinforced [21].

One final comment about Wessel's calculations concerns his method of choosing the initial guess zero order states. He compares the resonance region in the p-xylene spectrum with the isoenergetic region in the durene spectrum. The lines which appear in the durene spectrum are corrected by a first order perturbation procedure to give zero order durene energy levels. The zero order coupling strengths are estimated from the square root of the intensity of a durene peak. These positions and strengths are the first guess in the p-xylene calculation. Because of solvent shifts in both vibrational and electronic states, this estimation procedure should not be too accurate. This is verified in Wessel's first calculation. It has the further drawback that unless one has a "durene spectrum" from which to estimate the zero-order states of a "p-xylene spectrum," one is at a loss to find a beginning. This apparently is why Wessel was not able to refine the durene spectrum. We shall use a different procedure which extracts guesses for the zero order states from the perturbed spectrum itself. Thus, we can fit any spectrum that we can measure, given enough patience and computer time.

B. Our Treatment

The Green's function technique that we shall use here has been discussed previously by the authors [15] and [22]. According to

this technique, the Green's function matrix is given by

$$\underset{\sim}{G} = [\underset{\sim}{G}^{-1}_0 - \underset{\sim}{V}]^{-1} \tag{4}$$

where G is the true Green's function, G_0 is the diagonal zero-order Green's function matrix, and $\underset{\sim}{V}$ is the interaction matrix between zero order levels. The perturbed energy levels are given by the poles of the Green's function. The poles are found by equating the determinant of $[\underset{\sim}{G}^{-1}_0 - \underset{\sim}{V}]$ to zero.

$$\det|\underset{\sim}{G}^{-1}_0 - \underset{\sim}{V}| = \varepsilon - E_1 - \sum_{i=2}^{n} \frac{|V_{1i}|^2}{\varepsilon - E_i} \tag{5}$$

where E_1 is the zero-order energy of the primary state, the E_i's the zero-order energies of the secondary states, and ε is the energy variable. Moreover, one can calculate analytically the secular determinant of Wessel's matrix (Eq. (3)), and it is seen to be exactly Eq. (5), which is to be solved for its various eigenvalues (zeroes). Thus, at this point we are doing the same mathematics as Wessel.

Now, we allow the secondary states to become continuous, the sum is converted to an integral over a density of states function, and the discrete V_{1i} becomes continuous functions of energy. Eq. (5) becomes [15],

$$\varepsilon - E_1 - \mathcal{P} \int d\lambda \rho(\lambda) \frac{|\langle E_1|V|\lambda\rangle|^2}{\varepsilon - \lambda} + i\pi\rho(\varepsilon)|\langle E_1|V|\varepsilon\rangle|^2 = 0 \quad (6)$$

By this transformation we have converted our finite, discrete matrix into a continuous, infinite matrix. This is the chief advantage to our method over Wessel's. Now we can include secondary state widths in the calculation, phonon bands if necessary, and continua including that from the radiation field or from other low-lying electronic states (most probably triplets). In addition, we now do not have to numerically diagonalize the continuous, infinite matrix (an impossible job!), for we have already analytically done so. The fitting procedure is a roundabout, but simple way of calculating the eigenvalues. The calculation of the absorption spectrum is straightforward since it is proportional to the imaginary part of the Green's function [15]. Our fitting procedure is to guess a weighted density function ($\pi\rho(\varepsilon)|V(\varepsilon)|^2$), calculate a spectrum, compare it to the observed spectrum, make changes in the weighted density, and repeat until a satisfactory fit is obtained. More will be said about the details of the calculation later.

The continuous weighted density function deserves some attention. Normally in theoretical treatments, the secondary states are assumed to be discrete, infinitely sharp states. This is in reality a crude approximation to the real physical situation. First, all states interact with the radiation field. This in itself is

enough to justify the continuous density assumption since the radiation field is a true continuum. Secondly, the presence of anharmonicities will broaden out vibrational levels. For low-lying levels, this breadth may be very small, but for higher vibrational levels where the density of interacting states (combinations and overtones) is higher, the breadth should be correspondingly larger. Finally, in our solid state example, the phonon structure of the lattice contributes even further breadth to vibronic states. From these factors we see that the continuous density function is not really an approximation at all, but is a realistic physical picture.

We assume that the weighted density function is composed of two parts. One is a constant continuum which is composed of several continua including radiation field and molecular continua from lower-lying molecular states. The second part is the set of discrete states composed of vibrational states of the $^1B_{3u}$ state which must have the symmetry b_1g. We define in our calculations the weighted-density as a sum of normalized Gaussians:

$$WD(\varepsilon) = \frac{1}{\sqrt{\pi}} \sum_{i=1}^{\eta} \frac{DEL_i}{W_i} \exp\left[-1/2 \left(\frac{\varepsilon-\varepsilon_i}{W_i}\right)^2\right] \qquad (7)$$

where ε is the energy variable, DEL_i the interaction strength, W_i the width, and ε_i the position of level i. The number of coupled levels is η. In a stepwise fashion, the zero order primary state is first broadened into a Lorentzian by the constant continuum

which is then split up into many lines by the discrete continuum.

Some care must be applied when interpreting this density function. In some regions the density will look like a set of slightly broadened discrete peaks. In these regions the interpretation as a set of slightly broadened vibronic states is valid. However, in some regions the density appears as a smooth function even though the region is really made up of the superposition of several individual "states". Here one may not necessarily be justified in assuming that the Gaussians are assignable as vibronic states. The region might just as correctly be assigned to phonon states. Such a judgement depends, of course, on the particular situation in question. In any case, the density function derived from a spectrum fitting calculation correctly describes the weighted density no matter what the zero order interpretation is given to it.

The spectra were fit by a trial and error procedure. The first guess at zero order positions was made by measuring the positions of the valleys in the spectrum. In some earlier work [15b] it was found that such a procedure gave very good estimates to the correct zero order positions if the energy shift term was ignored. It turns out that this guess also provides a reasonable first choice for the correct calculations. The changes to be made are estimated visually using intuition as a guide. This intuition is built up after many hours of tedious laboring over differences between calculated and observed spectra. It often

was a considerable help to compare the weighted density function with the calculated and observed spectra. Some of these points will be illustrated as we discuss the individual spectra.

The calculations were performed in the reduced units of Ref. [15a]. The zero order position of the $^1B_{2u}$ origin (or a_g addition) was estimated visually and varied to give the best fit. The magnitude of the constant density was also varied to give the best fit.

Because we have not been concerned with the absolute units of our absorption curves, we must also estimate what the vertical scale of our calculated spectra is. This was done again by trial and error, but the choice made seems fairly correct judging from the goodness of the fits. A general baseline was used to account for instrumental baseline drift. This is due to light scattering and instrument response. For a particular spectrum, a linear baseline was estimated from Wessel's low resolution spectra. This was added to the calculated spectrum to give improved fit and was not varied. Finally, individual level interaction strengths, widths, and position were varied. Where necessary, new levels were inserted or taken out as required by the fit. On the order of 40 or more, iterations were generally required to fit a spectrum. We present here a total of seven different fitted spectra including the h-8 and d-8 $^1B_{2u}$ origin regions in both p-xylene and durene, and the supposed $^1B_{2u}$ 0-0 + $a_g(9)$ (501 cm^{-1}) symmetric addition regions of h-8 in durene and p-xylene and d-8

in p-xylene only.

IV. RESULTS--ORIGIN RESONANCES

A. h-8 Origin in p-xylene

In Fig. (2) we show the weighted-density function. The calculated spectrum, and the observed spectrum. The calculated and observed spectra are virtually identical with a few minor differences in certain areas. We are confident that, given enough time and patience on the part of the fitter, essentially exact fits could be obtained. Diminishing returns unfortunately comes into play and the last few changes necessary to achieve a good fit are difficult to estimate. The parameters of the fit are given in Table 2. The positions, widths, and interaction energies are given in both our reduced units and in wavenumbers. The zero order position of the $^1B_{2u}$ origin and its width due to the constant density is given in Table 1. Also included in Table 2 is a set of possible assignments which are generated by using both long axis values of symmetric modes and short axis values of b_{1g} modes. These assignments are most likely subject to considerable error as the frequencies, especially those of the b_{1g} modes, are uncorrected for vibronic interaction with the $^1B_{2u}$ state. Our assignments are somewhat different from Wessel's because he derives them from the

FIGURE 2

h-8 origin region is p-xylene host. The weighted density is shown at the bottom, the calculated spectrum just above, and the observed spectrum with wavelength designations on top. The observed spectrum is taken from Wessel's thesis.

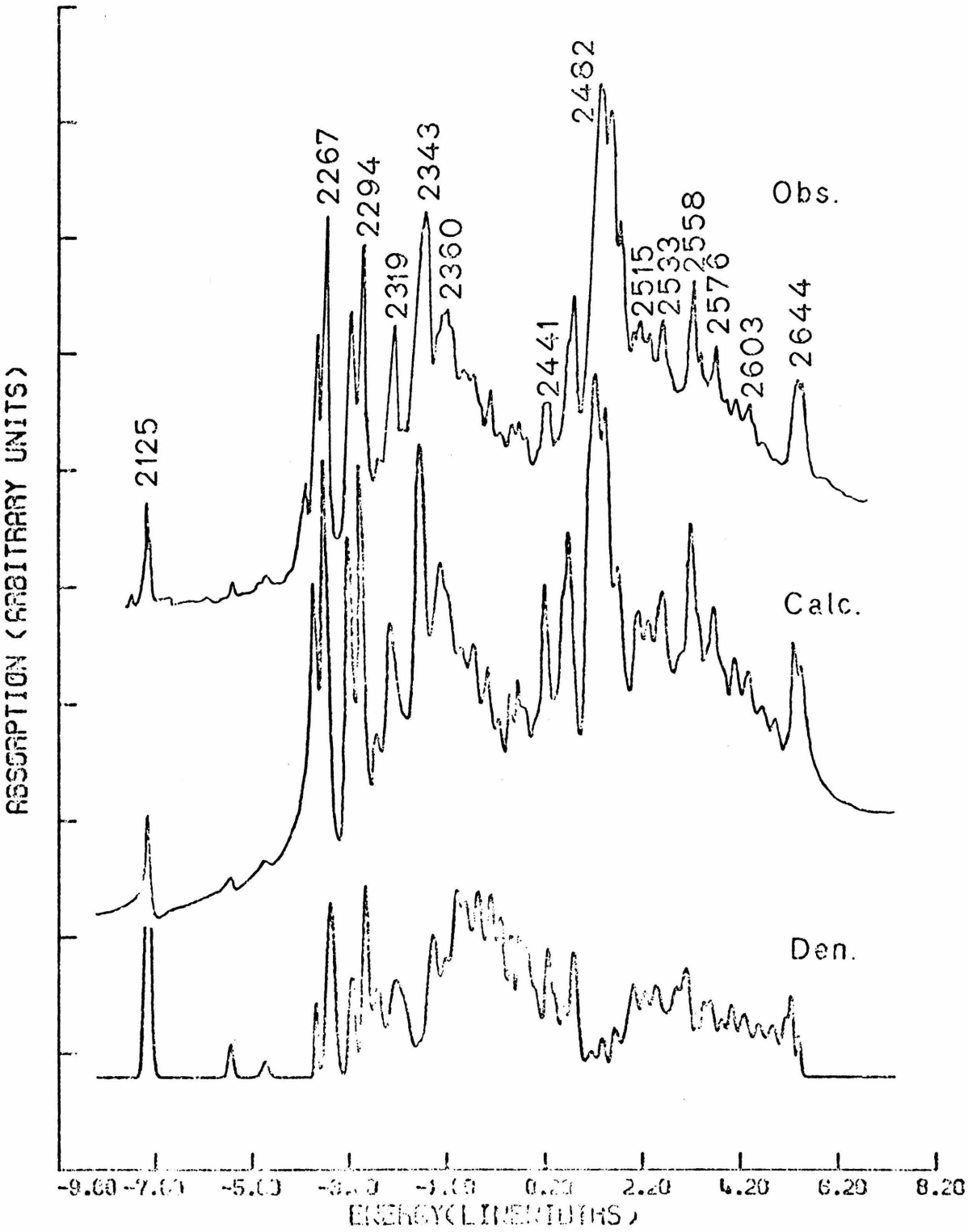
2125
2267
2294
2319
2343
2360
2441
2482
2515
2533
2558
2576
2603
2644
Obs.
Calc.
Den.
ABSORPTION (ARBITRARY UNITS)
-9.80
-7.80
-5.80
-3.80
-1.80
0.20
2.20
4.20
6.20
8.20

TABLE 1

$^1R_{2u}$ POSITION AND WIDTH

Spectrum	Position (cm^{-1} above $^1B_{3u}$ origin)	Width[a] (cm^{-1})
h-8 in p-xylene, origin	2433	38.2
d-8 in p-xylene, origin	2374	42.2
h-8 in durene, origin	2983	33.3
d-8 in durene, origin	2919	30.9
h-8 in p-xylene, origin + $a_g(9)$	2936	38.2
d-8 in p-xylene, origin + $a_g(9)$	2384	42.2
h-8 in durene, origin + $a_g(9)$	3477	33.3

[a] This is the half width at half maximum.

TABLE 2

h-8 IN p-XYLENE, ORIGIN

Position		Assignment		Width		Interaction	
Epsilon	cm^{-1}	Modes	cm^{-1} (calc.)	Epsilon	cm^{-1}	Epsilon	cm^{-1}
-7.95	2129	8,8+7	2125	0.060	2.3	0.539	21
-6.25	2194			0.050	1.9	0.173	7
-5.53	2222			0.070	2.7	0.141	5
-4.48	2262			0.030	1.1	0.200	8
-4.18	2273	8,8+6	2275	0.080	3.1	0.500	19
-3.74	2290			0.060	2.3	0.332	13
-3.47	2301			0.060	2.3	0.447	17
-3.23	2310	7,2x8	2315	0.100	3.8	0.400	15
-2.87	2324	7,5	2321	0.120	4.6	0.447	17
-2.64	2332			0.100	3.8	0.316	12
-2.37	2343	8,9+5	2344	0.090	3.4	0.224	9
-2.09	2353			0.100	3.8	0.500	19
-1.82	2364			0.100	3.8	0.447	17

TABLE 2 (continued)

Position		Assignment		Width		Interaction	
Epsilon	cm^{-1}	Modes	cm^{-1} (calc.)	Epsilon	cm^{-1}	Epsilon	cm^{-1}
-1.60	2372			0.080	3.1	0.480	18
-1.41	2379			0.090	3.4	0.500	19
-1.15	2389			0.110	4.2	0.600	23
-0.89	2399	7,3	2396	0.080	3.1	0.490	19
-0.68	2407	7,3x9	2409	0.080	3.1	0.469	18
-0.47	2415	8,2x7	2414	0.060	2.3	0.387	15
-0.32	2421	8,9+3	2419	0.040	1.5	0.283	11
-0.18	2426	8,2x9+7	2423	0.080	3.1	0.412	16
0.03	2434	8,4x9	2432	0.100	3.8	0.387	15
0.27	2444	8,8+5	2445	0.060	2.3	0.360	14
0.42	2449	7,9+6	2550	0.060	2.3	0.283	11
0.59	2456			0.060	2.3	0.264	10
0.80	2464			0.080	3.1	0.425	16
1.15	2477			0.110	4.2	0.224	9
1.39	2486			0.060	2.3	0.200	8

TABLE 2 (continued)

Position		Assignment		Width		Interaction	
Epsilon	cm^{-1}	Modes	cm^{-1} (calc.)	Epsilon	cm^{-1}	Epsilon	cm^{-1}
1.64	2496			0.070	2.7	0.245	9
1.88	2505			0.100	3.8	0.283	11
2.04	2511			0.080	3.1	0.332	13
2.25	2519			0.080	3.1	0.332	13
2.48	2528			0.100	3.8	0.387	15
2.73	2538			0.120	4.6	0.346	13
2.91	2545			0.080	3.1	0.300	11
3.11	2552			0.090	3.4	0.413	16
3.32	2560			0.040	1.5	0.200	8
3.44	2565	8,7+6	2564	0.040	1.5	0.173	7
3.59	2571	8,2x9+6	2573	0.110	4.2	0.387	15
3.83	2580			0.060	2.3	0.224	9
4.02	2587			0.080	3.1	0.316	12
4.28	2597			0.100	3.8	0.332	13
4.57	2608	7,8+7	2604	0.100	3.8	0.300	11

TABLE 2 (continued)

Position		Assignment		Width		Interaction	
Epsilon	cm^{-1}	Modes	cm^{-1} (calc.)	Epsilon	cm^{-1}	Epsilon	cm^{-1}
4.86	2619	8,8+3	2623	0.110	4.2	0.316	12
5.13	2629	8,9+8+7	2627	0.070	2.7	0.264	10
5.25	2634	8,3x9+8	2636	0.040	1.5	0.224	9
5.40	2640			0.040	1.5	0.173	7

durene spectrum where frequencies change slightly from the values in p-xylene. A somewhat more reliable assignment would be obtained if we would have fit the low energy region in p-xylene. Then we would have a good zero order set of mode frequencies to work with. We will not refer to assignments very often because we do not have much faith in them.

A most interesting comparison to make is between the weighted density and the calculated spectrum. It is here that one can get a feel for how the various lines in the spectrum derive from the zero order density. The most prominent features are the doublets at 2267 cm^{-1} and 2294 cm^{-1} and the single peaks at 2343 cm^{-1} and 2482 cm^{-1}. In examining the density for the doublets, we see that the major peak in the spectrum occurs shifted very slightly to lower energy from the corresponding density peak. The outer component of each doublet is almost not shifted at all from its zero order position. These are also good examples of the outer component intensification discussed by Wessel [23]. The outer component, though coupled weakly compared to the inner component, has comparable intensity. This is due to higher order coupling where, even though first order interactions result in little intensity borrowing, higher order terms contribute as much or more than the first order terms.

The two prominent singlet peaks are the result of the basic splitting pattern. From the density function there is roughly a broad peak running from $-1.8\ \xi$ ($\sim$2360 cm^{-1}) to $0.8\ \xi$ (2470 cm^{-1}). (ξ is the reduced energy unit.) This

interacts with the $^1B_{2u}$ origin to give the basic two humped intensity pattern. The fine structure on top of these humps is due to the fine structure in the zero order density. This is one of those regions in which some phonon activity may be present. If so, this may be the reason for the broad intensity under the sharp structure in the density function. There is no way to quantitatively determine if this is so, or if there is coincidentally a superposition of a number of $^1B_{3u}$ vibronic states. If the latter is the case, one might not expect the broadness because higher order interactions would possibly just split the levels up. Whatever the reason for the broadness, the density function is correct and does give the proper spectrum.

The peak at -7.95 ξ (2129 cm^{-1}) deserves further examination. From first order theory one expects that the shape of the spectrum should resemble the shape of the density function. We see here that this is not the case. This peak resembles a Fano-type line shape [24] with its dip to higher rather than lower energy. In general, all lines in the spectrum show some "antiresonance" behavior. The dip occurs toward the $^1B_{2u}$ origin position. For example, the dip to higher energy of the 2482 cm^{-1} peak in the calculated spectrum is due to this effect. The level at 5.13 ξ (2629 cm^{-1}) was added to the calculation to "fill in" the dip due to the two levels at 5.25 ξ (2634 cm^{-1}) and 5.40 ξ (2640 cm^{-1}). One encounters many such considerations throughout the iteration procedure.

A word about accuracy in the parameters is in order. We do not compute any error limits, but we can give some idea of what the variance might be based on experience in varying the parameters to achieve a fit. The absolute variance in the positions may be quite high, as much as 10-20 cm^{-1}. This is due to inherent errors in plotting, in converting from ξ units to wavenumbers, and the inaccuracies of the observed spectra that we used to fit our calculated spectra. However, the relative error in positions is quite good, easily less than 5 cm^{-1} and most likely 2-3 cm^{-1}. Because of the way we define our coupled levels, and the fact that they have finite width, makes the comparison of our interaction energies with Wessel's somewhat difficult. The way we define our coupled levels makes each one normalized. Whether that is necessary or not is difficult to decide. In viewing the interaction energies one should also look at the widths to get a true feel for the pre-exponential term in Eq. (7).

The sharper the level, the more accurate its position is. As far as widths are concerned, the error here, percentage wise, is fairly high in some cases, possibly as much as 20-40 percent. Again, the error depends on the level in question, some being very accurate and some not. Generally, the sharper the line, the more critical is its width to achieve a fit.. The relative interaction strengths are accurate to 2-3 cm^{-1}. Again, the variance depends on the level involved. One should notice that the interaction strength and the

width together determine the peak height of a level (see Eq. (7)). Thus, the broader a level, the stronger its interaction must be to have the same height in the density function.

The absolute values of the widths and interaction energies are also most likely not too accurate, but the relative values are fairly accurate. This is because both parameters derive their absolute value from the estimate of the zero order width of the primary ($^1B_{2u}$) state. This is a difficult parameter to estimate with accuracy (see Section VII for a discussion).

B. d-8 Origin in p-xylene

The density function and calculated and observed spectra are shown in Fig. (3). The zero order position and width of the $^1B_{2u}$ origin are given in Table 1. Parameters of the fit of Fig. (3) are given in Table 3. This spectrum is interesting from a number of aspects. The intensity distribution is much different from the two-humped, h-8 spectrum. Also we seem to have better evidence here of the presence of phonon excitation. Another interesting feature is that on the average the discrete levels in the density seem to be broader than the levels in h-8. This may be due to increased lattice coupling which is in turn due to higher vibrational amplitudes (d-8 shows this effect in the ground state [25]). Whether this observation is significant or not is uncertain.

FIGURE 3

d-8 origin region in p-xylene. Observed spectrum is Wessel's.

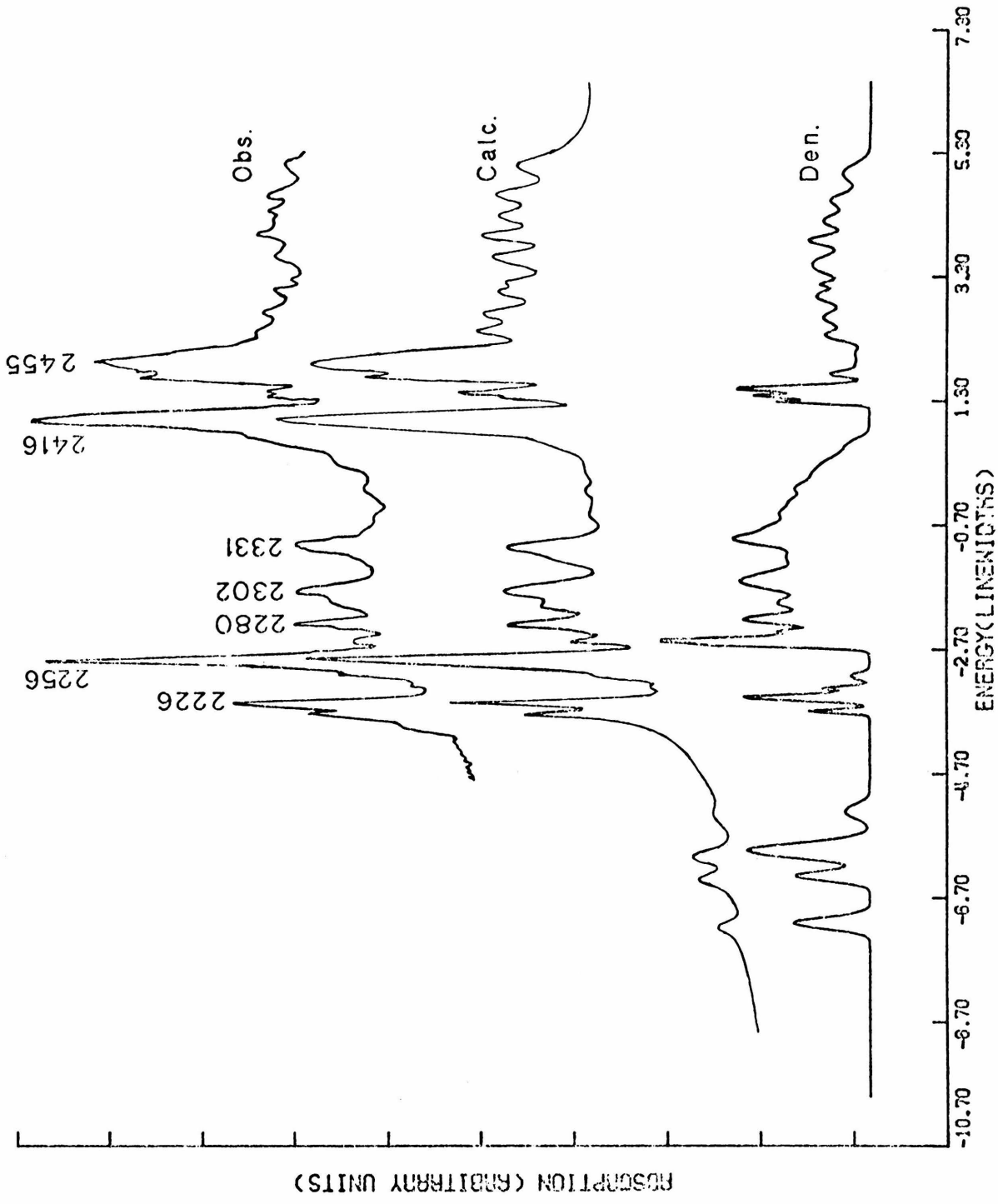
Obs.
Calc.
Den.
2455
2416
2331
2302
2280
2256
2226
ABSORPTION (ARBITRARY UNITS)
-10.70
-8.70
-6.70
-4.70
-2.70
-0.70
1.30
3.30
5.30
7.30
ENERGY(LINEWIDTHS)

TABLE 3

d-8 IN p-XYLENE, ORIGIN

Position		Assignment		Width		Interaction	
Epsilon	cm^{-1}	Modes	cm^{-1} (calc.)	Epsilon	cm^{-1}	Epsilon	cm^{-1}
-7.10	2074	4,9	2068	0.090	3.8	0.387	16
-6.34	2107	7,2x8	2107	0.080	3.4	0.361	15
-5.93	2124			0.120	5.1	0.565	24
-5.30	2150	7,9+6	2149	0.110	4.6	0.245	10
-3.68	2219	7,4	2215	0.030	1.3	0.200	8
-3.46	2228			0.050	2.1	0.374	16
-3.31	2234	4,8	2233	0.030	1.3	0.173	7
-3.12	2242	8,2x9+6	2234	0.050	2.1	0.141	6
-2.63	2263	7,3x9	2261	0.020	0.8	0.173	7
-2.55	2267	2	2268	0.060	2.5	0.529	22
-2.40	2273	7,3	2271	0.040	1.7	0.245	10
-2.21	2281	1	2280	0.090	3.8	0.490	21
-1.95	2292	6,3x9	2297	0.100	4.2	0.424	18
-1.71	2302	8,4+9	2302	0.110	4.6	0.245	10

TABLE 3 (continued)

Position		Assignment		Width		Interaction	
Epsilon	cm^{-1}	Modes	cm^{-1} (calc.)	Epsilon	cm^{-1}	Epsilon	cm^{-1}
-1.57	2308	6,3	2307	0.150	6.3	0.609	26
-1.18	2324			0.160	6.8	0.520	22
-0.92	2335			0.090	3.8	0.447	19
-0.73	2343	8,4x9	2348	0.100	4.2	0.425	18
-0.50	2353	6,8+6	2350	0.110	4.6	0.435	18
-0.30	2362	8,9+3 8,3x8	2358 2359	0.090	3.8	0.332	14
-0.10	2370			0.100	4.2	0.374	16
0.10	2378			0.100	4.2	0.283	12
0.31	2387	6,9+6	2385	0.140	5.9	0.361	15
0.60	2400	8,9+8+6	2401	0.100	4.2	0.200	8
1.29	2429	7,2x9+8	2426	0.030	1.3	0.245	10
1.38	2432			0.030	1.3	0.264	11
1.50	2438	4,6	2440	0.050	2.1	0.387	16
1.73	2447			0.050	2.1	0.200	8
1.86	2453			0.080	3.4	0.141	6

TABLE 3 (continued)

Position		Assignment		Width		Interaction	
Epsilon	cm^{-1}	Modes	cm^{-1} (calc.)	Epsilon	cm^{-1}	Epsilon	cm^{-1}
2.07	2462	6,2x9+8	2462	0.100	4.2	0.173	7
2.35	2473			0.080	3.4	0.264	11
2.64	2486			0.130	5.5	0.361	15
2.99	2500			0.110	4.6	0.346	15
3.19	2509	8,3x9+8	2513	0.040	1.7	0.141	6
3.50	2522	8,6+5 7,2x6	2518 2521	0.200	8.4	0.500	21
3.90	2539	7,9+5	2543	0.080	3.4	0.300	13
4.20	2551	4,2x9	2552	0.120	5.1	0.346	15
4.54	2566	8,2x8+6	2566	0.120	5.1	0.316	13
4.97	2584			0.150	6.3	0.300	13

The strong peak at 2256 cm^{-1} is interesting for two reasons. It is due principally to the levels in the density function at -2.55 ξ (2267 cm^{-1}) and -2.21 ξ (2281 cm^{-1}) respectively. There are no strong normal mode combinations involving $b_{1g}(8)$ or $b_{1g}(7)$ in this region. These were the only two modes which showed any substantial activity in the h-8 spectrum. In the durene d-8 spectrum Wessel assigns two strong peaks at 2261 cm^{-1} and 2276 cm^{-1} as $b_{1g}(2)$ and $b_{1g}(1)$ respectively. These two modes do not show activity in the h-8 spectra. The fact that the density function also shows these two strongly coupled levels in p-xylene lends credence to the assignment as Wessel has noted.

The second interesting feature is the broad band with superimposed fine structure which follows these two levels. This may indicate strong phonon absorption. If this is so, it falls in line with the statement above that there is larger amplitude in the d-8 modes and thus, one would assume, stronger phonon coupling. The same kind of broad-banded structure, although much less pronounced, appears after the triple peak in the density at 1.29 ξ, 1.38 ξ, and 1.50 ξ. The latter is possibly assignable as $b_{1g}(4) + a_g(6)$. The $b_{1g}(4)$ mode is again not seen in the h-8 system. Moreover, from Franck-Condon factor predictions, Wessel concludes that $a_g(6)$ assumes much more borrowing activity in d-8 than h-8. This reinforces somewhat this assignment.

The main double peak in the spectrum is due to the interaction of

the $^1B_{2u}$ origin and the triple peak centered at around +1.40 ξ. This origin, after interacting with the 2261 cm^{-1} and 2280 cm^{-1} levels, is pushed to higher energy where it interacts with the triplet. This region is reminiscent of the resonance spectra discussed previously by the authors [15b]. Another way of looking at this structure is to realize that the density function and spectrum are often approximately inversely related. That is, when the density is high, the spectrum shows a dip, and vice versa. The same notion is evidenced in the region just to the left of -2.70 ξ. The central region from -0.70 to 1.0 ξ was possibly the most difficult region to fit in this spectrum. The spectral shape is incredibly sensitive to the variations of the individual level parameters in this region.

C. h-8 Origin Region in Durene

The density function and calculated and observed spectra are shown in Fig. (4). The parameters of the fit are given in Tables 1 and 3. The durene host crystal produces the sharpest spectra of the two hosts discussed here. This can be seen both in the spectrum itself and in the density function. The spectrum's general appearance is similar to the h-8 spectrum in that both are double humped. There are differences between the two spectra. Most noticeable in the durene spectra are the two strong peaks at 3087 cm^{-1} and 3144 cm^{-1}. These have no parallel in the p-xylene spectrum.

FIGURE 4

h-8 origin region in durene host. Observed spectrum is Wessel's.

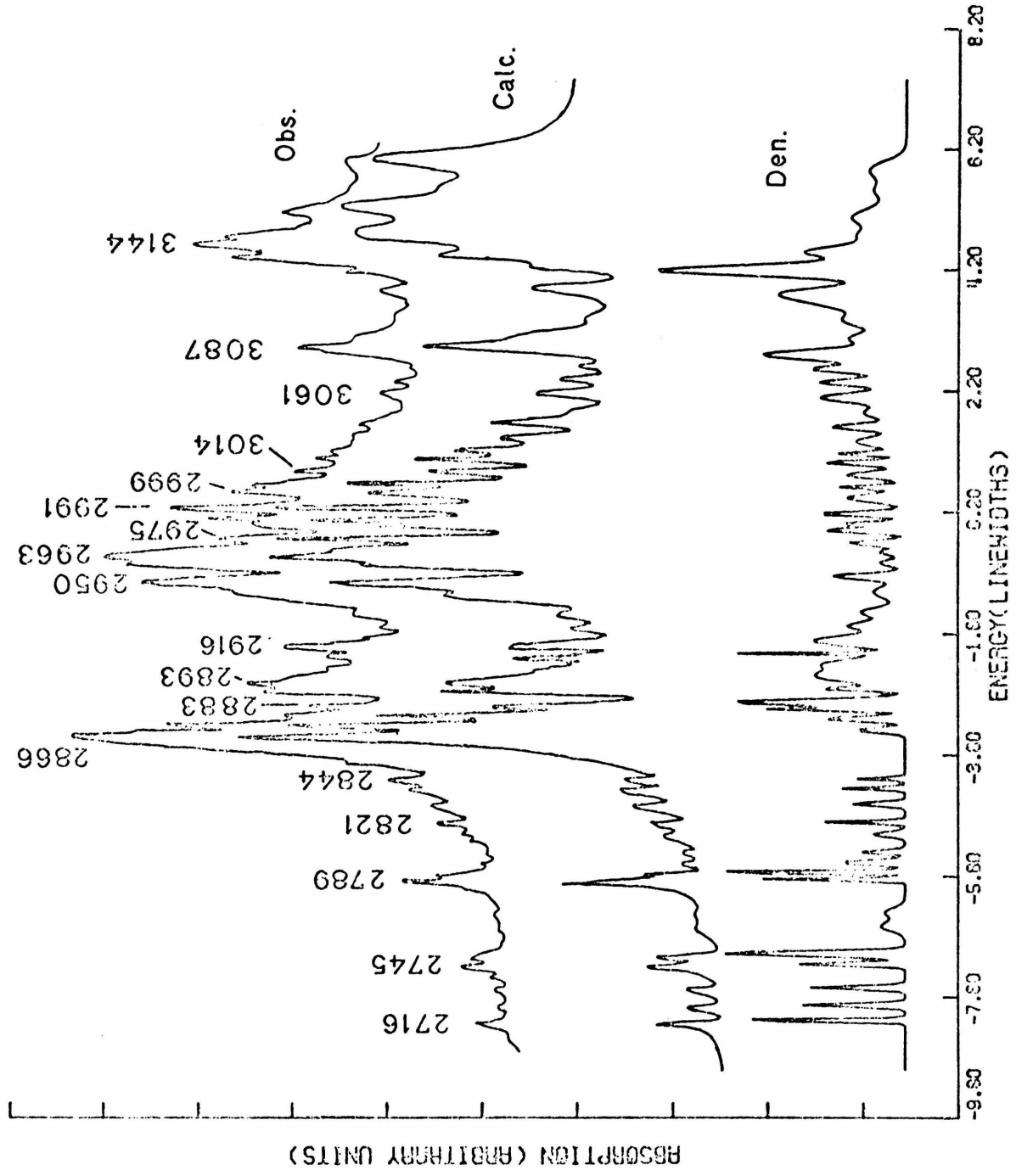
Obs.
Calc.
Den.
3144
3087
3061
3014
2999
2991
2975
2963
2950
2916
2893
2883
2866
2844
2821
2789
2745
2716
-9.80
-7.80
-5.80
-3.80
-1.80
0.20
2.20
4.20
6.20
8.20
ENERGY(LINEWIDTHS)
ABSORPTION (ARBITRARY UNITS)

TABLE 4

h-8 IN DURENE, ORIGIN

Position		Assignment		Width		Interaction	
Epsilon	cm^{-1}	Modes	cm^{-1} (calc.)	Epsilon	cm^{-1}	Epsilon	cm^{-1}
-22.44	2237			0.090	3.0	0.825	27
-21.67	2262			0.090	3.0	0.944	31
-20.94	2287	7,5	2290	0.090	3.0	1.440	48
-18.18	2378			0.090	3.0	0.741	25
-17.76	2392	7,3	2392	0.080	2.7	1.380	46
		7,7+9	2393				
-13.35	2539	8,3x8	2535	0.080	2.7	0.648	22
-12.14	2579			0.080	2.7	0.944	31
-10.83	2623	8,9+8+7	2621	0.030	1.0	1.330	44
-8.18	2711			0.020	0.7	0.346	12
-7.93	2720	8,2x6	2718	0.030	1.0	0.316	11
		8,2x8+7	2721				
-7.64	2729			0.030	1.0	0.300	10
-7.25	2742			0.030	1.0	0.316	11
-7.08	2748			0.040	1.3	0.480	16
-6.63	2763			0.080	2.7	0.245	8

TABLE 4 (continued)

Position		Assignment		Width		Interaction	
Epsilon	cm^{-1}	Modes	cm^{-1} (calc.)	Epsilon	cm^{-1}	Epsilon	cm^{-1}
-6.40	2770			0.080	2.7	0.224	7
-5.85	2789	7,8+6	2789	0.020	0.7	0.300	10
-5.73	2793	7,9+5	2791	0.020	0.7	0.374	12
-5.57	2798			0.040	1.3	0.282	9
-5.39	2804	8,7+5	2804	0.030	1.0	0.200	7
-5.10	2814	8,9+8+6	2817	0.040	1.3	0.200	7
-4.90	2820			0.020	0.7	0.224	7
-4.60	2830.			0.030	1.0	0.224	7
-4.34	2839	7,9+4	2835	0.020	0.7	0.200	7
-4.18	2844			0.020	0.7	1.732	6
-3.38	2871			0.040	1.3	0.245	8
-3.19	2877			0.040	1.3	0.316	11
-3.04	2882			0.025	0.8	0.316	11
-2.92	2886			0.050	1.7	0.520	17
-2.70	2894	7,2x9+7	2894	0.030	1.0	0.264	9

TABLE 4 (continued)

Position		Assignment		Width		Interaction	
Epsilon	cm^{-1}	Modes	cm^{-1} (calc.)	Epsilon	cm^{-1}	Epsilon	cm^{-1}
-2.50	2900	8,6+5	2900	0.100	3.3	0.520	17
		7,4x9	2901				
-2.28	2908	8,7+3	2906	0.090	3.0	0.458	15
		8,9+2x7	2907				
-2.12	2913			0.015	0.5	0.264	9
-1.91	2920	8,2x8+6	2917	0.090	3.0	0.510	17
		8,3x9+8	2922				
-1.66	2928			0.070	2.3	0.346	12
-1.44	2936	8,5x9	2937	0.080	2.7	0.332	11
-1.11	2947	8,6+4	2944	0.110	3.7	0.332	11
-0.85	2955			0.050	1.7	0.332	11
-0.63	2963	8,2x9+3	2961	0.050	1.7	0.200	7
-0.45	2969			0.050	1.7	0.200	7
-0.30	2974			0.040	1.3	0.264	9
-0.09	2980			0.040	1.3	0.316	11
0.02	2984			0.030	1.0	0.245	8
0.18	2989			0.040	1.3	0.332	11
0.44	2998			0.070	2.3	0.360	12
0.62	3004	8,6+3	3002	0.030	1.0	0.245	8

TABLE 4 (continued)

Position		Assignment		Width		Interaction	
Epsilon	cm^{-1}	Modes	cm^{-1} (calc.)	Epsilon	cm^{-1}	Epsilon	cm^{-1}
0.82	3011	7,3x8	3008	0.060	2.0	0.332	11
1.02	3017			0.040	1.3	0.316	11
1.17	3022			0.030	1.0	0.245	8
1.37	3029	7,8+5	3031	0.090	3.0	0.374	12
1.61	3037	7,7+6	3035	0.050	1.7	0.332	11
		8,9+3x8	3036				
1.84	3045			0.100	3.3	0.360	12
2.10	3053	7,2x9+6	3050	0.080	2.7	0.458	15
2.35	3062	8,9+8+5	3059	0.060	2.0	0.400	13
2.56	3069			0.060	2.0	0.412	14
2.80	3077	7,8+4	3075	0.090	3.0	0.632	21
		8,3x9+7	3078				
3.07	3086			0.090	3.0	0.387	13
3.37	3096			0.120	4.0	0.480	16
3.62	3104	8,9+8+4	3103	0.100	3.3	0.387	13
3.82	3111	7,3x9+8	3109	0.120	4.0	0.670	22
4.20	3123	7,8+3	3122	0.090	3.0	0.836	28

TABLE 4 (continued)

Position		Assignment		Width		Interaction	
Epsilon	cm^{-1}	Modes	cm^{-1} (calc.)	Epsilon	cm^{-1}	Epsilon	cm^{-1}
4.50	3133			0.100	3.3	0.556	19
4.77	3142			0.110	3.7	0.387	13
5.06	3152			0.130	4.3	0.141	15
5.28	3159	8,2x8+5	3159	0.130	4.3	0.264	9
5.53	3168			0.120	4.0	0.316	11
5.86	3179			0.150	5.0	0.412	14

The basic features of the durene spectrum can be understood by a two state argument similar to the h-8 p-xylene spectrum. If the region around -2.0 ξ (2915 cm^{-1}) is considered to be one state, then its interaction with the origin at 2983 cm^{-1} causes the basic splitting pattern. Assignments in the 2915 cm^{-1} region are not as interesting as in the d-8 p-xylene spectrum. The two strong peaks at 3087 cm^{-1} and 3144 cm^{-1} are due mainly to two strong coupled levels at 2.80 ξ (3077 cm^{-1}) and 4.20 ξ (3123 cm^{-1}) respectively. These two levels have been tentatively assigned as $b_{1g}(7) + a_g(8) + a_g(4)$ and $b_{1g}(7) + a_g(8) + a_g(3)$. In this region one would perhaps expect some contribution from the $a_g(9)$ addition to the origin. Thus, most conclusions about interaction strengths in this region are somewhat dubious.

The density function is amazingly sharp. The number of levels is high, but they are all for the most part resolved. Only in the regions around -2.00 ξ and from +3.00 ξ to +6.20 ξ is there any appreciable broadness underlying the sharp structure. This is in marked contrast to the situations in h-8 and d-8 p-xylene spectra. It may indicate that there is less molecule-lattice interaction resulting in less phonon activity. A second explanation may be that solvent shifts of the triplet levels with respect to the singlet levels are different for durene and p-xylene hosts. It thus can be argued that the triplet level shift in durene leads to less broadening than in p-xylene if such a triplet exists. Along these lines, the broadening from +3.00 ξ on may be due to the

presence of a triplet level originating at about that position. This is a similar type of argument to that made by Hochstrasser [4]. Both of the above arguments should be recognized as being highly speculative since we can offer no real quantitative evidence for either one (or for any other explanation).

D. d-8 Low Resolution, Low Energy and Origin in Durene

The density function and calculated and observed spectra are shown in Fig. (5). The parameters of the fit are given in Tables 1 and 5. Because this is a low resolution spectrum, very little of the interesting detail around the resonance region can be resolved. The low energy region is easily understood by first order theory if one ignores the Franck-Condon overlap calculations as discussed earlier. The resonance region appears to be different from the previous spectra in that there does not appear to be any one or two strongly coupled levels which determine the intensity pattern. The levels around the origin are mostly of similar coupling strength and width. The result, as shown in the spectrum, is no overall splitting as seen previously (especially the broad doublet as in h-8 origins in p-xylene and durene). The spectrum can be described as a broad peak with superimposed fine structure. Little more can be said about this particular spectrum. No assignments of the zero

FIGURE 5

d-8 origin plus some of the low energy spectrum in durene host. Observed spectrum is Wessel's.

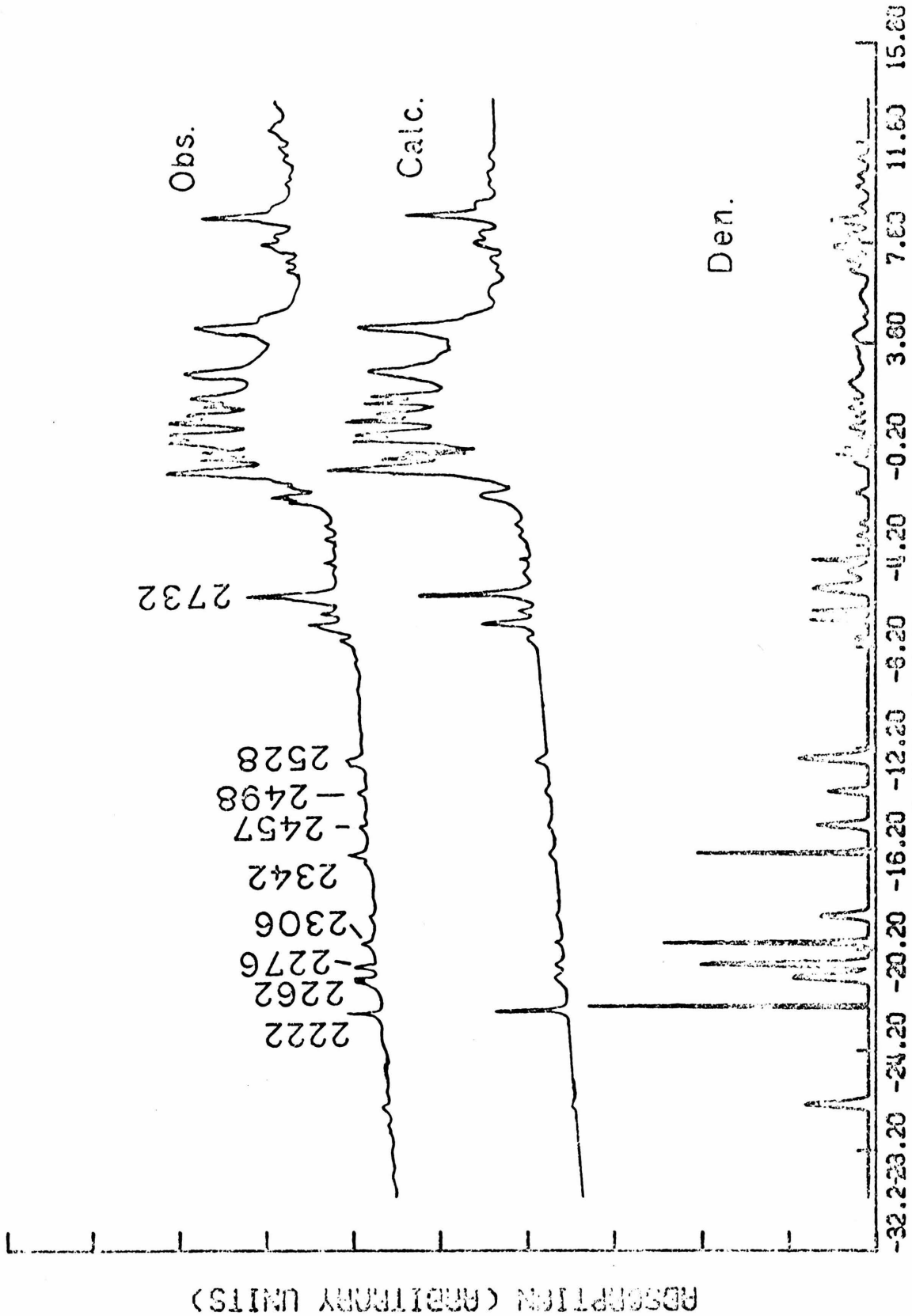
Obs.
Calc.
Den.
2732
2528
2498
2457
2342
2306
2276
2262
2222
-32.20 -28.20 -24.20 -20.20 -16.20 -12.20 -8.20 -4.20 -0.20 3.80 7.80 11.80 15.80
ENERGY(LINEWIDTHS)
ABSORPTION (ARBITRARY UNITS)

TABLE 5

d-8 IN DURENE, ORIGIN

Position		Width		Interaction	
Epsilon	cm^{-1}	Epsilon	cm^{-1}	Epsilon	cm^{-1}
-26.33	2107	0.100	3.1	1.166	36
-22.44	2227	0.020	0.6	1.070	33
-21.27	2263	0.110	3.4	1.340	41
-20.75	2279	0.070	2.2	1.660	51
-19.90	2305	0.040	1.2	1.340	41
-18.83	2338	0.090	2.8	0.980	30
-16.32	2416	0.030	0.9	1.180	37
-15.23	2449	0.090	2.8	0.975	30
-13.90	2490	0.080	2.5	0.806	25
-12.57	2531	0.110	3.4	1.263	39
-7.85	2677	0.040	1.2	0.413	13
-7.13	2699	0.040	1.2	0.741	23
-6.73	2712	0.030	0.9	0.749	23

TABLE 5 (continued)

Position		Width		Interaction	
Epsilon	cm^{-1}	Epsilon	cm^{-1}	Epsilon	cm^{-1}
-5.87	2738	0.140	4.3	1.263	39
-5.21	2759	0.170	5.2	0.836	26
-4.73	2773	0.030	0.9	0.706	22
-3.78	2803	0.070	2.2	0.400	12
-3.32	2817	0.070	2.2	0.360	11
-2.11	2854	0.090	2.8	0.480	15
-0.91	2891	0.120	3.7	0.583	18
-0.56	2902	0.020	0.6	0.413	13
-0.29	2910	0.020	0.6	0.436	13
0.08	2922	0.100	3.1	0.436	13
0.48	2934	0.100	3.1	0.625	19
0.89	2947	0.090	2.8	0.480	15
1.27	2959	0.090	2.8	0.600	19
1.57	2968	0.070	2.2	0.447	14
1.93	2979	0.140	4.3	0.530	16

TABLE 5 (continued)

Position		Width		Interaction	
Epsilon	cm^{-1}	Epsilon	cm^{-1}	Epsilon	cm^{-1}
2.26	2989	0.150	4.6	0.768	24
2.62	3000	0.120	3.7	0.374	12
2.98	3011	0.190	5.9	0.470	14
3.30	3021	0.170	5.2	0.500	15
3.68	3033	0.160	4.9	0.565	17
4.14	3047	0.190	5.9	0.775	24
4.85	3069	0.110	3.4	0.316	10
5.71	3096	0.270	8.3	0.670	21
6.70	3126	0.110	3.4	0.648	20
7.10	3138	0.110	3.4	0.685	21
7.66	3156	0.120	3.7	0.938	29
8.12	3170	0.120	3.7	0.706	22
8.70	3188	0.120	3.7	0.975	30
9.25	3205	0.120	3.7	0.490	15

TABLE 5 (continued)

Position		Width		Interaction	
Epsilon	cm^{-1}	Epsilon	cm^{-1}	Epsilon	cm^{-1}
10.04	3229	0.120	3.7	0.548	17
10.48	3243	0.120	3.7	0.500	15
11.18	3264	0.110	3.4	0.480	15

order levels were attempted.

V. RESULTS -- $a_g(9)$ ADDITIONS

A. h-8 p-xylene

The density function, calculated spectrum and observed spectrum are shown in Fig. (6). The parameters of the fit are given in Tables 1 and 6. The resemblance of the origin and $a_g(9)$ addition spectra is really quite remarkable. This resemblance also carries over into the density functions. It appears that on this basis the main features of the spectrum are determined by adding a single $a_g(9)$ quantum to both the $^1B_{2u}$ 0-0 and to the $^1B_{3u}$ levels in resonance with it. Other mode combinations seem to be less significant in determining density. Most of the features of this spectrum can be readily explained in the same manner as the features of the h-8 origin spectrum. No assignments were attempted for the zero order levels.

The major difference between the origin and $a_g(9)$ addition density functions is the different shape and shift in the maximum of the main peak. In the h-8 spectrum its shape can be crudely described as a peak with a high energy tail. This tail, as noted earlier, could possibly be attributed to phonon mode coupling. However, in the $a_g(9)$ addition density, the peak seems to have a

FIGURE 6

h-8 origin + $a_g(9)$ addition in p-xylene. Observed spectrum is Wessel's.

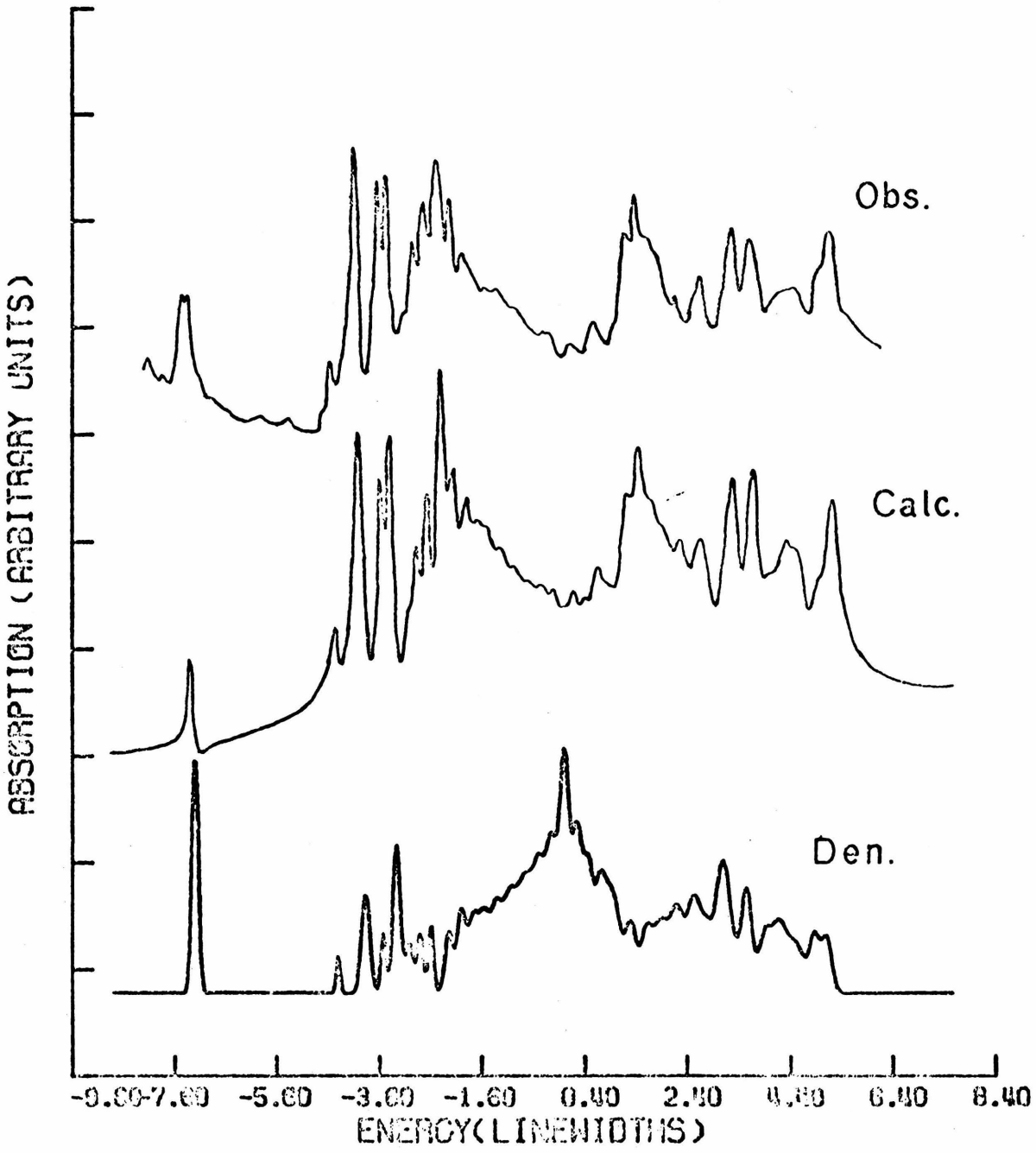
Obs.
Calc.
Den.
ABSORPTION (ARBITRARY UNITS)
-9.00 -7.60 -5.60 -3.60 -1.60 0.40 2.40 4.40 6.40 8.40
ENERGY(LINEWIDTHS)

TABLE 6

h-8 IN p-XYLENE, ORIGIN + $a_g(9)$

Position		Width		Interaction	
Epsilon	cm^{-1}	Epsilon	cm^{-1}	Epsilon	cm^{-1}
-7.20	2652	0.060	2.3	0.539	21
-4.40	2760	0.040	1.5	0.173	7
-3.87	2780	0.080	3.1	0.400	15
-3.52	2794	0.050	1.9	0.245	9
-3.27	2804	0.070	2.7	0.458	18
-3.02	2813	0.080	3.1	0.283	11
-2.80	2822	0.060	2.3	0.264	10
-2.59	2830	0.050	1.9	0.264	10
-2.24	2843	0.080	3.1	0.316	12
-2.00	2853	0.080	3.1	0.346	13
-1.75	2862	0.120	4.6	0.436	17
-1.53	2871	0.090	3.5	0.332	13
-1.33	2878	0.100	3.9	0.374	14

TABLE 6 (continued)

Position		Width		Interaction	
Epsilon	cm^{-1}	Epsilon	cm^{-1}	Epsilon	cm^{-1}
-1.06	2889	0.150	5.8	0.539	21
-0.74	2901	0.140	5.4	0.539	21
-0.47	2912	0.120	4.6	0.530	20
-0.26	2920	0.090	3.5	0.458	18
-0.09	2926	0.090	3.5	0.458	18
0.02	2931	0.070	2.7	0.480	19
0.18	2937	0.090	3.5	0.458	18
0.30	2941	0.080	3.1	0.400	15
0.46	2948	0.080	3.1	0.412	16
0.68	2956	0.120	4.6	0.490	19
0.95	2967	0.150	5.8	0.530	20
1.30	2980	0.100	3.9	0.360	14
1.59	2991	0.110	4.2	0.346	13
1.89	3003	0.160	6.2	0.480	19
2.20	3015	0.120	4.6	0.412	16

TABLE 6 (continued)

Position		Width		Interaction	
Epsilon	cm^{-1}	Epsilon	cm^{-1}	Epsilon	cm^{-1}
2.54	3028	0.150	5.8	0.539	21
2.79	3038	0.090	3.5	0.264	10
3.06	3048	0.130	5.0	0.469	18
3.18	3053	0.170	6.6	0.447	17
3.55	3067	0.100	3.9	0.447	17
3.90	3080	0.120	4.6	0.374	14
4.17	3091	0.130	5.0	0.400	15
4.49	3103	0.170	6.6	0.412	16
4.87	3118	0.100	3.9	0.332	13
5.11	3127	0.100	3.9	0.332	13

low energy tail. This cannot be rationalized in terms of phonon modes (at least at low temperatures). It appears that one can only say that the interaction strength has been redistributed among the individual levels which combine to give the broad "level". This may be an indication that phonon modes play less of a role in determining the intensity pattern, but such a conclusion is quite tenuous. Most other parts of the density functions are quite similar.

B. d-8 in p-xylene

The density and calculated and observed spectra are shown in Fig.(7). The parameters of the fit are given in Tables 1 and 7. Again, as in the h-8 p-xylene case, the spectra of origin and $a_g(9)$ are remarkably similar in many respects. However, there are also some striking differences. Most notable is the disappearance of the major origin peak 2256 cm^{-1} (attributed to $b_{1g}(2)$) in the $a_g(9)$ addition. Also, the two strong peaks at 2417 cm^{-1} and 2455 cm^{-1} are much reduced in intensity. The set of four peaks (2267, 2280, 2301, 2331 cm^{-1}) is still present in the $a_g(9)$ addition with much the same intensity pattern. Also, the structure on the high energy end of the spectrum is different but not drastically so.

The big problem is to explain what happens to the 2256 cm^{-1} peak in the $a_g(9)$ addition. If the origin assignment of $b_{1g}(2)$

FIGURE 7

d-8 origin + $a_g(9)$ addition in p-xylene. Observed spectrum is Wessel's.

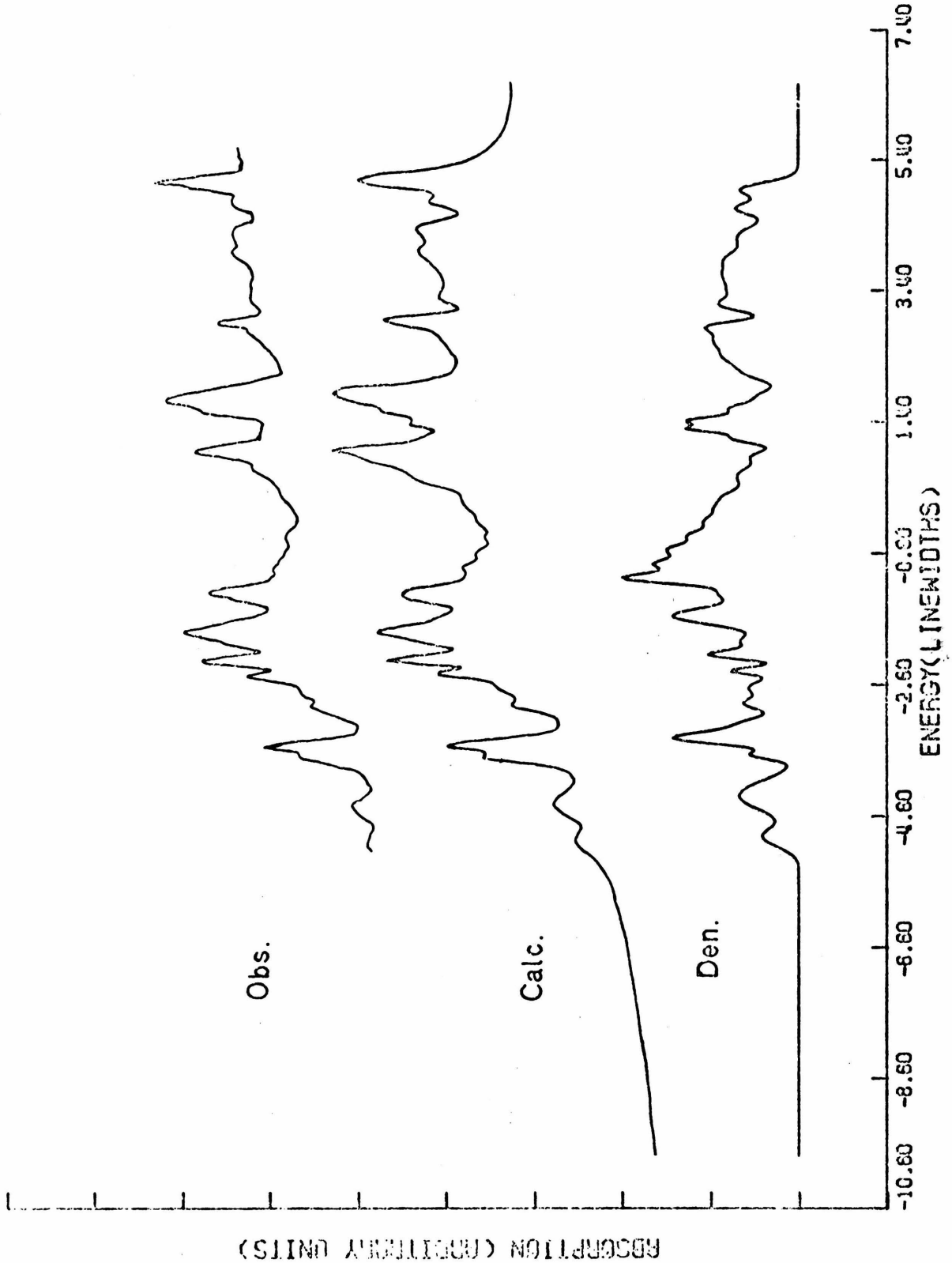
Obs.
Calc.
Den.
-10.60
-8.60
-6.60
-4.60
-2.60
-0.60
1.40
3.40
5.40
7.40
ENERGY(LINEWIDTHS)
ABSORPTION (ARBITRARY UNITS)

TABLE 7

d-8 IN p-XYLENE, ORIGIN + $a_g(9)$

Position		Width		Interaction	
Epsilon	cm^{-1}	Epsilon	cm^{-1}	Epsilon	cm^{-1}
-4.92	2695	0.150	5.8	0.316	12
-4.29	2719	0.230	8.9	0.510	20
-3.67	2743	0.070	2.7	0.245	9
-3.42	2753	0.090	3.5	0.447	17
-3.20	2761	0.110	4.2	0.346	13
-2.90	2773	0.090	3.5	0.283	11
-2.64	2783	0.130	5.0	0.346	13
-2.38	2793	0.060	2.3	0.264	10
-2.15	2802	0.070	2.7	0.332	13
-1.95	2809	0.100	3.8	0.316	12
-1.73	2818	0.110	4.2	0.200	8
-1.54	2825	0.140	5.4	0.565	22
-1.20	2838	0.110	4.2	0.387	15

TABLE 7 (continued)

Position		Width		Interaction	
Epsilon	cm^{-1}	Epsilon	cm^{-1}	Epsilon	cm^{-1}
-0.98	2847	0.080	3.1	0.480	18
-0.77	2855	0.100	3.8	0.500	19
-0.54	2864	0.100	3.8	0.469	18
-0.33	2872	0.090	3.5	0.387	15
-0.13	2879	0.100	3.8	0.387	15
0.07	2887	0.100	3.8	0.346	13
0.25	2894	0.100	3.8	0.316	12
0.46	2902	0.130	5.0	0.332	13
0.65	2909	0.110	4.2	0.283	11
0.88	2918	0.100	3.8	0.283	11
1.15	2929	0.080	3.1	0.316	12
1.29	2934	0.050	1.9	0.283	11
1.41	2939	0.060	2.3	0.332	13
1.58	2945	0.090	3.5	0.332	13
1.79	2953	0.100	3.8	0.264	10

TABLE 7 (continued)

Position		Width		Interaction	
Epsilon	cm^{-1}	Epsilon	cm^{-1}	Epsilon	cm^{-1}
2.05	2963	0.100	3.8	0.200	8
2.20	2969	0.120	4.6	0.316	12
2.40	2977	0.110	4.2	0.332	13
2.64	2986	0.130	5.0	0.435	17
2.86	2994	0.090	3.5	0.346	13
3.15	3006	0.100	3.8	0.346	13
3.37	3014	0.130	5.0	0.374	14
3.62	3024	0.130	5.0	0.374	14
3.86	3033	0.130	5.0	0.346	13
4.22	3047	0.220	8.5	0.500	19
4.66	3064	0.100	3.8	0.316	12
4.94	3075	0.110	4.2	0.346	13

fundamental is correct, it appears that the Franck-Condon overlap factors cause a drastic reduction of the intensity of this component. A comparison of the widths shows that this level increases in width from 2.5 cm^{-1} to either 4.2 or 3.8 cm^{-1}. It is difficult to ascertain if this is significant. This aspect of the $a_g(9)$ addition remains a puzzle. The decrease in intensity of the doublet 2417 and 2455 cm^{-1} is most likely due to the absence of a state corresponding to the strong 2267 cm^{-1} origin level. In the origin region its interaction with the $^1B_{2u}$ 0 origin shoves intensity into the doublet. In the $a_g(9)$ addition it is not present and the doublet is less intense even though the states corresponding to the origin triplet have roughly the same interaction energy in the origin and the $a_g(9)$ addition. The comments on phonon mode activity made for the origin region still seem to apply to the $a_g(9)$ addition region. We ignore, of course, the possible intensity sources $^1B_{2u} + a_g(6)$ or $a_g(7)$ which should lie around 830 cm^{-1} above the origin, relatively close to the region of the $a_g(9)$ addition. Possibly multiple source interference causes the reduction of the 2267 cm^{-1} analog in the $a_g(9)$ addition region.

C. h-8 in Durene

The density, calculated spectra and observed spectra are shown in Fig. (8). The parameters of the fit are given in Tables 1 and 8.

FIGURE 8

h-8 origin + $a_g(9)$ addition in durene. Observed spectrum is Wessel's.

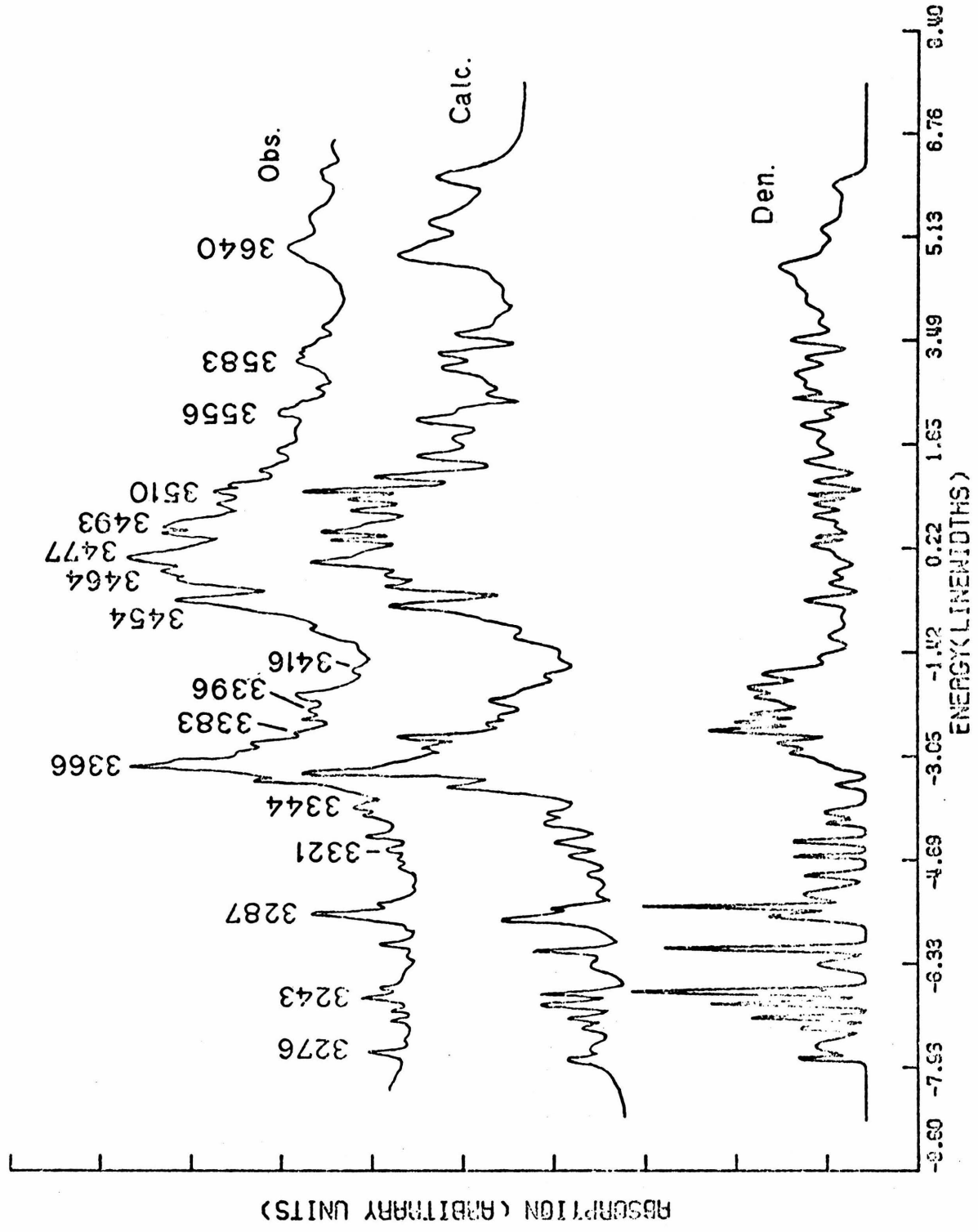
Obs.
Calc.
Den.
3640
3583
3556
3510
3493
3477
3464
3454
3416
3396
3383
3366
3344
3321
3287
3243
3276
-8.60
-7.53
-6.33
-4.69
-3.05
-1.42
0.22
1.65
3.49
5.13
6.76
8.40
ENERGY(LINEWIDTHS)
ABSORPTION (ARBITRARY UNITS)

TABLE 8

h-8 IN DURENE, ORIGIN + $a_g(9)$

Position		Width		Interaction	
Epsilon	cm^{-1}	Epsilon	cm^{-1}	Epsilon	cm^{-1}
-7.82	3215	0.020	0.7	0.224	8
-7.62	3222	0.110	3.7	0.425	14
-7.33	3231	0.030	1.0	0.264	9
-7.17	3237	0.030	1.0	0.346	12
-6.95	3244	0.030	1.0	0.387	13
-6.76	3250	0.040	1.3	0.549	18
-6.33	3265	0.070	2.4	0.332	11
-6.08	3273	0.030	1.0	0.447	15
-5.57	3290	0.060	2.0	0.435	15
-5.42	3295	0.025	0.8	0.412	14
-5.23	3302	0.090	3.0	0.425	14
-4.92	3312	0.040	1.3	0.283	9
-4.62	3322	0.020	0.7	0.245	8

TABLE 8 (continued)

Position		Width		Interaction	
Epsilon	cm^{-1}	Epsilon	cm^{-1}	Epsilon	cm^{-1}
-4.39	3330	0.030	1.0	0.283	9
-4.10	3340	0.030	1.0	0.200	7
-3.93	3345	0.060	2.0	0.283	9
-3.50	3360	0.040	1.3	0.200	7
-3.24	3369	0.040	1.3	0.173	6
-3.12	3373	0.060	2.0	0.300	10
-2.99	3377	0.050	1.7	0.332	11
-2.84	3382	0.060	2.0	0.412	14
-2.64	3389	0.050	1.7	0.500	17
-2.51	3393	0.030	1.0	0.332	11
-2.38	3397	0.060	2.0	0.469	16
-2.23	3402	0.050	1.7	0.332	11
-2.12	3406	0.050	1.7	0.387	13
-1.97	3411	0.070	2.4	0.510	17
-1.75	3419	0.080	2.7	0.510	17

TABLE 8 (continued)

Position		Width		Interaction	
Epsilon	cm^{-1}	Epsilon	cm^{-1}	Epsilon	cm^{-1}
-1.49	3427	0.100	3.4	0.387	13
-1.16	3438	0.090	3.0	0.316	11
-0.85	3449	0.140	4.7	0.332	11
-0.59	3458	0.060	2.0	0.332	11
-0.33	3466	0.060	2.0	0.264	9
-0.15	3472	0.060	2.0	0.245	8
0.13	3482	0.100	3.4	0.316	11
0.28	3487	0.050	1.7	0.264	9
0.41	3491	0.025	0.8	0.200	7
0.57	3496	0.080	2.7	0.283	9
0.74	3502	0.050	1.7	0.283	9
0.92	3508	0.060	2.0	0.316	11
1.07	3513	0.025	0.8	0.707	8
1.28	3520	0.060	2.0	0.316	11
1.48	3527	0.050	1.7	0.173	6

TABLE 8 (continued)

Position		Width		Interaction	
Epsilon	cm^{-1}	Epsilon	cm^{-1}	Epsilon	cm^{-1}
1.59	3531	0.060	2.0	0.316	11
1.89	3541	0.160	5.4	0.500	17
2.17	3550	0.070	2.4	0.346	12
2.38	3557	0.070	2.4	0.300	10
2.58	3564	0.040	1.3	0.283	9
2.75	3570	0.090	3.0	0.400	13
2.98	3577	0.100	3.4	0.469	16
3.23	3586	0.070	2.4	0.360	12
3.50	3595	0.070	2.4	0.400	13
3.76	3604	0.120	4.0	0.413	14
4.08	3614	0.130	4.4	0.469	16
4.39	3625	0.140	4.7	0.530	18
4.68	3634	0.120	4.0	0.548	18
4.97	3644	0.110	3.7	0.360	12
5.24	3653	0.110	3.7	0.374	13

TABLE 8 (continued)

Position		Width		Interaction	
Epsilon	cm^{-1}	Epsilon	cm^{-1}	Epsilon	cm^{-1}
5.48	3661	0.130	4.4	0.283	9
5.70	3669	0.120	4.0	0.265	9
5.96	3677	0.110	3.7	0.332	11

Both the spectra and densities of the origin and $a_g(9)$ addition regions are remarkably similar, perhaps even more so than the h-8 p-xylene case. The only real difference occurs at the high energy end of the $a_g(9)$ spectrum where the two peaks corresponding to the origin peaks at 3087 and 3144 cm^{-1} appear with much reduced intensity. Rationalizations about Franck-Condon factors could be one explanation. Another might be multiple source interference. As these peaks occur on the high energy end of the origin spectrum, they might be subject to interference (around the origin constructive) between $^1B_{2u}$ 0-0 and $^1B_{2u}$ 0-0 + $a_g(9)$. In the $a_g(9)$ region, the contribution of the 0-0 is reduced and the interference may now become destructive. This is only a speculation as we have not done the phasing calculations to justify it.

VII. $^1B_{2u}$ ORIGINS AND THEIR WIDTHS

A subject which we have as yet not touched upon is the "zero order" width of the $^1B_{2u}$ states. By "zero order" width we mean the width due to the constant component of the weighted density function. It was noted earlier, and can be seen in Table 1, that these widths are much greater than those observed for the $^1B_{3u}$ levels. We are fairly confident that these widths are not in error by the order of magnitude difference between $^1B_{3u}$ and $^1B_{2u}$ levels. Thus, the increased width of the $^1B_{2u}$ state seems real. We have plotted in

Figs. (9) and (10) examples of the width of the $^1B_{2u}$ origin. The pure Lorentzian (plus baseline) is superimposed on the calculated spectrum. One can see how the wings of the pure Lorentzian determine the wings of the spectrum. It was this type of judgement, plus considerations of the general intensity pattern near resonance, that lead to the estimation of the widths. One can see that it would be very difficult to estimate the width to an accuracy of a few wavenumbers, but variation of this parameter does indeed show that some accuracy is attainable.

To what can this width be due? We can offer no definitive answer to this question. It is surely not due to an increase in the radiative lifetime over the $^1B_{3u}$ state since this would lead to a drastic increase in the intensity of the transition which is not observed. The only other reasonable explanation seems to be interaction with some other electronic states which broaden the $^1B_{2u}$ state, but not the $^1B_{3u}$ state. The only other possible electronic states would seem to be triplets. This seems to be a difficult question to resolve and deserves further attention. Our spectral fitting procedure cannot suggest an answer, but can only point up the problem.

Also in Figs. (9) and (10) one gets a somewhat clearer picture of how the basic intensity patterns discussed earlier are determined. One can visually perform a crude, first order perturbation splitting argument to arrive at the overall intensity patterns. Also, it is

FIGURE 9

Calculated h-8 origin region in durene. The density is plotted above. The dashed line superimposed on the spectrum is the pure Lorentzian due to the constant component of the density. Its width is 33.3 cm^{-1} (HWHM).

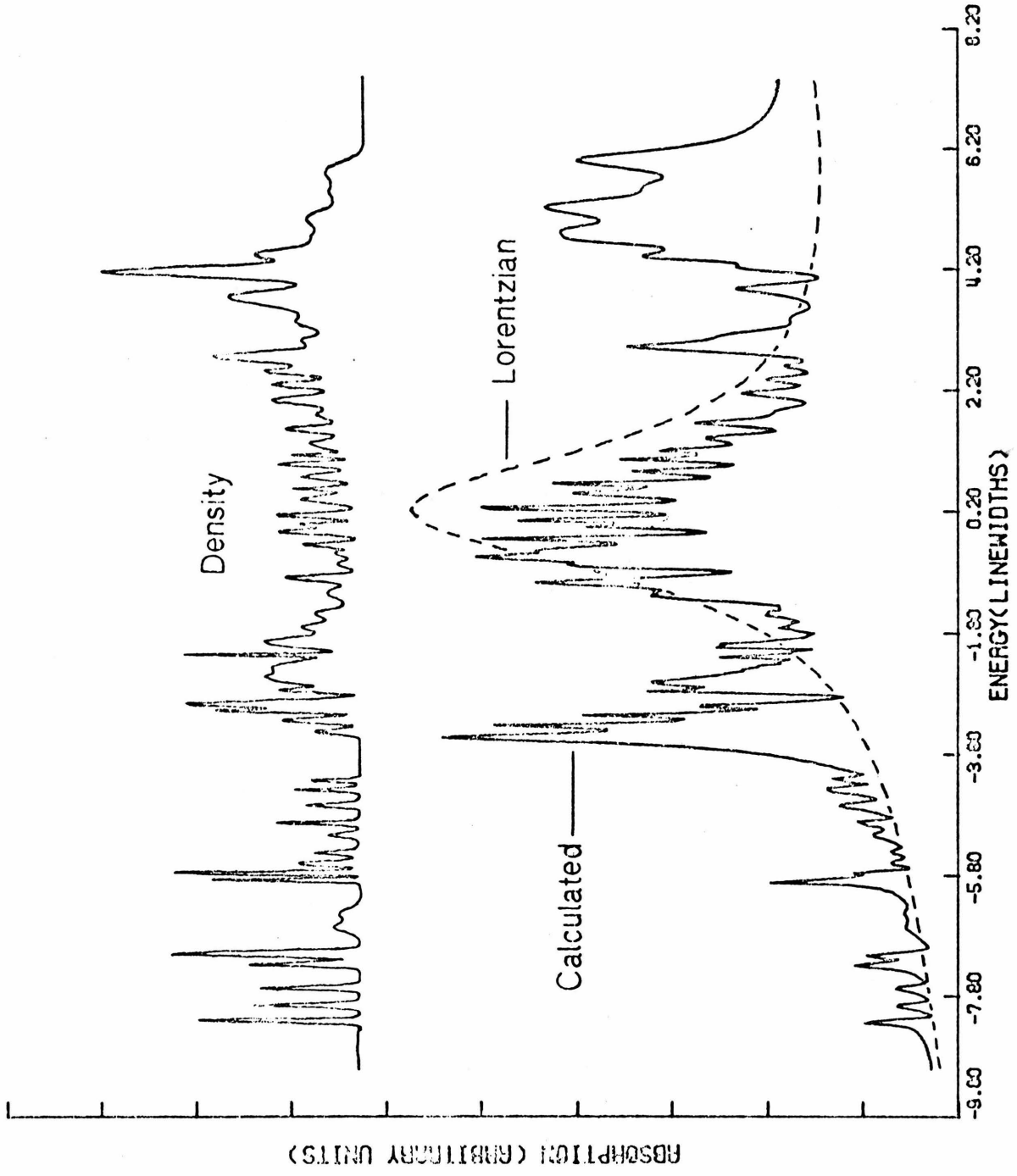
Density
Lorentzian
Calculated
ABSORPTION (ARBITRARY UNITS)
-9.00
-7.80
-5.80
-3.80
-1.80
0.20
2.20
4.20
6.20
8.20
ENERGY(LINEWIDTHS)

FIGURE 10

Calculated d-8 origin region in p-xylene. Same as Fig. 9 The width of the Lorentzian is 42.2 cm^{-1} (HWHM).

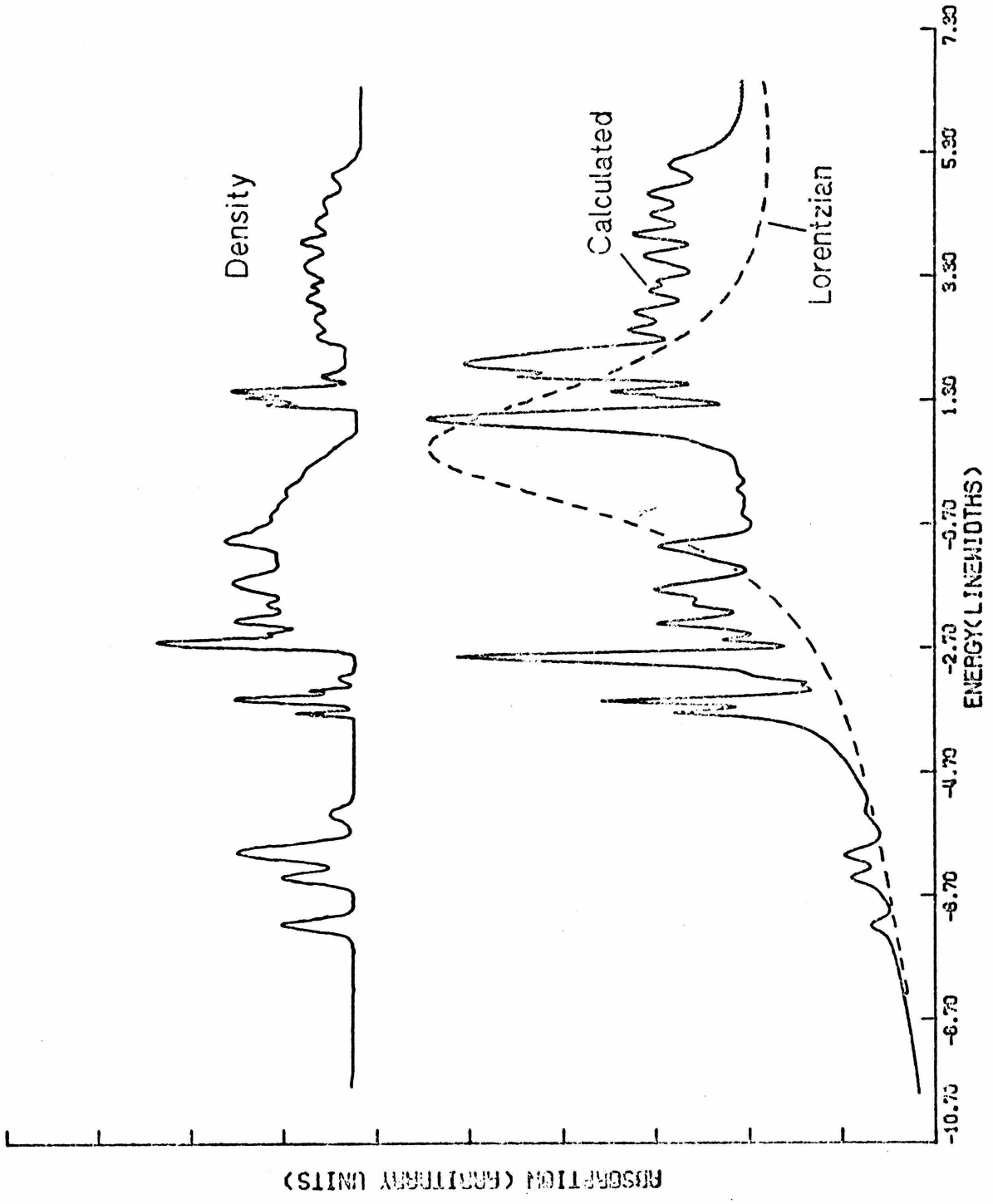
Density
Calculated
Lorentzian
-10.70
-6.70
-8.70
-4.70
-2.70
-0.70
1.30
3.30
5.30
7.30
ENERGY(LINEWIDTHS)
ABSORPTION (ARBITRARY UNITS)

easy to see how, if the Lorentzian were much narrower, the overall intensity patterns would not be correct. The difficulty in determining accurately the zero order positions and widths of the $^1B_{2u}$ state is the weakest link in our fitting procedure. One further fact must be noted. Wessel places the zero order $^1B_{2u}$ positions at much lower energies ($\sim$100-200 cm^{-1}) than we do. He included in his calculations all the low energy lines in his diagonalization which supposedly push the $^1B_{2u}$ state up into the region where resonance structure is observed. We place the $^1B_{2u}$ where it seems to give the best fit to the resonance structure, ignoring the low energy lines. This is the reason for this discrepancy in our $^1B_{2u}$ positions. If we also calculated the low energy lines, our zero order position would most likely have to be moved to lower energy.

VIII. PREDICTED EMISSION DECAY CURVES

Using our calculated spectra and the Fourier transform technique outlined previously [15a], we can compute what the resonance emission decay curves should look like. Caution must be used in comparing this with vapor phase emission decay curves [7]. Our system is not a vapor phase spectrum. The vapor spectrum at low temperatures has not been measured, but at room and slightly below room temperature, the spectrum is very broad and

complicated by strong sequence structure. Moreover, our decay curves are computed for ideal, minimum uncertainty-principle width excitation pulses. Even the experiments of Wannier, et. al. [7], using the fourth harmonic of the Nd^{3+} glass laser, do not have the uncertainty-principle minimum width. This, as shown [15b], will tend to wash out any nonexponential behavior of the decay.

We have plotted two examples of decay curves. These are shown in Figs. (11) and (12). The first uses the h-8 origin region in durene. Using the values in Table 1 for the width of the $^1B_{2u}$ state, we can now give absolute values to our relative units of time. Thus, one epsilon is equal to 33.3 cm^{-1} for the h-8 origin in durene. This means, employing the uncertainty principle $\Delta t \Delta w \sim 1$, that one lifetime unit is equal to 0.159 picoseconds. It should be noted that these numbers are in error by approximately 20-30 percent at most. The second example is the d-8 origin in p-xylene. Here the width is $\xi = 42.2$ cm^{-1} giving a lifetime unit of 0.126 picoseconds.

We give three examples of different widths and positions of the excitation pulse for each spectrum. All decay curves show quantum beat effects as expected [15a]. The spacing of the beats in time is inversely related to the separation of the excited peaks in the spectrum. Thus, in Figs. (11c) and (12c), the beats are very closely spaced corresponding to the relatively large separation of the major excited peaks in the spectrum. As we narrow the

FIGURE 11

Various calculated emission decay curves for h-8 origin region in durene. The Gaussian excitation parameters are:

	Position (ξ)	Width (ξ)
(a)	-3.8	1.2
(b)	-3.0	2.5
(c)	0.0	6.0

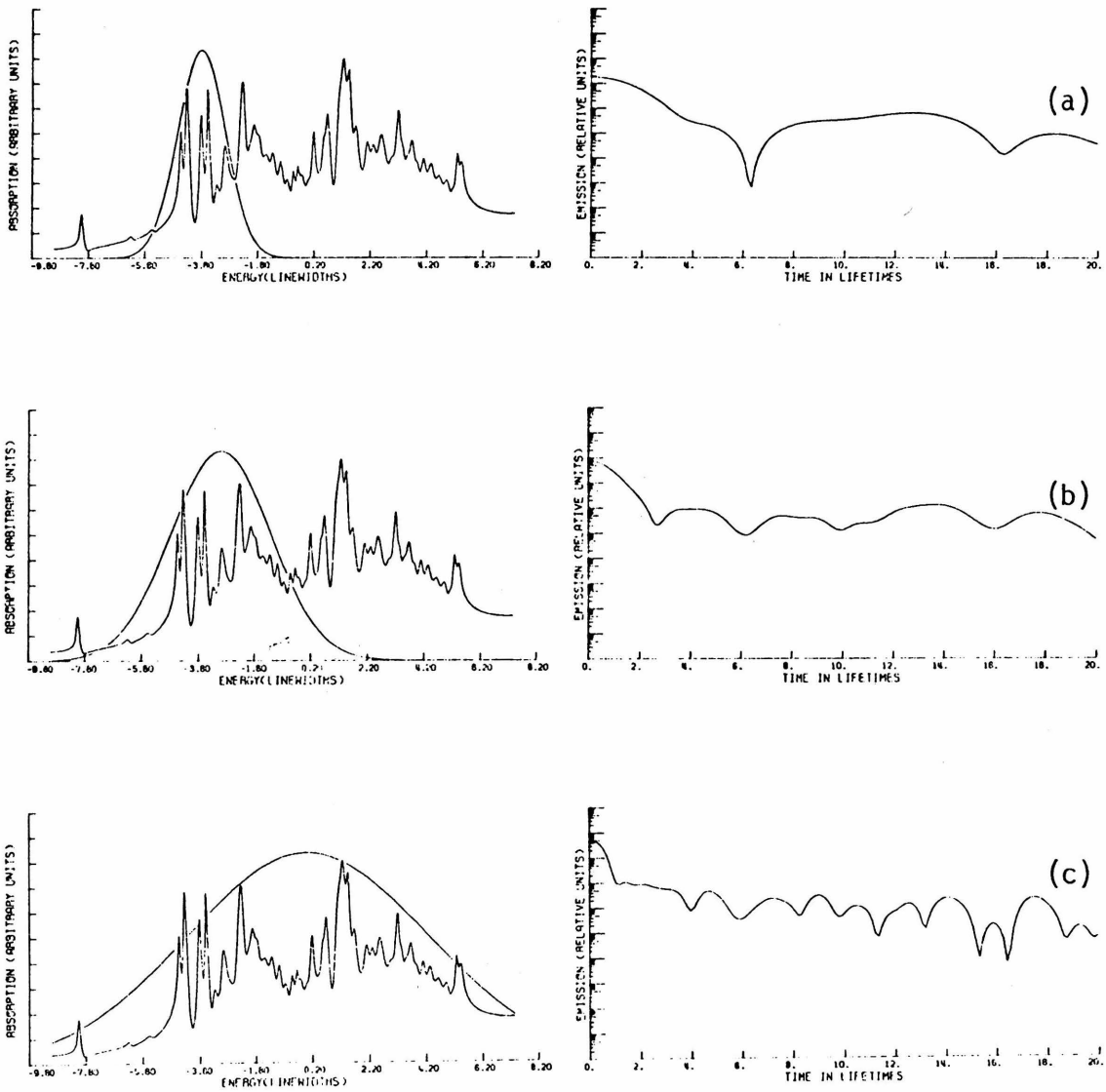
ABSORPTION (ARBITRARY UNITS)
ENERGY(LINEWIDTHS)
EMISSION (RELATIVE UNITS)
TIME IN LIFETIMES
(a)
(b)
(c)

FIGURE 12

Various calculated emission decay curves for d-8 origin region in p-xylene. The Gaussian excitation parameters are:

	Position (ξ)	Width (ξ)
(a)	1.3	2.0
(b)	-1.7	1.0
(c)	-0.7	6.0

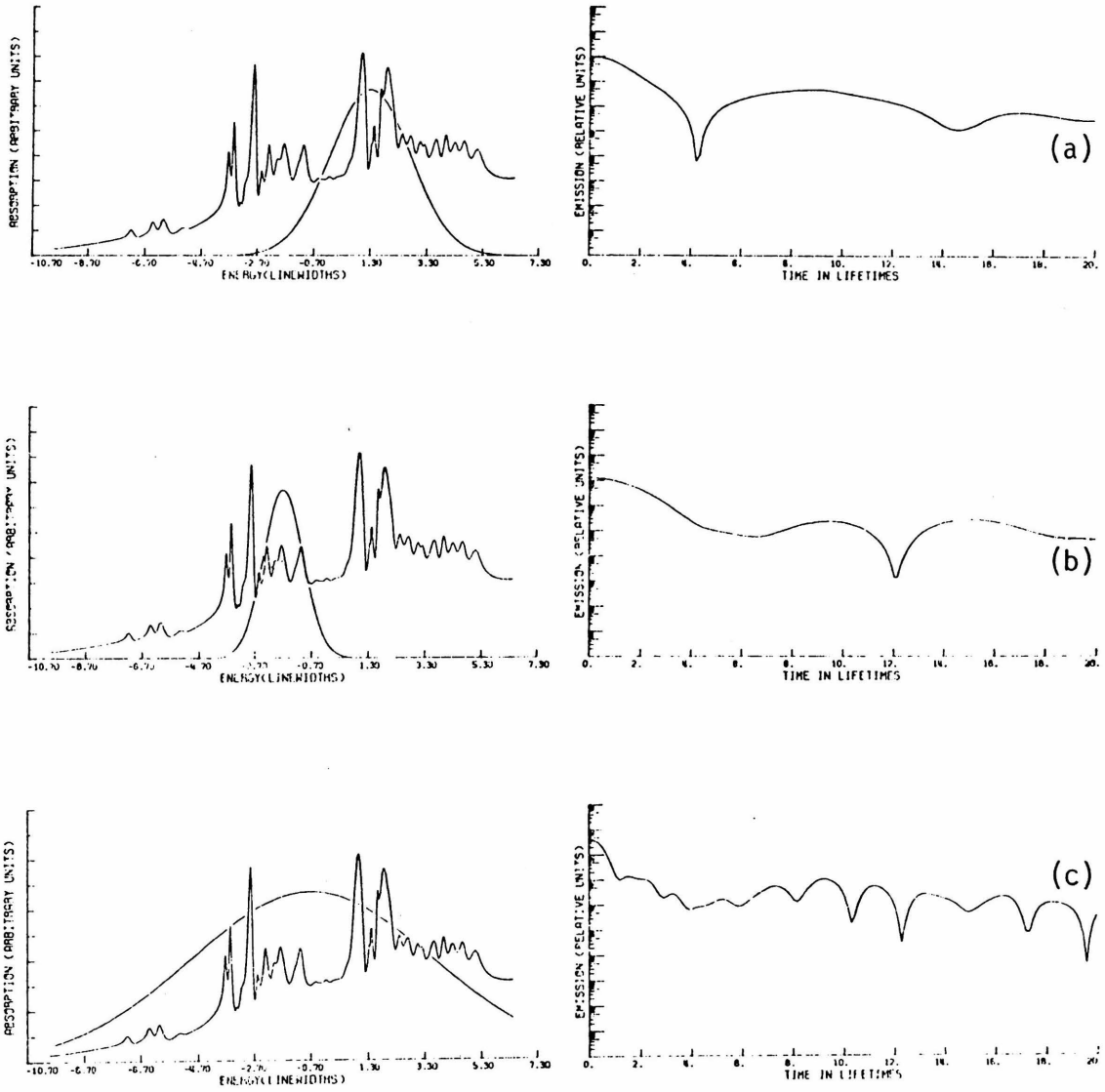
ABSORPTION (ARBITRARY UNITS)
ENERGY(LINEWIDTHS)
EMISSION (RELATIVE UNITS)
TIME IN LIFETIMES
(a)
(b)
(c)

bandwidth of the excitation pulse, the peaks which contribute to the decay curve are more closely spaced given beats which are relatively widely spaced in time. The irregular pattern of the beat structure is due to the irregular spacing of the spectral peaks. See Fig. (1) for a more regular peak spacing in the spectrum and a more expected beat pattern.

The long decay in the curves results from the very narrow line widths of some of the peaks in the spectrum. This is what most ordinary experiments measure. These long decay times are due mainly to the width of the coupled levels of the $^1B_{3u}$ state. Thus, it is not unexpected that the exponential lifetimes measured by various workers (which correspond to our long decay times) in the region of the second singlet are close to those measured in the first singlet [26]. This also is a partial confirmation of our criticism of the Douglas "dilution" effect discussed earlier.

As one can see from our numbers, it is difficult to understand how the experiments of Wannier, et. al. [7] were able to see beat decays on the basis of the time resolution of the experiment. Our entire plotted decay curves cover roughly three picoseconds. The beats occur on times less than this. There is no way that Wannier, et. al.'s time resolution could have detected these beats. Also, if one plots our curves linearly instead of logarithmically, the beats are so weak it would seem difficult to be able to observe them given the weakness of the resonance fluorescence. Thus, the results of this experiment

seem doubtful as far as their having been quantum beats observed.

IX. SUMMARY

We have presented here a general discussion of the intermediate or narrow energy gap class of molecules in terms of their spectra and emission decay curves. There we showed that the speed of the emission decay is related not to the integrated intensity of the absorption band, but to the width of the peaks in the absorption spectrum. The general results were then made more specific by calculating the spectra and emission decay curves of the second singlet of naphthalene in two host crystals where fine structure is resolvable. From these calculations one can get values of the position, width, and interaction energies of the vibronic levels of the first singlet which interact with the second singlet giving rise to the fine structure. From a few sample computed decay curves considerable doubt is cast on the experiments of Wannier, et. al. [7] where quantum beats were reported in the resonance fluorescence of the second singlet.

REFERENCES

[1] (a) McClure, D. S., 1954, J. Chem. Phys., 22, 1668.

(b) Ibid., 1956, J. Chem. Phys., 24, 1.

[2] Hollas, J. M., 1962, J. Mol. Spec., 9, 138.

[3] Bixon, M., and Jortner, J., 1968, J. Chem. Phys., 48, 715.

[4] Hochstrasser, R. M., 1968, Acc. Chem. Res., 1, 266.

[5] Fischer, G., 1969, Mol. Cryst. Liq. Cryst., 6, 105.

[6] Bree, A., and Vilkos, V. V. B., 1971, Spectrochim. Acta, 27A, 2333.

[7] Wannier, P., Rentzepis, P. M., and Jortner, J., 1971, Chem. Phys. Lett., 10, 193.

[8] (a) Van Den Bogaardt, P. A. M., Rettschnick, R. P. H., and Von Voorst, J. D. W., 1973, Chem. Phys. Lett., 18, 351.

(b) Geldof, P. A., Rettschnick, R. P. H., and Hoytink, G. J., 1969, Chem. Phys. Lett., 4, 59.

(c) Wannier, P., Rentzepis, P. M., and Jortner, J., 1971, Chem. Phys. Lett., 10, 102.

[9] (a) Busch, G. E., Retnzepis, P. M., and Jortner, J., 1972, J. Chem. Phys., 56, 361.

(b) Hochstrasser, R. M., and Wessel, J. E., 1973, Chem. Phys. Lett., 19, 156.

[10] Douglas, A. E., 1967, J. Chem. Phys., 45, 1007.

[11] Mulliken, R. S., 1939, J. Chem. Phys., 7, 14.

[12] Bixon, M., and Jortner, J., 1969, J. Chem. Phys., 50, 3284.

[13] Nitzan, A., and Jortner, J., 1972, Proc. Roy. Soc. Land. A., 327, 367.

[14] Harris, R. A., 1961, J. Chem. Phys., 39, 1866. Note that Harris calculates a cross section, not an absorption coefficient. The problem is one of the constants. The correct expression is given in the paper.

[15] (a) Langhoff, C. A., and Robinson, G. W., 1973, Mol. Phys., (in press).

(b) Langhoff, C. A., and Robinson, G. W., (in preparation).

[16] (a) Robinson, G. W. and Frosch, R. P., 1962, J. Chem. Phys., 37, 1962.

(b) Ibid., 1963, J. Chem. Phys., 38, 1187.

[17] Wessel, J. E., 1971, Thesis, U. of Chicago.

[18] See Ref. [17], p. 60, 62.

[19] See Ref. [17], pp. 151-159.

[20] Nitzan, A., and Jortner, J., 1972, Mol. Phys., 24, 109.

[21] See Ref [17], p. 132-138.

[22] Langhoff, C. A., and Robinson, G. W., (in preparation).

[23] See Ref. [17], pp. 161-164

[24] Fano, U., 1961, Phys. Rev., 124, 1866.

[25] (a) Freeman, D., and Ross, I. G., 1960, Spectrochim. Acta, 16, 1393.

(b) Scully, D. B., and Wiffen, D. H., 1960, Spectrochim. Acta, 16, 1409.

[26] (a) Uy, J. O., and Lim, E. C., 1970, Chem. Phys. Lett., 7, 306.

(b) Laor, U., and Ludwig, P. K., 1971, J. Chem. Phys., 54, 1054.

(c) Schlag, E. W., Schneider, S., and Chandler, D. W., 1971, Chem. Phys. Lett., 11, 474.

PART 6

PROPOSITIONS